

PURIFICATION, SIZE SEPARATION AND IONIC
FUNCTIONALIZATION OF HALLOYSITE NANOTUBES

By

SANAZ ABBASI

Submitted to the Graduate School of Engineering and Natural Sciences
in partial fulfillment of
the requirements for the degree of
Master of Science

Sabanci University

January 2018

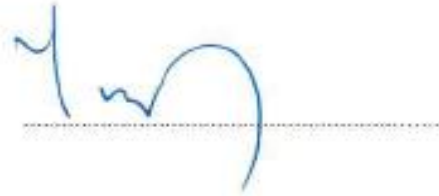
PURIFICATION, SIZE SEPARATION AND IONIC FNCTIONALIZATION
OF HALLOYSITE NANOTUBES

APPROVED BY:

Asst. Prof. Dr. Serkan Ünal
(Thesis Supervisor)



Prof. Dr Yusuf Menceoğlu



Assoc. Prof. Dr. Derya Yüksel İmer



DATE OF APPROVAL: 10/01/2018

© Sanaz Abbasi 2018
All Rights Reserved

ABSTRACT

PURIFICATION, SIZE SEPARATION AND IONIC FNCTIONALIZATION OF HALLOYSITE NANOTUBES

SANAZ ABBASI

Master Dissertation, January 2018

Supervisor: Asst. Prof. Dr. Serkan Ünal

Keywords: halloysite, size separation, purification, silane-amine coupling reaction, ionic functionalization

Halloysite nanotubes (HNTs) are tubular clay minerals, with unique chemical composition and surface charge that can be utilized in composite materials for various applications. However, it is critical to utilize well-defined, non-agglomerated HNTs to obtain homogenous nanocomposites. Additionally, functionalization of HNTs by organosilanes improves their physicochemical and mechanical properties. Here, two studies regarding the preparation of HNTs with enhanced characteristics were carried out. First, the purification and size separation of HNTs were introduced by three hierarchical procedures: alkaline treatment, ultrasonication, and three-step viscosity gradient centrifugation. Secondly, the ionic functionalization of HNTs was examined using an ionic solution through the coupling reaction between an organosilane, 3-(Triethoxysilyl)propyl isocyanate (ISO) and an N-Methyltaurine sodium salt (N-MTSS), as the grafting agent. DLS, FE-SEM, XRD, FTIR, and TGA were used to characterize the size distribution, morphology, structure, chemical and thermal behavior of all HNTs, respectively. Raw HNTs (150 – 1103 nm in length) that

exist in the form of relatively large agglomerations were considerably broken, and cut in individual nanotubes during the alkaline treatment and ultrasonication. Impurities have been successfully removed from pure HNTs (average length of 126 – 179 nm) by a three-step centrifugation. Characterization of ionically functionalized HNTs showed that although modification did not affect the structure of HNTs, modified samples were well-dispersed compared to unmodified ones, indicating the improvement of dispersion behavior due to the ionically charged outer surface. In addition, most suitable conditions for ISO and N-MTSS reaction, along with pirhana and oxygen plasma pre-treatment of HNTs illustrated the highest level of grafting on HNT surface.

ÖZET

HALLOSIT NANOTÜPLERİN SAFSIZLAŞTIRILMASI, BOYUT AYRIMI VE İYONİK

FONKSİYONELLENDİRİLMESİ

SANAZ ABBASI

Yüksek lisans Tezi, Ocak 2018

Tez Danışmanı: Yrd. Doç. Dr. Serkan Ünal

Anahtar kelimeler: halloysit nanotüpler, boyut ayrımı, saflaştırma, silan-amin bağlama reaksiyonu, iyonik fonksiyonelleştirme.

Halloysite nanotüpler (HNTs) su arıtma da dahil olmak üzere çeşitli uygulamalar için kompozit materyallerde kullanılabilen benzersiz kimyasal yapıları ve yüzey yükü olan, tüp şeklinde kil mineralleridir. Bununla birlikte, homojen nanokompozitler elde etmek için iyi tanımlanmış, aglomere olmayan HNT'lerin kullanılması kritik önem taşır. Ek olarak, organosilan ajanlarla HNT'lerin fonksiyonelleştirilmesi, doğal olarak bulunan bu nanotüplerin tüm uygulamalarda özelliklerini arttırdığı düşünülmektedir. Burada, geliştirilmiş özelliklere sahip HNT'lerin hazırlanması ile ilgili iki araştırma yürütülmüştür. İlk olarak, HNT'lerin saflaştırılması ve boyut ayrımı, üç hiyerarşik prosedürle gerçekleştirilmiştir, bunlar alkali işlem, ultrasonikasyon ve üç adımlı viskozite değişimine bağlı santrifüjlemedir. İkinci olarak, bir organosilan bileşiği olan 3-(trioksisilil)propil izosiyanat (ISO) ve bir amin tuzu olan n-metiltaurin sodium tuzu (N-MTSS) aşırı ajanı olarak kullanılarak her ikisi arasındaki bağlama reaksiyonu ile oluşan bir iyonik solüsyon hazırlanıp

HNT'lerin iyonik fonksiyonlandırılması incelenmiştir. Hazırlanan örnekler DLS, FE-SEM, XRD, FTIR ve TGA kullanarak karakterize edilmiştir. Nispeten büyük aglomerasyon formunda bulunan ham HNT'ler (150-1103 nm boyutunda), alkali muamele ve ultrasonifikasyon sırasında bireysel nanotüplere önemli ölçüde kırılmış, dağılmıştır ve kesilmiştir. HNT demeti veya micro parçacıklardan gelen safsızlıklar, üç aşamalı sentrifüleme ile saf HNT'den (126-179 nm ortalama boyut) başarıyla ayrılmıştır. İyonik fonksiyonellendirme, nanotüplerin yapısı ve geometrisi üzerinde hiç bir etki göstermemiştir. Sonuçlar, modifiye edilmemiş HNT'lere kıyasla tüm modifiye edilmiş HNT'lerin su içerisinde çok daha iyi dağıldığını göstermektedir. İyonik modifikasyon ile yüklü HNT'lerin dış yüzeyi yüklü olması nedeniyle dağılım sürecini geliştirdiği gösterilmiştir. Ek olarak ISO ve N-MTSS reaksiyonu için en uygun koşulların HNT'lerin pirhana ve oksijen plazma ile ön-muamele ile birlikte, en iyi aşılama seviyesinde olduğu gösterilmiştir.

**«»To My parents; whose unconditional love and support built the necessary
foundations to achieve this work. «»**

ACKNOWLEDGEMENTS

I wish to express my sincere gratitude and appreciation to my thesis advisor, Assistant Professor Dr. Serkan Ünal and my thesis committee member Professor Dr. Yusuf Mencelođlu for their productive guidance and knowledge in all the duration of thesis and for their significant inspiration and encouragement.

My sincere gratitude to Assoc. Prof. Dr. Derya Yüksel İmer, for her prospective collaboration in this work.

Special thanks to Dr. Özlem Karahan for her constructive suggestions, motivation and comprehensive advice throughout the thesis study.

I would like to express my gratefulness to Sabanci University and all faculty members for providing a productive and competitive academic environment.

This project was funded by Scientific and Technological Research Council of Turkey (TUBITAK) under the grant agreement number 113Y376.

TABLE OF CONTENTS

1. Introduction.....	1
1.1 Introduction	1
1.2 Chemical Composition and Morphology of halloysite.....	2
1.3 Introduction to purification and size separation of HNTs	5
1.4 Introduction to ionic functionalization of HNTs	6
1.5 Aim of this work.....	7
2. Part I: Purification and size separation of HNTs	8
2.1 Literature Survey	8
2.1.1 Studies on the general nanoparticles separation techniques.....	8
2.1.1.1 Separation by filtration	9
2.1.1.2 Separation by gel electrophoresis	10
2.1.1.3 Separation by size exclusion chromatography (SEC).....	11
2.1.1.4 Separation by centrifugation.....	13
2.1.2 Studies on the effect of pH treatment on the structure, morphology and precipitation behavior of HNTs	17
2.1.3 A study on the preparation of homogeneous HNTs in length by ultrasonication and viscosity gradient centrifugation	21
2.1.4 Aim of this work	22
2.2 Materials and experimental procedures.....	23
2.2.1 Materials.....	23
2.2.2 Experimental procedures.....	23
2.2.2.1 Preparation of PVP solution for HNTs dispersion.....	23

2.2.2.2	Preparation of purified and size-separated HNTs	24
2.2.2.3	Preparation of alkaline treated HNTs	25
2.2.3	Characterization methods	25
2.2.3.1	Size distribution analysis	25
2.2.3.2	Morphological analysis	26
2.2.3.3	Structural and phase purity analysis	26
2.2.3.4	Chemical analysis	26
2.2.3.5	Thermal analysis	26
2.3	Results and discussion	26
2.3.1	Characteristics of raw and purified HNTs	26
2.3.2	The effect of re-purification on the yield of purified HNTs	33
2.3.3	The effect of Ultrasonic power on the dispersion and size distribution of purified HNTs	34
2.3.4	The effect of PVP concentration on the dispersion and size distribution of purified HNTs	37
2.3.5	The effect of alkaline treatment on the dispersion and agglomeration of pristine HNTs	45
2.3.6	The effect of alkaline treatment of pristine HNTs on the purification and size separation of purified HNTs	54
2.4	Conclusions	61
3.	Part II: Ionic functionalization of HNTs	62
3.1	Literature survey	62
3.1.1	Studies on the surface modification of HNTs by organosilane agents	62
3.1.2	Aim of this work	66
3.2	Materials and experimental procedures	67

3.2.1 Materials.....	67
3.2.2 Experimental procedures.....	67
3.2.2.1 Reaction of ISO with N-MTSS.....	67
3.2.2.2 Modification of HNTs surface by silane-amine agent solution.....	68
3.2.3 Characterization Methods	69
3.2.3.1 Morphological analysis.....	69
3.2.3.2 Chemical analysis	69
3.2.3.3 Thermal analysis	69
3.3 Results and discussion.....	69
3.3.1 Characterization of ionic silane agent	69
3.3.2 Properties of raw and ionically modified HNTs	71
3.4 Conclusions	79
4. Conclusions and future work	79
5. References.....	81

LIST OF FIGURES

Fig.1. Chemical structure of halloysite [21].	3
Fig.2. FE-SEM images of a) spheroidal halloysite b) tubular halloysite c) kaolinite [18]. ...	3
Fig.3. TEM image of Halloysite nanotubes [18].	5
Fig.4. Diagram displaying the purification of polymersomes from micelles by filtration through 50 nm pores [40].....	10
Fig.5. Separated Au NPs. (A) Schematic drawing of a centrifuge tube after the centrifugation and the color of resulting solutions. (B) The color of the solution taken from 2 different locations shown in A. TEM images of Au NPs. (A) Mother; (B) after centrifugation, NRs deposited on the side wall of the tube; and (C) after centrifugation, nanotubes, spheres, and NRs with larger diameter, sedimented at the bottom of the tube [53].....	15
Fig.6. HNTs structural changes under strong acidic and alkaline treatments, causing the appearance of amorphous SiO ₂ nanoparticles and Al(OH) ₃ nanosheets, respectively [63].....	19
Fig.7. Schematic view of HNTs behavior in relation to each other (a) inner-space of HNTs (b) HNT positions after suspension in solutions with different values of pH [64].....	20
Fig.8. Graphic view of preparation of pure HNTs by ultrasonication and viscosity gradient centrifugation [36].	22
Fig.9. Schematic preview of purification and size separation raw HNT.	24
Fig.10. Schematic preview of purification and size separation raw HNT.	25
Fig.11. Photographs of HNT suspensions in PVP solution (a) pristine HNTs; (b) sonicated HNTs at 120 w for 1 hr; (c) HNTs after sonication and centrifugation at 1170 g; (d) HNTs after sonication and centrifugation at 8800 g; (e) HNTs after sonication and centrifugation at 15557g.....	27
Fig.12. DLS measurement of size distribution for (a) pristine HNTs; (b) sonicated HNTs at 120 w for 1 h; (c) supernatant of HNTs suspension after sonication and	

centrifugation at 1170 g; (d) supernatant of HNTs suspension after sonication and centrifugation at 8800 g.	28
Fig.13. FE-SEM images of (a) pristine HNTs; (b) sonicated HNTs at 120 w for 1 h; (c) Purified HNTs obtained after sonication and centrifugation at 8800 g; (d) Purified HNTs obtained after sonication and centrifugation at 15557 g.	30
Fig.14. Statistical survey for size distribution by FE-SEM for (a) pristine HNTs; (b) sonicated HNTs at 120 w for 1 h; (c) Purified HNTs obtained after sonication and centrifugation at 8800 g; (d) Purified HNTs obtained after sonication and centrifugation at 15557 g (each bar color indicates the average length size range: Red is for particles <200 nm, orange represents particles 200-600 nm and blue shows particles >600 nm).	31
Fig.15. XRD patterns of (a) pristine HNTs; (b) Purified HNTs obtained after sonication at 120 w for 1 h and centrifugation at 8800 g; (c) Purified HNTs obtained after sonication at 120 w for 1 h and centrifugation at 15557 g.....	32
Fig.16. FTIR spectra of (a) pristine HNTs; (b) sonicated HNTs (c) Purified HNTs obtained after sonication at 120 w for 1 h and centrifugation at 8800 g; (d) Purified HNTs obtained after sonication at 120 w for 1 h and centrifugation at 15557 g....	33
Fig.17. Effect of re-purification on the total yield of purified HNTs.	34
Fig.18. FE-SEM images of (a) pristine HNTs (b) Purified HNTs obtained after sonication at 70 w for 1 h and centrifugation at 8800 g; (c) Purified HNTs obtained after sonication at 90 w for 1 h and centrifugation at 8800 g; (d) Purified HNTs obtained after sonication at 120 w for 1 h and centrifugation at 8800 g.	35
Fig.19. Statistical survey for the effect of ultrasonication power on the dispersion and size distribution of (A) Pristine HNTs (B) Purified HNTs obtained after sonication at 70 w for 1 h and centrifugation at 8800 g; (C) Purified HNTs obtained after sonication at 90 w for 1 h and centrifugation at 8800 g; (D) Purified HNTs obtained after sonication at 120 w for 1 h and centrifugation at 8800 g. (B'), (C') and (D') are the same as (B), (C) and (D) with 15557 g centrifugation force.	36

Fig.20. XRD patterns of (a) pristine HNTs (b) Purified HNTs obtained after sonication at 70 w for 1 h and centrifugation at 8800 g; (c) Purified HNTs obtained after sonication at 90 w for 1 h and centrifugation at 8800 g; (d) Purified HNTs obtained after sonication at 120 w for 1 h and centrifugation at 8800 g.	37
Fig.21. DLS measurement of Size distribution for HNT suspensions in (a) 3% wt. PVP-0.1 mol/L CTAB solution; (b) 6% wt. PVP-0.2 mol/L CTAB solution ((I) pristine HNTs; (II) sonicated HNT at 120 w for 1 h; (III) supernatant of HNTs suspension after sonication and centrifugation at 1170 g; (IV) supernatant of HNTs suspension after sonication and centrifugation at 8800 g).....	38
Fig.22. FE-SEM images of (a) pristine HNTs (b) sonicated HNTs in 3% wt. PVP-0.1 mol/L CTAB solution at 120 w for 1 h; (c) sonicated HNTs in 6% wt. PVP-0.1 mol/L CTAB solution at 120 w for 1 h.....	40
Fig.23. FE-SEM images of (a) Purified HNTs obtained from 3% wt. PVP solution, after sonication at 120 w for 1 h and centrifugation at 8800 g; (b) Purified HNTs obtained from 6% wt. PVP solution, after sonication at 120 w for 1 h and centrifugation at 8800 g.	41
Fig.24. FE-SEM images of (a) Purified HNTs obtained from 3% wt. PVP solution, after sonication at 120 w for 1 h and centrifugation at 15557 g; (b) Purified HNTs obtained from 6% wt. PVP solution, after sonication at 120 w for 1 h and centrifugation at 15557g.	42
Fig.25. Statistical survey for the effect of PVP concentration on the dispersion and size distribution of (A) Pristine HNTs (B) Purified HNTs obtained from 3% wt. PVP solution, after sonication at 120 w for 1 h and centrifugation at 8800 g; (C) Purified HNT obtained from 6% wt. PVP solution, after sonication at 90 w for 1 hr and centrifugation at 8800 g..	43
Fig.26. XRD patterns of (a)Pristine HNTs (b) purified HNTs obtained from 3% wt. PVP solution, after sonication at 120 w for 1 h and centrifugation at 8800 g; (c) Purified HNTs obtained from 6% wt. PVP solution, after sonication at 120 w for 1 h and centrifugation at 8800 g.	44

Fig.27. FT-IR spectra of (a)Pristine HNTs (b) purified HNTs obtained from 3% wt. PVP solution, after sonication at 120 w for 1 h and centrifugation at 8800 g; (c) Purified HNTs obtained from 6% wt. PVP solution, after sonication at 120 w for 1 h and centrifugation at 8800 g.	45
Fig.28. FE-SEM images of (a) pristine HNT (b)alkaline treated HNTs with NaOH (0.0005 mol/L) (c) alkaline treated HNTs with NaOH (0.001 mol/L).	48
Fig.29. Statistical survey by FE-SEM for the effect of alkaline treatment on the dispersion and agglomeration of pristine HNTs: (a) average length size of HNTs before and after treatment with 0.0005, 0.02 and 1.0 mol/L NaOH solution (b) average external diameter of HNTs before and after treatment with 0.0005, 0.02 and 1.0 mol/L NaOH solution.	50
Fig.30. XRD patterns of pristine and alkaline-treated HNTs.	52
Fig.31. FT-IR spectra of pristine and alkaline-treated HNTs.	53
Fig.32. TGA curves of pristine and alkaline-treated HNTs.	54
Fig.33. FE-SEM images of (a) Pristine HNTs (b) Purified HNTs precipitated at 8800 g centrifugal force; (c) Purified alkaline-treated HNTs obtained from 0.0005 mol/L NaOH solution and precipitated at 8800 g centrifugal force; (d) Purified alkaline-treated HNTs obtained from 0.002 mol/L NaOH solution and precipitated at 8800 g centrifugal force.	56
Fig.34. FE-SEM images of (a) Pristine HNTs (b) Purified HNTs precipitated at 15557 g centrifugal force; (c) Purified alkaline-treated HNTs obtained from 0.0005 mol/L NaOH solution and precipitated at 15557 g centrifugal force; (d) Purified alkaline-treated HNTs obtained from 0.002 mol/L NaOH solution and precipitated at 15557 g centrifugal force.	57
Fig.35. Statistical survey by FE-SEM for the effect of alkaline treatment on the purification and size separation of purified HNTs: (a) average length size of purified alkaline-treated HNTs with 0, 0.0005 and 0.002 mol/L NaOH concentration precipitated at 8800 g c centrifugal force (b) average length size of purified alkaline-treated HNTs with 0, 0.0005 and 0.002 mol/L NaOH concentration precipitated at 15557 g centrifugal force.	58

Fig.36. XRD patterns of (a) Pristine HNTs (b) Purified HNTs precipitated at 8800 g centrifugal force; (c) Purified alkaline-treated HNTs obtained from 0.0005 mol/L NaOH solution and precipitated at 8800 g centrifugal force; (d) Purified alkaline-treated HNTs obtained from 0.002 mol/L NaOH solution and precipitated at 8800 g centrifugal force.	59
Fig.37. FTIR spectra of (a) Pristine HNT (b) Purified HNT precipitated at 8800 g centrifugal force; (c) Purified alkaline-treated HNT obtained from 0.0005 mol/L NaOH solution and precipitated at 8800 g centrifugal force; (d) Purified alkaline-treated HNT obtained from 0.002 mol/L NaOH solution and precipitated at 8800 g centrifugal force.	60
Fig.38. TGA curves of (a) Pristine HNTs (b) Purified HNTs precipitated at 8800 g centrifugal force; (c) Purified alkaline-treated HNTs obtained from 0.0005 mol/L NaOH solution and precipitated at 8800 g centrifugal force; (d) Purified alkaline-treated HNTs obtained from 0.002 mol/L NaOH solution and precipitated at 8800 g centrifugal force.	61
Fig.39. Reaction pathway for ISO and N-MTSS.	70
Fig.40. FTIR spectra of ionic silane agent solutions (a) sample SA-1-17A and SA-1-22A (b) SA-1-18A.	71
Fig.41. Reaction pathway for modifying the HNT external surface by the ionic silane agent solution for samples SA-1-17B and SA-1-18B.	72
Fig.42. Reaction pathway for grafting the ionic silane agent on the HNT surface for samples SA-1-22B and SA-1-22C.	72
Fig.43. FTIR spectra of ionically modified HNTs.	74
Fig.44. TGA curves of ionically modified HNTs.	75
Fig.45. FE-SEM images of (a) pristine HNT (b) sample SA-1-18B (c) sample SA-1-22B.	77
Fig.46. FE-SEM images of (a) pristine HNT (b) PT-HNT (c) sample SA-1-22B (d) sample SA-1-22C.	78

LIST OF TABLES

Table 1. Nanoparticles separation techniques.....	8
Table 2. pH values of the prepared alkaline suspensions for pristine HNT treatment.	46
Table 3. Mass change of ionically modified HNTs during heat treatment, obtained from TGA analysis.....	76

LIST OF ABBREVIATIONS

¹ HNMR	Proton Nuclear Magnetic Resonance
Ag NPs	Silver Nanoparticles
APTES	γ -aminopropyltriethoxysilane
Au NPs	Gold Nanoparticles
Au NR	Gold Nanorod
CFF	Cross Flow Filtration
CNT	Carbon Nanotube
CTAB	Hexadecyltrimethylammonium Bromide
DAS	Diaminosilane
DC	Differential Centrifugation
DGC	Density Gradient Centrifugation
DGM	Density Gradient Medium
DLS	Dynamic Light Scattering
DMF	N-dimethylformamide
EPDM	Ethylene Propylene Diene Monome
FE-SEM	Field Emission Scanning Electron Microscope
FTIR	Fourier Transform Infrared
GOPTMS	3-(glycidyloxy)propyl trimethoxysilane
HNT	Halloystie Nanotube
IPDI	Isophorone Diisocyanate
ISO	3-(Triethoxysilyl)propyl isocyanate
KH-792	N- β -aminoethyl- γ -aminopropyl trimethoxysilane
MAPTMS	3-(methylamino)propyl trimethoxysilane
MWCNT	Multi Walled Carbon Nanotube
NF	Nanofiltration
N-MTSS	N-Methyltaurine Sodium Salt
OTES	Octyltriethoxysilane
PDI	Polydispersity Index

PHBV	Poly(hydroxybutyrate-co-hydroxyvalerate)
PT-HNT	Piranha Treated HNT
PU	Polyurethane
PVP	Polyvinylpyrrolidone
SEC	Size Exclusion Chromatography
SWCNT	Single Walled Carbon Nanotube
TAS	Triaminosilane
TEA	Triethyl Amine
TEM	Transmission Electron Microscopy
TGA	Thermogravimetric Analysis
XPS	X-ray photoelectron spectroscopy
XRD	X-ray Diffraction
γ -MPS	γ -methacryloxypropyl trimethoxysilane

1. Introduction

1.1 Introduction

Nanoclays are defined as mineral nanoparticles in the form of layers of silicates. Based on the chemistry and physics of the nanoclay particles, they are categorized into various forms such as bentonite, hectorite, montmorillonite, kaolinite, and halloysite. Various benefits of using nanoclays such as environmentally friendly, low economical price, and facile accessibility enabled the application of these natural materials in numerous technical and industrial areas such as pharmacy [1], cosmetics [2], catalysis [3, 4], textile industry [5, 6], medicine [7, 8], and food packaging [9, 10]. Furthermore, nanoclays applications in the field of environmental engineering attracts researcher's attention as adsorbents for volatile organic compounds and waste water treatments agents for a wide variety of contaminations including organic and inorganic pollutants [11-13]. The major reason which encourages researchers to investigate nanoclays in various applications is the outstanding compatibility of nanoclays for optimizations, and the ability to obtain desired separated layers by delamination of stack nanoclays. The compatibility of nanoclays for optimizations is due to the given fact that inter-layered cations are replaceable with desired cations or any other molecules. Surface chemistry modification of nanoclays derived from some simple treatments is the key point for manipulating the characteristics of clays such as acidity, pore size, interlayer spacing, surface area, polarity, and lots of properties which are responsible for various performances in many applications. Additionally, high aspect ratio derived from separation/delamination approach of nanoclays into separated singular nanosheets is a key property besides other useful characteristics [14].

Halloysite is defined as a natural mineral clay like kaolinite, dickite, and nacrite which are considered multiwalled aluminosilicates with 1:1 sheet positioning. The layered structure of the halloysite is known to host water molecules are in the between the layers and the layers are composed tetrahedrally coordinated Si^{4+} and octahedrally coordinated Al^{3+} in a 1:1 positioning. In 1826, Berthier discovered the halloysite and it was introduced as a 1:1 silicate layer in the clay mineral group of kaolin. In 2000, based on Churchman reported [15] that halloysite are created throughout the time of rocks weathering, without considering the fiery

state of the halloysite. The wide variety of the morphologies of the halloysite particles are obtainable. Although the elongated tubule of the halloysite particles is the most common morphology, other forms of the halloysite depending on their specified application such as spheroidal, short tubular, and platy particle shapes were reported frequently [15-17].

Halloysite nanotube (HNT) with the tubular structure showed wide variety of applications in various research areas. There are many benefits of the HNT including non-toxic, considerable aspect ratio, bio-compatibility, porousness and surface area, regeneration potential, great thermal stability, high mechanical resistivity, different inside and outside chemistry, adequate hydroxyl groups on the surface as a characteristic properties, abundance (low cost) and high cation exchange capacity that caused HNT to be superior choice for different applications such as novel drug delivery systems (NDDS), retard and fast release of active agents, catalysts, waste water treatments, disposable and reusable, acting as nanofillers in hybrid clay-polymer nanocomposites, etc.

1.2 Chemical Composition and Morphology of halloysite

Although theoretical chemical composition of the halloysite is same as kaolinite, the water content of the halloysite is higher than kaolinite. The ideal unit formula for halloysite-(7 Å) and halloysite-(10 Å) can be introduced as $\text{Al}_2\text{Si}_2\text{O}_5(\text{OH})_{4.n}\text{H}_2\text{O}$ where $n = 0$ and 2 , respectively [17] which the composition of each layer includes a tetrahedral (Si–O) and an octahedral (Al–OH) sheet (see Fig.1) [18, 19]. The interaction of water molecules with the halloysite in the form of hydrated halloysite (when $n=2$) is defined as “halloysite-(10 Å)”, in which one layer of water molecules is present between the multilayers as sandwich mode and the “10 Å” term represents the d001-value of the layers. In contrast, the dehydrated structure of halloysite (when $n=0$) is defined as “halloysite-(7 Å)”, and the lack of water molecules layer as intermediate can be derived from mild heating and/or a vacuum environment conditions [20]. However, presence of some typical impurities (Iron oxides or poorly arranged minerals, some of which may also be localized within halloysites tubes) is always the challenging subject to evaluate the chemical analysis of many halloysites that

represents the considerable amounts (up to 12.8 wt%) of Fe_2O_3 [20]. This result can be attributed to Iron oxides such as hematite or maghemite, and somewhat to isomorphous substitution of Fe^{3+} for Al^{3+} in the octahedral sheet [15].

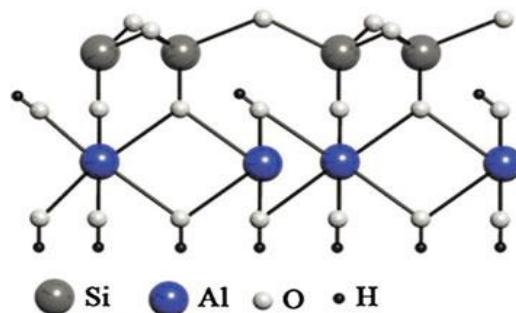


Fig.1. Chemical structure of halloysite [21].

The morphology of the halloysite particles (Fig.2) is attributed to the crystallization conditions and geological phenomenon [21]. It has been shown in the literature that halloysite particles morphology is forcefully assigned to geological conditions and the crystallization routine. Joussein *et al.* [20] studied the relationship of various morphologies of halloysite's particles with their geographical locations. From the view point of the morphological study, halloysite nanoparticles can be categorized in three main classes: spherical, platy and tubular [18, 20].

The most favorable shape for many applications in the nano-based research is the tubular, however, all above-mentioned different categorizes are present [18].

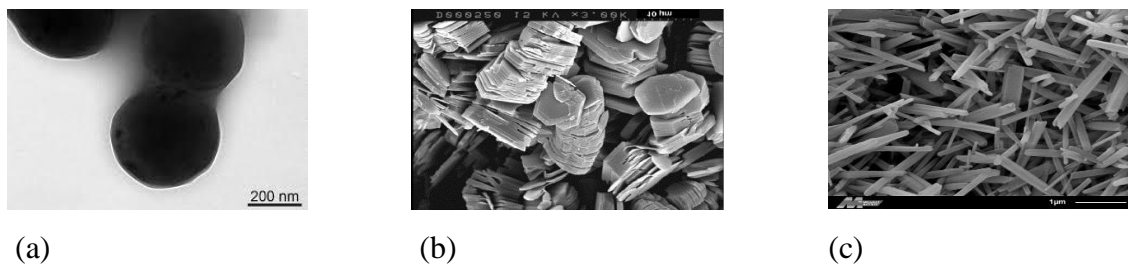


Fig.2. FE-SEM images of a) spheroidal halloysite b) tubular halloysite c) kaolinite [18].

Spheroidal halloysite is present with a wide range of structure around the world, depending on the location of their occurrence. It is mostly common to see pseudo-spherical or

spheroidal particles in weathered volcanic ashes and pumices. Saturated state of solutions is associated with the spheroidal morphology. Highly tendency to be supersaturated of the solution in contact with the glass is due to high dissolution rate of volcanic glass. Comparing with the spheroidal kaolinite formation condition reveals that this condition is associated to spheroidal kaolinite precipitation [22].

Different shapes of the tubules may be emerged in tubular halloysite including long and thin, short and stubby or even appearing form other tubes (Fig.2). Based on the tubes sources, length and inner diameter of halloysite tubes vary from 200 to 1000 nm and 15 to 100 nm respectively [23]. In order to clarify the exact reason for planar kaolinite to roll and getting the tubular halloysite shape, Dixon & McKee *et al.* [24] claimed that owing to presence of interlayer water molecules, bond interactions which they are linking the octahedral and tetrahedral sheets together are weakened [18], thus absence of dimensional analogy between the layers is enhanced and forces the Si-O sheet to curve toward the Al-OH side.

Similar to feldspars and micas, tubular halloysite is derived from crystalline minerals. Although Singh and Gilkes *et al.* [25] claimed that deformation of platy kaolinite is the reason of formation of tubular morphology, the crystallization process from solution rather than topotactic alteration is the mechanism of tubular shape halloysite formation from micas. Transmission electron microscopy (TEM) study conducted by Robertson & Eggleton *et al.* [26] claimed a model for halloysite tube development from platy kaolinite. The initial point of the process has been claimed as a progressive change of kaolinite which is inducing a loss of rigidity of structure at points along the crystal, interpreted as hydration to halloysite. A TEM image of tubular halloysite is presented in Fig.3.

By progressing the kaolinite change, the development of the halloysite is occurred, the primary planar shape of the kaolinite changes into curly shape evenly.

The influence of individual clay minerals on formation damage of reservoir sandstones: A critical review with some new insights, owing to special characteristics of HNTs is that the

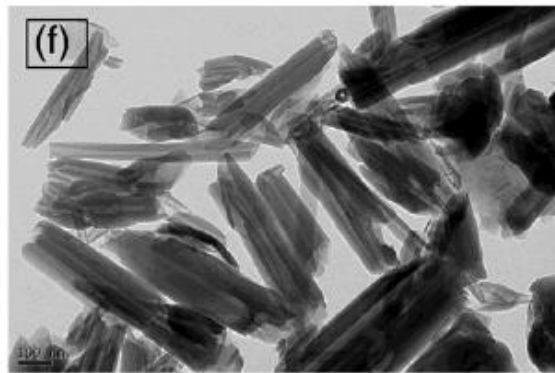


Fig.3. TEM image of Halloysite nanotubes [18].

great deal of researcher's interests is attracted to use of halloysite nanotubes in wide variety of applications.

Halloysite nanotubes can be obtained easily from the environment as natural nanoclays including various chemical compositions for interior and exterior walls and is very cost effective acquirable in contrary to synthetic nanotubes such as carbon nanotubes (CNTs) [27, 28]. Non-toxicity and biocompatibility characteristics of the HNTs are the key points in biomaterial applications such as a nanoscale filler. In the novel drug delivery systems and biocides applications, HNTs are capable to carry the active materials by encapsulating and acting as the controlling agent in releasing the substances [29]. High thermal and corrosion resistivity, acting as the filler for other nanocomposites and drug delivery agent of biomaterials, acting as the purifying agent in water waste treatment applications, textile wastes, etc. of the HNTs all are due to the chemistry and mechanical properties of HNTs [30].

1.3 Introduction to purification and size separation of HNTs

The on-demand availability of nanomaterials with selected size and well-defined chemical/physical properties is fundamentally important for their widespread application. Likewise, considerable potentials of HNTs in various fields of applications is dependent to its high mechanical properties, enhanced thermal resistivity, great biocompatibility and

abundant deposition [31, 32]. Although HNTs have been used in applications such as ceramics and polymeric composites industries [33, 34] and water waste treatment [35] for a long time, heterogeneous quality of natural HNTs has caused difficulties in the wide-ranging uses of HNTs for developing cost effective, high performance and multifunctional polymer or hybrid nanocomposites. For purification of inhomogeneous natural pristine HNTs into homogenous fractions, which is a vital factor in the applications of these nanomaterial, an extensive experimental method is needed [36]. However, conventional separation approaches of nanoparticles are not applicable for HNTs due to their naturally existing properties. In this regard, a comprehensive method using multiple separation and purification methods, along with necessary modification applied to these techniques is crucial to prepare pure HNTs with uniform dispersion in size. This context will be discussed further in the literature.

1.4 Introduction to ionic functionalization of HNTs

The elimination of dangerous heavy metals from drinking, domestic and industrial water is significantly vital. In general, naturally available HNTs without any functionalization are able to eliminate the pollutants from waste water by physical or chemical adsorption. However, with the purpose of increasing the performance of HNT, they are often modified with some specific functional groups. Functionalization of HNTs by organosilane agents is considered to enhance the properties of this naturally available nanotubes for its previously mentioned applications. The use of organosilanes with the chemical formula $R-Si-(OR')_3$ is widely known, due to advantages such as low cost and potential for hydrolysis and thus, condensation reactions with hydroxyl groups existing on the surface of other particles [66]. Multiple research has been dedicated to this field, which will be explained further in the future.

1.5 Aim of this work

This work focuses on two crucial subjects regarding the preparation of HNTs with improved characteristics: (i) purification and size separation of HNTs, and (ii) ionic functionalization of HNTs by a silane compound.

In the purification and size separation investigation of HNTs, the aim was to provide purified and homogeneous HNTs in size, as a critical adjustment for the improved performance of these natural clay minerals in its application. The selected method should be potentially applicable for large scale production of purified HNTs. For this purpose, the whole purification and size separation of pristine HNTs was studied by three hierarchical procedures: alkaline treatment (for improving the dispersion behavior of HNT suspensions), ultrasonication (to break apart any agglomerations including impurities in the pristine HNT such as kaolinite and other similar clay minerals), and three-step viscosity gradient centrifugation (to sort HNTs into two distinct uniform fractions based on their size) of pristine HNTs. The effect of ultrasonication power, concentration of the density gradient media (polyvinylpyrrolidone (PVP) Solution containing hexadecyltrimethylammonium bromide (CTAB) surfactant), and alkaline treatment on the size distribution and yield of purified HNTs were investigated.

In the ionic functionalization of HNTs, the ionic functionalization of HNTs by an ionic solution prepared from the coupling reaction of a organosilane agent 3-(Triethoxysilyl)propyl isocyanate (ISO) with n-methyltaurine sodium salt (N-MTSS) was examined. Considering in the terms of hydrophilicity, diffusion and absorbance, no work has been done on ionic covering of the external surface of HNTs in the literature. The objective of this work was to illustrate the best reaction conditions for grafting the newly synthesized ionic agent on the outer surface of HNT, and to investigate the effect of modification on the structure, morphology and dispersion behavior of HNTs.

2. Part I: Purification and size separation of HNTs

2.1 Literature Survey

2.1.1 Studies on the general nanoparticles separation techniques

In order to prepare pure nanoparticles for fundamental research and applications, the size-based separation of them in purification stage is still the challenging step. Development of methods that provide convenient access to stabilized nanoparticles, offer greater control of structural definition, and can be conducted at larger scales is becoming increasingly important for fundamental studies and applications of nanoparticles. Especially, a considerable value of purity and monodispersity are vital parameters which can make the evaluation of structure-property relationships complicated. They can also perplex the electronic and optical measurement, or block the chemical/physical process by which nanostructures are used [37, 38]. Eliminating the impurities and pollutants from outlined nanoparticle structure is still important challenging topic. Although the effect of impurity removal on the chemistry and nanoparticles performance in the term of purification has been neglected, recently it was found that purification processes have important effects [39]. In order to separate of heterogenous nanoparticle solution into homogenous fractions, various methods have been utilized with regard to desired physical and structural properties. The most efficient and trustworthy techniques are presented in Table 1.

Table 1. Nanoparticles separation techniques

Technique	Nanoparticles
Filtration	Polymersomes, gold nanoparticles (Au NPs).
Gel electrophoresis	Charged colloids, C-dots, silver nanoparticles (Ag NPs).
Size exclusion chromatography	CNTs, polymer/nanoparticles hybrid materials, polymersomes, (AuNPs).
Centrifugation (rate-zonal and isopycnic)	Metallic nanoparticles, gold nanorods, ploymersomes, Organic polymers, silicon nanocrystals, carbon dots (C-dots), CNTs, HNTs.

2.1.1.1 Separation by filtration

Filtration is one of the common purification methods based on size distribution of particles. S. F. Sweeney *et al.* [39] reported the diafiltration as a fast and convenient trend for purification of water-soluble AuNPs. This method has great potential for size separation of inhomogeneous nanoparticle samples. Diafiltration was compared to conventional purification methods and the X-ray photoelectron spectroscopy (XPS), thermogravimetric analysis (TGA), and proton nuclear magnetic resonance (^1H NMR) analyses resulted in high purity in less time and less waste with diafiltration rather than conventional purification methods such as centrifugation, chromatography, and dialysis extractions.

Also, they investigated the fractionation of a polydisperse 3 nm sample into four fractions of differing mean core diameter. TEM and UV-visible measurements revealed that diafiltration as a purification method has great potential for fractionation and represented the possible field to the pore morphology of diafiltration membranes. Diafiltration was proved as useful purification method with high efficiency and yield in the size separation applications and nanoparticle preparation uses [39].

In another work, the purification of polymersomes pre-treated from a block copolymer sensitive to pH by cross-flow filtration was investigated by J. D. Robertson *et al.* [40]. Owing to “filter cake” phenomena, which means blocking the filter by nanoparticle aggregation, dead-end filtration method could not represent the acceptable results. The filter cake problem was solved by Cross flow-filtration (CFF) by creating the particle flow at a tangent to the pore under high pressure. Schematic Fig.4 Shows the CFF mechanism under high pressure. In this method, smaller particles compared with the pore size penetrate the membrane in presence of high pressure while tangential flow intercepts the filter cake phenomena.

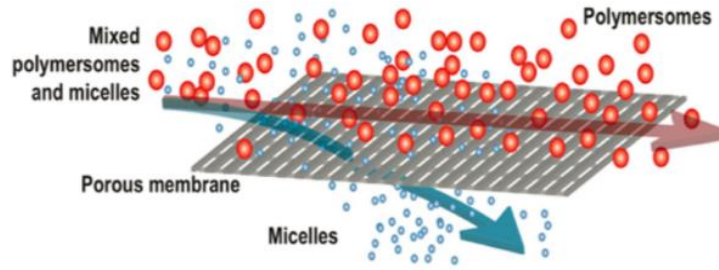


Fig.4. Diagram displaying the purification of polymersomes from micelles by filtration through 50 nm pores [40].

2.1.1.2 Separation by gel electrophoresis

Gel electrophoresis is introduced as a highly efficient method for separating and determining the characteristics of nanoparticles, nanospheres, and biological macromolecules. This method has various forms including different degrees of dimensionality and applying time-varying electric fields.

Au NPs and Ag NPs were separated according to their size and shape by agarose gel electrophoresis after coating them with a charged polymer layer in the M. Hanauer *et al.* [41] research. The size- and shape-dependent plasmon resonance of noble metal particles and TEM were used for verifying the separation procedure. According to Henry formula, a formula was driven which illustrate the electrophoretic mobilities. This model gives a theoretical framework for estimating the mobility behavior of polymer coated nanoparticles. In another work, the electrophoretic propagation of charged colloidal objects, monodisperse, anionically stabilized polystyrene spheres were investigated by D. Bikos *et al.* [42]. They found that the ring-like front of monodisperse nanospheres propagates stably in polyethylene glycol (PEG)-passivated agarose gels and that the measured ring radius as a function of time agrees with a simple model that incorporates the electric field of a cylindrical geometry by making a full-ring cylindrical gel electrophoresis chamber. Additionally, they illustrated that the cylindrical geometry gives a potential advantage when acting electrophoretic separations of objects that have widely size distribution: smaller objects can still be retained in a

cylindrical gel that has a limited size over long electrophoretic run times required for separating larger objects.

2.1.1.3 Separation by size exclusion chromatography (SEC)

Separation by size exclusion chromatography (SEC) is another efficient method for the separation of macromolecules in solution based on size distributions [43]. The hydrodynamic volume is the fundamental mechanism of this method for separation. The mechanism of this method is based on moving the mixture through the stationary phase of a SEC column that smaller molecules flow in and out of pores within the gel, whilst larger molecules cannot penetrate into the pores, letting them to pass through the stationary phase quicker and elute from the column earlier. Compared to filtration, yield of SEC is higher as most of the material loaded onto a column will be eluted [44]. General uses of SEC is based on the separation of free small molecules from those encapsulated within nanoparticles [40].

In another work, the efficient purification of single-wall carbon nanotubes (SWCNTs) by SEC was represented (44) by G.S. Duesberg *et al.* By size exclusion chromatography applied to surfactant stabilized dispersions of SWNT raw material, carbon nanospheres, metal particles, and amorphous carbon could be successfully eliminated. Additionally, the tubes were separated by their lengths as well. The atomic force microscopy (AFM) measurement proved that equal fractions of both individual SWNTs and ropes of SWNTs were in the purified material.

In another investigation, G.S. Duesberg *et al.* [45] also performed SEC on micellar aqueous dispersions of soot from an arc discharge experiment to yield chemically unmodified, almost impurity free and size separated multiwall carbon nanotubes (MWCNT). The chromatographic technique was an effective, non-destructive method for purification and size separation of CNTs.

In addition to size separation, SEC can also be used for the separation of Au NPs according to their shape. This was achieved based on the adsorption behavior of Au NPs (spherical and rodlike) on the surface of column materials. A surfactant compound containing

poloxyethylene dodecanol (Brij-35) and sodium dodecyl sulfate (SDS) was added to the eluent for this purpose. Adding SDS eliminated the irreversible adsorption of Au NPs [43].

A novel purification method for SWCNTs was introduced. This method was based on SEC and vacuum filtration, and took advantage of the fact that during a swelling procedure in distilled water, the size of polymer cavities increases. These cavities are not so small in size to block the movement nanoparticle bundles, and not so large that nanotubes could escape. The stationary phase used in this work was potassium polyacrylate [46]. As an alternative method to density gradient centrifugation, SEC was carried out to separate CNTs to two categories of SWCNTs and DWCNTs. Sephacryl gel S-200 was used as the stationary phase material, and the average diameter of prepared DWCNTs and SWCNTs were 1.64 ± 0.15 nm and 0.93 ± 0.03 nm, respectively. This offered technique was highly capable of being scaled up for industrial applications [47].

The common application of SEC is the separation of small particles which are free from those entrapped inside nanoparticles. As an effort to resolve the problem of separation of nanoparticles specifically by their size and shape, a solution of polymersomes was concentrated by passing through a cross-flow membrane. This part was performed as an improvement process for SEC resolution, and as a result, the required time for the absorption of liquid to the stationary phase was reduced. The results obtained from chromatography indicated that the dividing of polymersomes into fractions with different sizes was efficient. This method was effectual for separation of samples containing various sizes of particles into many individual fractions with discrete sizes. The separated samples by SEC and differential centrifugation (DC) were both tested for measuring their monodispersity, and it was found out that samples separated by SEC were better dispersed than those purified by DC. The only drawbacks in this technique were the higher chance of material loss and it took longer to achieve separated particles than DC [40].

2.1.1.4 Separation by centrifugation

Recently, attention has been paid to centrifugation as a separation technique for directly dividing nanoparticles by size in liquid medium, since this method has proven to be a great potent for nanoparticles purification due to the efficiency in breaking agglomerations, high amount of yield and its ability to be scaled up for industrial applications [48]. Two of most reported centrifugation techniques are isopycnic centrifugation, which is a density-based method, and velocity-based rate zonal centrifugation. Small nanoparticles (average size < 10 nm) are usually less dense than the gradient medium, thus they can be separated by using isopycnic centrifugation. However, density of large nanoparticles is higher than that of the solution gradient medium. In this case, the difference in the velocity which particles sediment depending on their size can be considered as a separation factor. Rate zonal centrifugation is a suitable method for the separation of large nanoparticles [49].

Isopycnic centrifugation: In this separation method, all fractions of a desired sample are divided based on their density during the experienced centrifugal force. According to the equilibrium precipitation, a density gradient is built. After that, analyte components are concentrated in the form of bands where their density is equal to that of their surrounding media.

In an earlier work, selective separation of AuNPs with various sizes was exploited. Used AuNPs were composed of different surface chemistries. The separation was carried out in water or an organic medium. The applied technique can be extended to other NPs separation. In this research, no solutes were used in order to avoid any possibility of contamination. An advantage of this method was that it could be processed at low centrifugational forces, thus it was easily attainable using benchtop machines. In the used sedimentation separation, no density gradient medium (DGM) or any other solute was utilized. A suitable centrifugation rate was selected. After centrifugation, different fractions with different dimensions were prepared after each run in a sequential way. At the end of the procedure, fractions containing largest nanoparticles in size to fractions with smallest size distribution in the solution were sedimented. The products of this method were AuNPs with size range from 9.5 to 20 nm,

with standard deviations of 11% and 18%, respectively. Another outcome of this separation technique was that there was no need for modification of the raw nanoparticles to enhance their dispersion within the solution [50].

Rate-zonal centrifugation: This centrifugation method is based on the hydrodynamic properties of materials during the separation procedure. In this approach, the required medium consists of different viscosities attributed to separate zones within the solution. For preparation of this type of medium, solutions of a specific chemical compound, such as aqueous sucrose or ficoll, with different concentrations are layered on top of each other inside the centrifuge tube. Different zones with different viscosities have advantage over a homogeneous medium in viscosity in a way that using multiple layers with changing viscosities facilitates the collection and enrichment of purified samples. Separated nanoparticles of each region have narrower size distributions. However, these layers are not stable, and they tend to collapse during centrifugal acceleration or deceleration. They can also get disrupted by diffusion of other regions at the centrifugation time. These drawbacks make the collection of separated samples problematic. Therefore, for this purpose, sharp and stable boundaries between each viscosity zones are necessary to achieve homogeneous fraction with distinct sizes [51].

In a novel work, the length separation of SWCNTs was exploited through centrifugation in a high-density medium. It is reported that, in order to maximize the density differences among SWCNT types, the medium density is set about the average density of the nanotubes in the case of type separation. In another case of length separation, in order to minimize the influence of the differences in density of various SWCNTs types, much higher or lower density medium was used. In order to make length and electronic type-ordered categorizes, the consecutive separations can be used. Different parameters such as lower separation rate, higher SWCNTs concentration, and lower temperature improved the separation. It is claimed that length separation by above mentioned technique is relatively straightforward compared to other methods. SWCNTs with long lengths, proving previous results, show great optical properties [52].

The effect of centrifugation on efficient separation of gold nanorods suspended in a mixture of nanorods and nanospheres was investigated. In Fig.5, shape separation of gold nanorods, in which they have been synthesized by seed-mediated through the centrifugation method was shown. Hydrodynamic analysis of the shape and rods explained the centrifugation conditions under which the shape separation was done. It was claimed that separation of all types of nanoparticles shape through proceed centrifugation can be the promising research subject about separation techniques. It is proposed as an important, high efficiency method to obtain monodispersity and dispersion of the nanoparticles by shape [53].

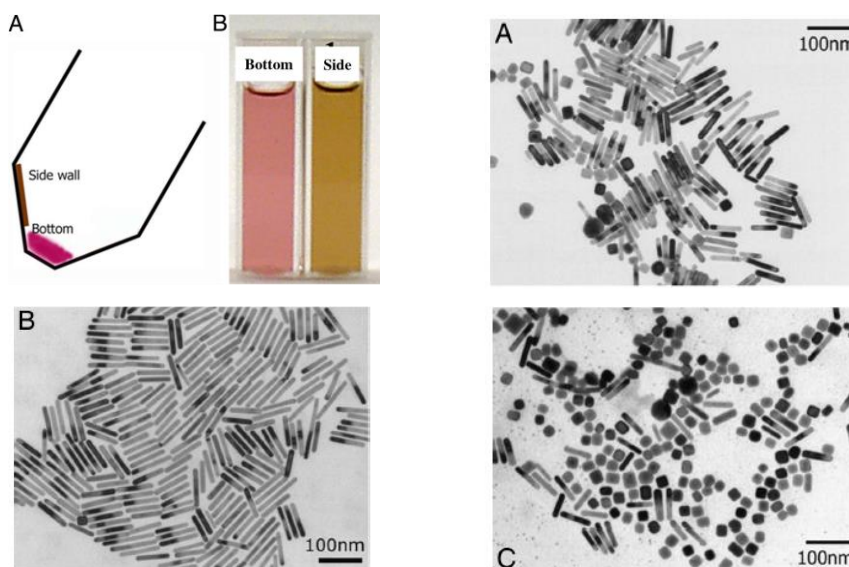


Fig.5. Separated Au NPs. (A) Schematic drawing of a centrifuge tube after the centrifugation and the color of resulting solutions. (B) The color of the solution taken from 2 different locations shown in A. TEM images of Au NPs. (A) Mother; (B) after centrifugation, NRs deposited on the side wall of the tube; and (C) after centrifugation, nanotubes, spheres, and NRs with larger diameter, sedimented at the bottom of the tube [53].

In another work, the effect of separation through ultracentrifugal rate technique was studied on metallic nanoparticles with different size, suspension composition, inclusive of Au NPs and FeCo@C. Finally, it was claimed that the method yields high resolution for colloid nanoparticles separation with various compositions, wide range of size, and various bundles

of nanoparticles in short time through density gradient centrifugation (DGC) with various rates of nanoparticles sedimentation [54].

Recently, the nanoparticle separation and purification by various colloidal nanoparticles such as Ag, Au, and CdSe inside an organic density gradient through ultracentrifugation was done. Size and shape separation of colloidal particles and gold nanowires can be successfully achieved. By using this technique post-treatment procedure was facilitated and the following monodisperse colloids assembly was simplified. The major benefits of the organic polymer dissolution inside the gradient medium enhanced the efficiency of separation and straightforward creation of functional composite films with segregate monodisperse nanoparticles which they are embedded inside [55].

Density gradient solution is composed of layers of a specific chemical solutions with different concentrations. This causes the viscosities as well as densities in each layer to be different. In one research, this change in viscosity has been examined during separation by density gradient centrifugation. A viscosity gradient was built by using PVP as the specific chemical. The densities were nearly similar, but viscosity values were hugely different. This insured a better separation by size for nanoparticles. In the category of rate zonal centrifugation for achieving an efficient nanoparticle size separation, this work ensured the conceptual importance of using a gradient as a function of viscosity, instead of density. An original approach for distinct size separation of NPs with using PVP solution as the viscosity gradient was carried out. AuNPs were stabilized by PVP solution and separated into fractions with small differences in size with high resolution. Using viscosity gradient solution, compared to using density gradient solution to achieve a complete NPs size separation, especially for large NPs, was highly successful. Furthermore, different solutions of PVP with different molecular weights, but equal viscosities were utilized to gain similar purification results, illustrating the pliability of the new approach [56].

A novel method which was based on employing rate zonal centrifugation for separation of nanoparticles by size and shape was conducted by using “aqueous multiphase systems (MuPSs)” as media. The aim of this work was to divide Au NRs (main synthesis product) from gold nanospheres and other large nanoparticles (synthesis byproducts). As a

conclusion, a new method utilizing thermodynamically stable aqueous phases for separation media was exploited. This method presented an improved and enhanced performance for rate zonal centrifugation as a separation technique. Separation of media based on phase eliminated the problems such as sample collection and short stability duration, which were related to using previously developed layered media [51].

In another research, with respect to interfacial science, colloidal particles were purified by density gradient centrifugation according to their electronic and optical properties as well as their sizes. The contribution of electronic, optical and mechanical properties in purification of thin films was investigated. Isopycnic and transient density gradient centrifugation using both organic and aqueous media were employed to fractionate the thin films into their colloidal components, SWCNTs and silicon nanocrystals [57].

Despite the interest of employing density and viscosity centrifugation techniques in separation of CNTs since Fagan *et al.* [58, 59], these methods are not applicable for purification of HNTs in large scales. Besides, Chen *et al.* [49] demonstrated the problem of short stability time after centrifugation. To overcome these challenges for separation of HNTs, a new method was introduced using viscosity centrifugation in two steps [36]. The aim was to introduce a homogeneous dispersion of HNTs in length, and the procedure was based on the combination of ultrasonication and ultracentrifugation in two steps. The obtained results showed the effectiveness and convenience of treating HNTs by ultrasonication in cutting and dispersion. In addition, the impact of ultrasonication time and power in dispersion of HNTs were studied. Furthermore, HNTs concentration determination was investigated by employing UV-visible spectroscopy [36].

2.1.2 Studies on the effect of pH treatment on the structure, morphology and precipitation behavior of HNTs

Prior to preparation of purified nanotubes, eliminating the existing agglomerations in natural HNTs has proven to be a contributing factor in achieving more homogeneous nanoparticles in size. Suspensions of HNTs in basic solutions has been effective in breaking the bundles

of nanotubes and dispersing the particles in aqueous or organic media. This action will preserve the properties of HNTs in long term for different applications, without any disturbance in their structure or shape [60].

From the theoretical point of view, strong acidic or basic environments have a potential to damage HNTs structure, due to the occurrence of desilication and dealumination. However, it is shown that mild acidic or basic environments (pH= 2 - 11) would not harm HNTs [61], and an obvious relation exists between the suspension's pH value and dispersion of HNT powders [28].

The stability of natural HNTs in acidic, neutral and basic environment at room temperature were previously studied. In strong acidic or basic solutions (0.01–1 mol/L), Al–OH started to dissolve, causing the gradual thinning of the inner walls of HNT. For example, in solutions of NaOH, the higher level of solubility for Si(IV), compared to Al(III) results in fragmentation and appearance of Al(OH)₃ layers and scaly particles (see Fig.6) [60].

In another study concerning the pH treatment effect on HNT structure, dispersion and aggregation degree of COOH functionalized HNT under acidic, neutral and basic conditions were investigated. It was shown that in spite of aggregate formation in neutral environment, HNTs were well dispersed inside the acidic or basic solutions. This phenomenon is caused by the fact that although hydrogen bonds between COOH functionalized HNTs are strong in neutral conditions, and thus leads to aggregation, they tend to decrease in acidic or basic environments due to the change in charge dispersion [62].

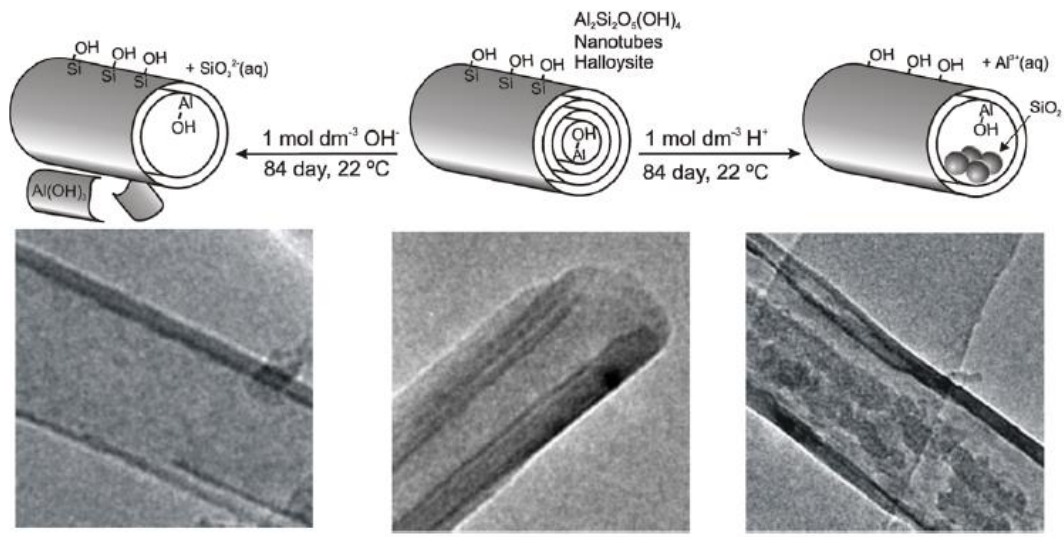


Fig.6. HNTs structural changes under strong acidic and alkaline treatments, causing the appearance of amorphous SiO_2 nanoparticles and $\text{Al}(\text{OH})_3$ nanosheets, respectively [63].

In an investigation concerning the properties of halloysite from six different regions in the world, it was noteworthy that prior to any characterization, all HNT samples were washed and maintained in the pH conditions of 7.5-8 in order to achieve a clearly dispersed suspension [18].

The examination of individual HNTs behavior in relation to other HNTs in a suspension was carried out under the title of “blocking and opening of HNTs under acidic, neutral and alkaline environments”. It was claimed that one nanotube acts like a door for another nanotube, in the way that it either blocks any access to the other nanoparticle by aggregation or it opens the access to the mentioned HNT by dispersion. It was observed that the acidic solutions of HNT were unstable, thus huge bundles and agglomerates were formed at pH values below neutrality. Meanwhile, HNT suspension at pH values above eight (basic environment) showed high dispersion without any precipitation. This is due to the increased van der Waals interactions between nanotubes. The highest dispersion was seen at pH = 11. In conclusion, in alkaline solutions, HNTs were successfully dispersed and individual HNTs were separated from each other (opening phenomenon), and in acidic conditions HNTs tended to form bundles and positioned at the end of other HNT bundles and thus blocking the access to their inner pores (see Fig.7) [63].

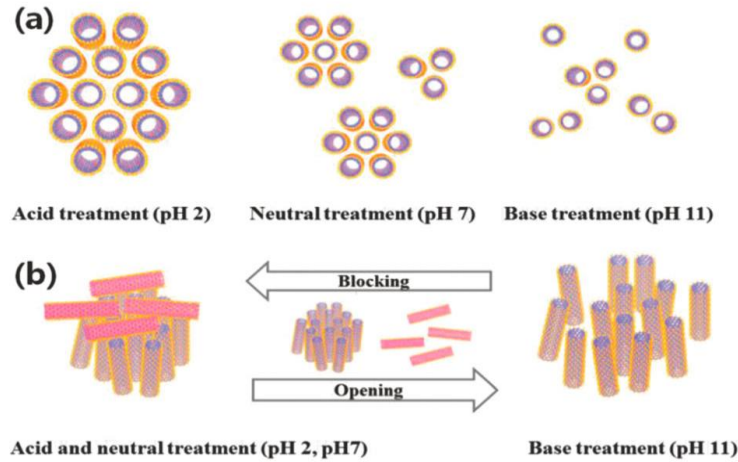


Fig.7. Schematic view of HNTs behavior in relation to each other (a) inner-space of HNTs (b) HNT positions after suspension in solutions with different values of pH [64].

The impact of alkali activation on the chemistry and physics of HNTs for adsorption and release of ofloxacin were reported. It was proved that this activation could enhance the adsorption ability of HNTs for ofloxacin and increase the duration for the release mechanism. Furthermore, it was observed that alkaline treatment with NaOH concentrations below 4.0 mol/L at room temperature did not affect the structure of HNTs [64].

Morphological and structural changes of halloysite with acid or alkaline activation were also studied in another approach. Similar to results obtained by Joo *et al.* [63], it was shown that for pH values less than two, HNT suspension became unstable and they eventually formed agglomerates and thus, bundles. But for pH values higher than eight, no precipitation or bundle formation occurred due to van der Waals interactions. And again, pH = 11 was found to contain the highest level of dispersion among other tested pH values. This occurrence considerably had an impact on the surface area, pore diameter and pore volume of HNTs. In basic solution, HNTs were completely dispersed with all the ends of each nanotubes separated from others. In comparison, in acidic solutions, all nanotube ends were blocked. However, in strong concentration of acids or bases, significant changes were observed in the structure and morphology of halloysite [28].

New outcome about HNTs surface charge was measured by ζ potential considering different pHs. It was claimed that by increasing the value of pH, surface charge existing at the outer

space will become dominant over that at the inner space of HNT. Consequently, this change in the surface charge can lead to separating individual nanotubes and hence, dispersing them in the solution [65].

2.1.3 A study on the preparation of homogeneous HNTs in length by ultrasonication and viscosity gradient centrifugation

As previously mentioned, depending on the origin, commercial HNTs are inhomogeneous in size (0.1-5 μm), and present usually in the form of agglomerates and bundles. The previously applied conventional nanoparticle separation techniques are difficult to employ on these natural clay minerals. Here, we review an approach presented by R. Rong *et al.* [36], in which ultrasonication and viscosity centrifugation (performed in two steps) were carried out to break the agglomerates and bundles, cutting long nanotubes into short fractions and finally separate HNTs according to their length, respectively (Fig.8).

A PVP solution in aqueous media was prepared as the viscosity gradient solution. This solution also contained 0.1 mol/L CTAB as a surfactant for better suspension of HNTs [36].

Study of the ultrasonication time on the size and yield of prepared HNTs showed that long duration of treatment resulted in shorter HNTs but less amount of yield. In addition, the investigation of ultrasonication power on the length and yield of prepared HNTs showed that by increasing the power of ultrasonication treatment, the amount of yield also increases [36]. Another studied effect was related to the centrifugation time. It was proven that after ultrasonication, by centrifugation of HNTs for long times (75 min), HNT yield drops down. Thus 45 min was found to be the optimum centrifugation time to achieve the highest yield for purified HNTs [36].

Finally, the effect raw HNTs concentration on the obtained yield of purified HNTs was also reported. For this purpose, solutions of HNT with different concentrations were processed by the proposed method. In the end, it was observed that as the raw HNTs concentration is increased, the amount of yield decreased [36].

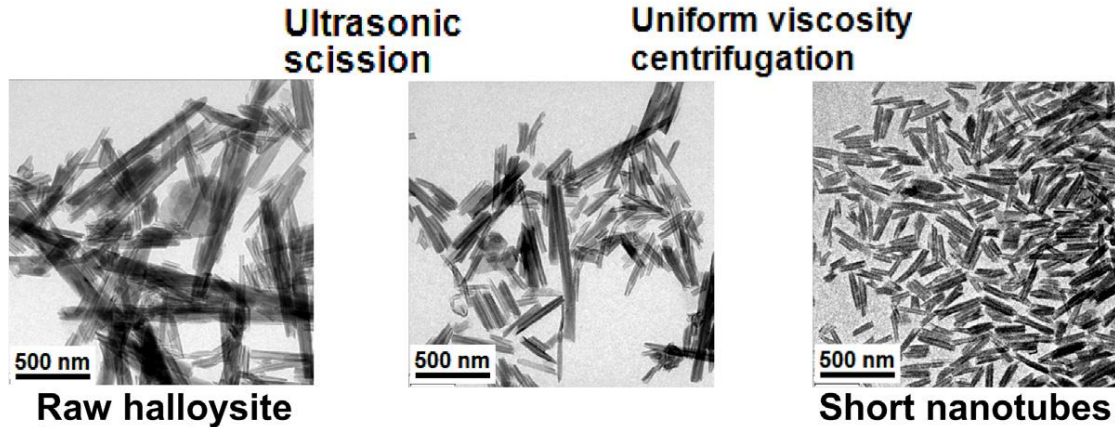


Fig.8. Graphic view of preparation of pure HNTs by ultrasonication and viscosity gradient centrifugation [36].

The results attained by R. Rong *et al.* [36] illustrated the achievement of homogeneous HNTs in length with high yield through ultrasonication and viscosity gradient centrifugation in two steps. The main benefit of this method can be described as its potential to be applied in large scales for the preparation of pure HNTs for industrial applications.

2.1.4 Aim of this work

In order to obtain purified and homogeneous HNTs in size, as a crucial process for the enhanced behavior of these naturally available nanotubes for all their applications, the described method in the previous section was employed with additional parameters. The purification and size separation of pristine HNTs mined in Turkey was investigated by three hierarchical procedures: First, the effect of alkaline treatment on dispersion and deagglomeration of pristine HNTs was studied. Second, ultrasonication was carried out to cut long HNTs to short nanotubes, and break the bundles and huge agglomerates, and finally, three-step viscosity gradient centrifugation was applied to eliminate the existing impurities in the pristine HNT such as kaolinite and other kaolin clay minerals, and to sort HNTs into two distinct uniform fractions based on their size. In addition to the effect of ultrasonication power on the yield of HNT, the effect of the concentration of PVP and CTAB as the chemical

and surfactant of the density gradient media, respectively were investigated. Another new examination was related to usage of pre-alkaline treated HNTs instead of raw HNTs as the input material for the separation process. The objective was to determine the effect of alkaline treatment on the yield as well as the size distribution of the prepared HNTs that were mined in local sources in Turkey.

2.2 Materials and experimental procedures

2.2.1 Materials

Pristine HNT powder was provided by Esan, Eczacıbaşı Industrial Raw Materials company (Istanbul, Turkey) and were dried at 110° C for 12 h to eliminate any residual physically absorbed water content before use. PVP (M_w = 40000, Sigma-Aldrich), CTAB (M = 364.46 g/mol, Sigma-Aldrich) and deionized water were used for the preparation of the viscosity gradient media in the purification of raw HNTs. Ethanol (Sigma-Aldrich), Chloroform (Sigma-Aldrich) and deionized water were the washing solvents for purified HNT. Sodium hydroxide (NaOH, >97%, 2.0 mol/L) was used for the alkaline treatment of HNTs.

2.2.2 Experimental procedures

2.2.2.1 Preparation of PVP solution for HNTs dispersion

For the preparation of the PVP solution, two different concentrations of PVP and CTAB; 1) 3 g PVP and 3.64 g CTAB [36] and 2) 6 g PVP and 7.28 g CTAB- were added separately to 100 ml of deionized water, stirred at 60° C for 15 min and ultrasonicated for 20 min to achieve a complete transparent solution. CTAB acted as surfactant for maximum dispersion of HNT powders in the media.

2.2.2.2 Preparation of purified and size-separated HNTs

Approximately 2 g of pristine HNT was added to 100 ml of PVP solution. The solution was ultrasonicated at 70, 90 and 120 w for 1 h using a probe sonicator. The HNT suspension resulting from ultrasonication was poured into 50 ml centrifuge tubes and then immediately centrifuged at 1170 g for 45 min. The turbid supernatant was collected and centrifuged at 8800 g for 20 min. This procedure was done for one more set at 15557 g for 20 min, until the supernatant became completely transparent. All precipitations were collected and washed multiple times with excessive water, chloroform and ethanol alternately. After washing, they were dried at 110°C for 20 h.

The precipitation obtained from centrifuging at 1170 g, after washing and drying, was considered as raw material and was subjected to the whole purification procedure described above for two more times. This was performed in order to maximize the final yield for purified HNTs. A schematic preview of preparation of purified HNT is given in Fig.9.

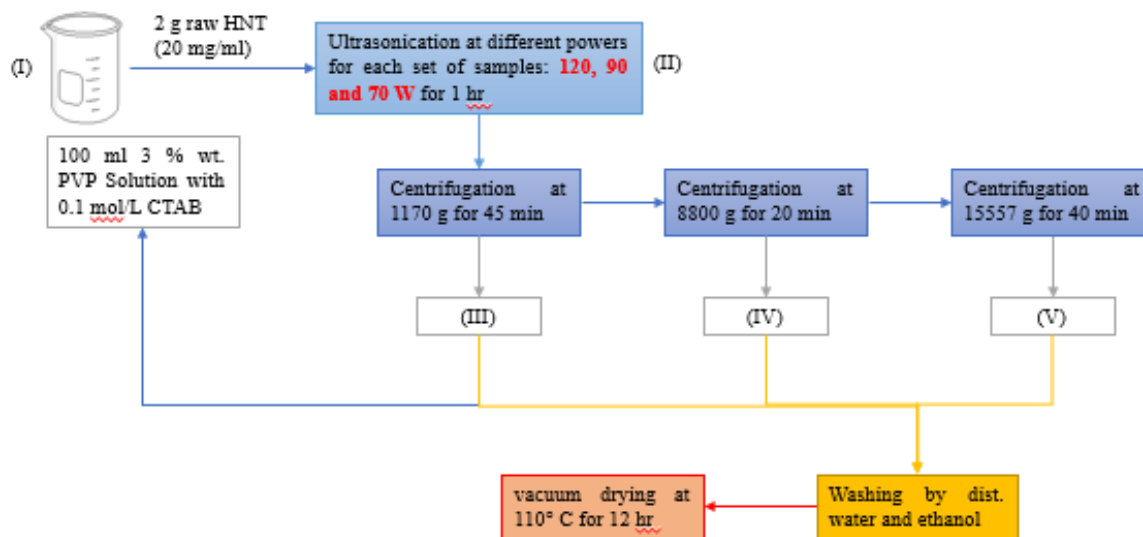


Fig.9. Schematic preview of purification and size separation raw HNT.

2.2.2.3 Preparation of alkaline treated HNTs

The alkaline treatment of HNT samples were performed according to the procedure mentioned elsewhere [64]. Approximately 4 g pristine HNT was added to 40 ml NaOH solution with six different concentrations (0.0005, 0.001, 0.002, 0.02, 0.2 and 1 mol/L) separately. The suspensions were ultrasonicated at 50 °C for 1 h. Then, they were washed with distilled water five times. All samples were collected, and vacuum dried at 110 °C for at least 12 h. A schematic preview of alkaline treatment of HNT is given in Fig.10.

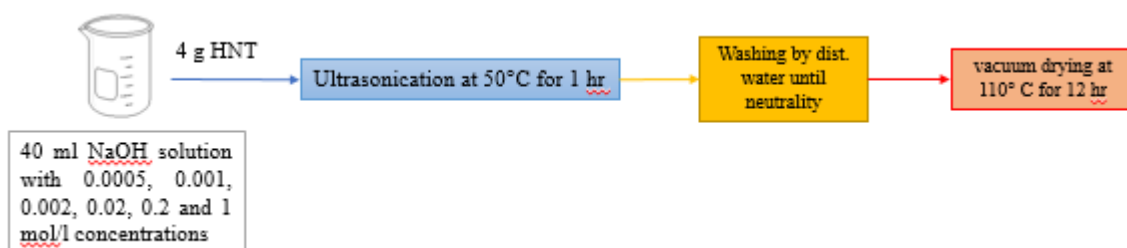


Fig.10. Schematic preview of purification and size separation raw HNT.

2.2.3 Characterization methods

2.2.3.1 Size distribution analysis

Determination of the hydrodynamic diameter of raw and purified HNT samples was investigated by the dynamic light scattering (DLS) instrument (Zetasizer Nano - ZS, Malvern Instruments Ltd., UK) at 25 °C. In addition, size distribution of HNTs before and after purification was calculated by Gemini 35 VP Field Emission Scanning Electron Microscope (FE-SEM).

2.2.3.2 Morphological analysis

The morphology of raw and purified HNTs were studied using Gemini 35 VP FE-SEM.

2.2.3.3 Structural and phase purity analysis

Examination of phase purity for pristine and purified HNTs was done by X-ray diffraction patterns (XRD) using a Bruker D2 Phaser XRD (Desktop) instrument.

2.2.3.4 Chemical analysis

Fourier Transform Infrared (FTIR) spectroscopy was used for the chemical analysis of raw, alkaline treated and purified HNT samples.

2.2.3.5 Thermal analysis

Thermal behavior of all samples was studied by TGA using a Netzsch STA 449 C Jupiter instrument at 10 °C/min, which is a simultaneous thermal analyzer and is capable of measuring the data with 0.1 °C sensitivity.

2.3 Results and discussion

2.3.1 Characteristics of raw and purified HNTs

As shown in Fig.11, color density of the HNT suspension did not change after sonication treatment in 3% wt. PVP solution containing 0.1 mol/L CTAB. However, the turbidity of supernatants after each centrifugation step gradually decreased until complete transparency was achieved.

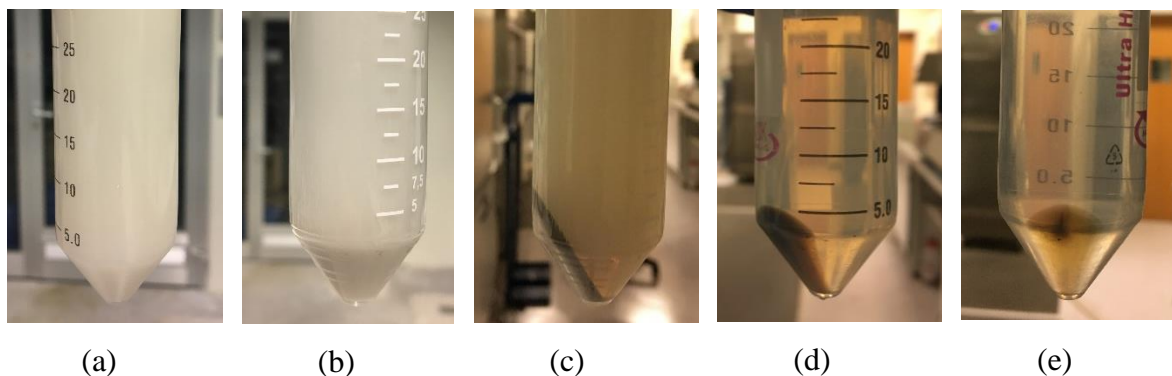


Fig.11. Photographs of HNT suspensions in PVP solution (a) pristine HNTs; (b) sonicated HNTs at 120 w for 1 hr; (c) HNTs after sonication and centrifugation at 1170 g; (d) HNTs after sonication and centrifugation at 8800 g; (e) HNTs after sonication and centrifugation at 15557g.

Measured DLS results (Fig.12) illustrated a broad size range for raw HNTs from < 100 nm to $>1 \mu\text{m}$ and bimodal size distribution in this interval. Z-average diameter and polydispersity index (PDI) for pristine HNT were 3478 nm and 0.735, respectively. After sonication, Z-average size and PDI values both decreased to 569.8 nm and 0.650, respectively. This suggests that ultrasonic treatment effected the HNT size distribution by breaking agglomerations and cutting large nanotubes to smaller nanoparticles. After the first level of centrifugation, Z-average diameter further decreased to 342.8 nm with the PDI value of 0.249. In the second centrifugation step, the average hydrodynamic diameter became 302.3 nm and PDI was measured as 0.217. These decreased values indicate that a monodispersity in the HNT suspension was present after purification.

Since the given size distribution data is theoretically based on models conducted for measuring the hydrodynamic diameter of spherical particles, DLS solely could not be considered as a reliable method for an accurate size analysis of nanotubular particles. Hence, FE-SEM technique was employed as an alternative and more precise method to validate the length range of nanotubes as well as existence of other impurities.

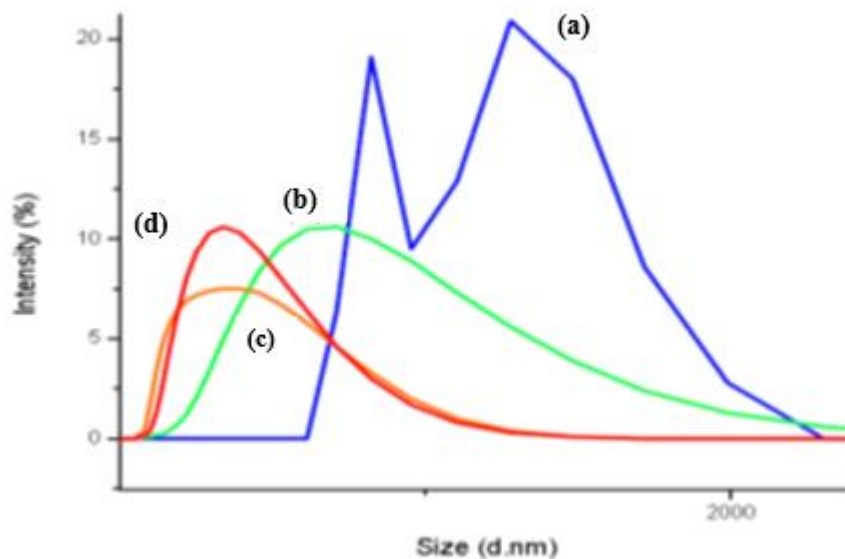


Fig.12. DLS measurement of size distribution for (a) pristine HNTs; (b) sonicated HNTs at 120 w for 1 h; (c) supernatant of HNTs suspension after sonication and centrifugation at 1170 g; (d) supernatant of HNTs suspension after sonication and centrifugation at 8800 g.

FE-SEM images of dried HNTs before and after purification are presented in Fig.13. It can be seen from the images that ultrasonication has considerably broken the bundles of nanotubes; however, impurities such as kaolinite plates and similar other structures still remain within the HNTs content. After the three-step centrifugation process, impurities have been eliminated completely and in the meantime, a highly homogeneous HNTs dispersion was observed in size. A statistical survey of pristine and purified HNTs size distribution by FE-SEM is given in Fig.14. It was observed that while pristine HNTs have a broad range of average length from 150 ± 20 nm to 1103 ± 20 nm (all three colors of blue, orange and red representing different size ranges are present), sonicated HNTs have the same range of lengths as well. Though the majority of sonicated nanotubes population is composed of particles with $202-527 \pm 20$ nm average length, which is smaller than the pristine HNTs. This means that by ultrasonication, HNTs were cut in shorter length, hence a decline in average length size is observed in the FE-SEM images. However, purified HNTs obtained after centrifugation at 8800g involves nanotubes with average length of $157-327 \pm 20$ nm (red and orange bars). Final purified HNTs products from 15557 g includes only tubular

particles with average length size of $126-179 \pm 20$ nm (red bar). These results comprehend that by proceeding through each purification step, along with removing impurities, size distribution for HNT lengths narrows down, and finally two categories of purified HNTs with distinct average length sizes are acquired.

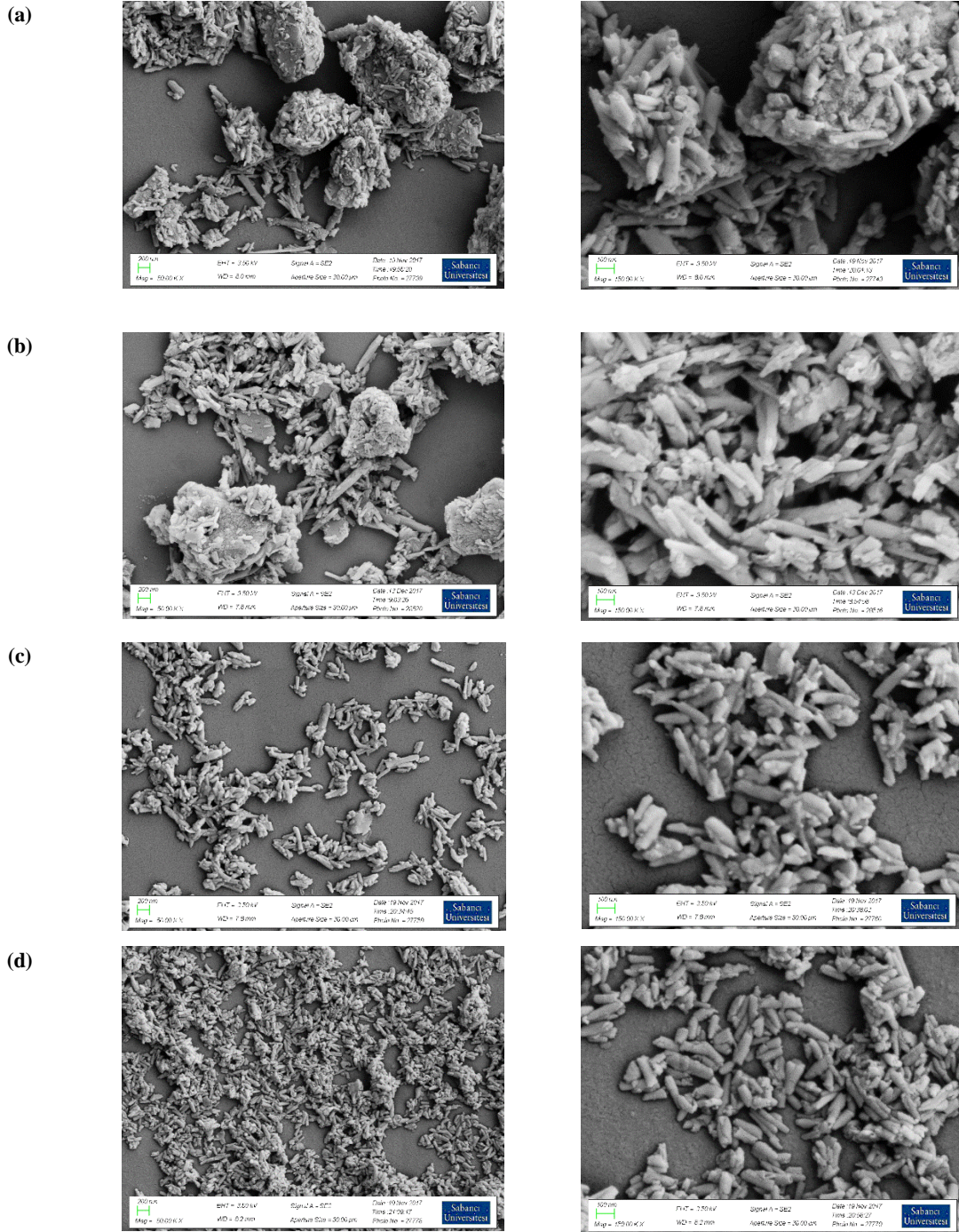


Fig.13. FE-SEM images of (a) pristine HNTs; (b) sonicated HNTs at 120 w for 1 h; (c) Purified HNTs obtained after sonication and centrifugation at 8800 g; (d) Purified HNTs obtained after sonication and centrifugation at 15557 g.

XRD patterns of pristine and purified HNTs are shown in Fig.15. The dominant diffraction peaks referring to the hexagonal structure of halloysite - $\text{Al}_2\text{Si}_2\text{O}_5(\text{OH})_4$ - are present in XRD

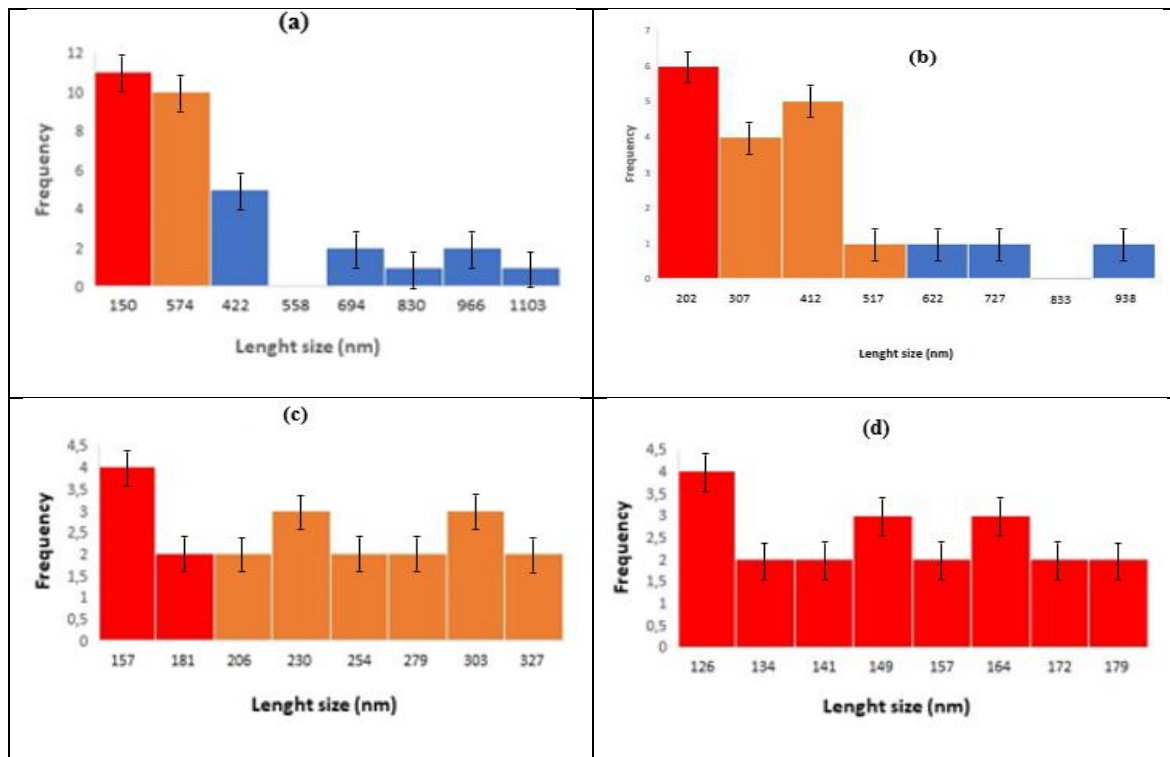


Fig.14. Statistical survey for size distribution by FE-SEM for (a) pristine HNTs; (b) sonicated HNTs at 120 w for 1 h; (c) Purified HNTs obtained after sonication and centrifugation at 8800 g; (d) Purified HNTs obtained after sonication and centrifugation at 15557 g (each bar color indicates the average length size range: Red is for particles <200 nm, orange represents particles 200-600 nm and blue shows particles >600 nm).

pattern of pristine HNTs. Also, most of the other present diffraction peaks indicate the standard dehydrated halloysite- 7\AA , with lattice constants “a” and “b” equal to 5.133 and 7.160, respectively [66]. A sharp peak at 12.1° corresponds to 7.3\AA and is attributed to [001] basal reflections. A second sharp peak at 20.1° attributing to 4.4\AA indicates the tubular structure of halloysite [100] [67]. The third dominant peak at 24.6° belonging to 3.6\AA is responsible for [002] basal reflection. Aside from halloysite peaks, there are several other peaks which belong to other clay minerals such as kaolinite and nacrite or other impurities. For example, present peaks at 18.1° , 29° , 25.6° , 26.6° , 38.5° , 43° , 47° , 50° , 52.4° and 55.3° belong to

kaolinite, nacrite and other impurities. From the XRD pattern of purified HNT, it is obvious that all peaks except the ones contributing to standard halloysite structure have disappeared upon purification. This confirms the elimination of impurities during the purification process.

FTIR was employed to characterize the raw and purified HNTs. As shown in Fig.16, characteristic peaks of halloysite are as follows: 3698 cm^{-1} , 3621 cm^{-1} are indicating the O-H stretching vibrations of Al-OH bond in internal surface and in interface of Al-O

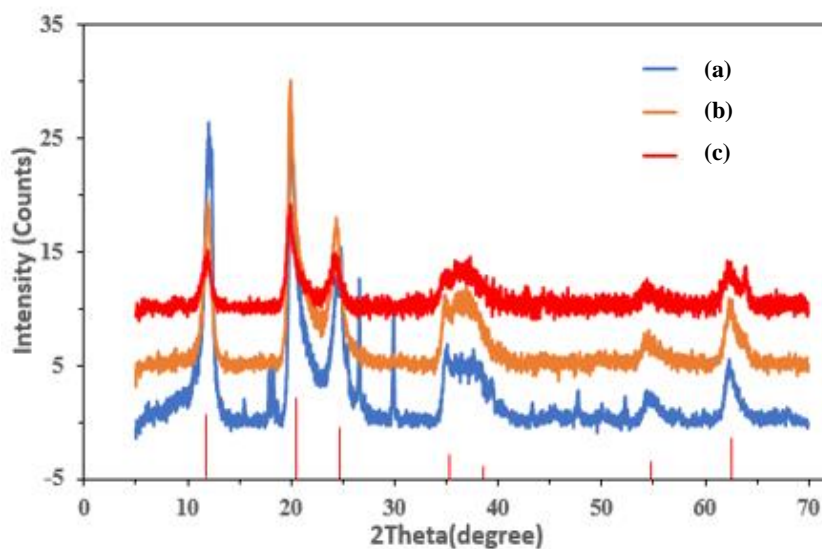


Fig.15. XRD patterns of (a) pristine HNTs; (b) Purified HNTs obtained after sonication at 120 w for 1 h and centrifugation at 8800 g; (c) Purified HNTs obtained after sonication at 120 w for 1 h and centrifugation at 15557 g.

octahedron and Si-O tetrahedron, respectively. 1635 cm^{-1} is attributed to the water deformation vibration. Stretching vibration of apical Si-O and in-plane Si-O are observed at 1114 cm^{-1} , 1089 cm^{-1} and 1031 cm^{-1} , respectively. Peaks at 940 cm^{-1} and 913 cm^{-1} belong to inner-surface O-H deformation and Al-OH deformation of internal surface. Si-O-Si symmetric stretching is shown at 796 cm^{-1} . 754 cm^{-1} is attributed to Si-O-Al perpendicular stretching [36]. By comparing all FTIR spectra shown in Fig.16, it is confirmed that

purification and separation did not alter any characteristic peaks of HNTs, hence this is an effective method for achieving pure nanoparticles.

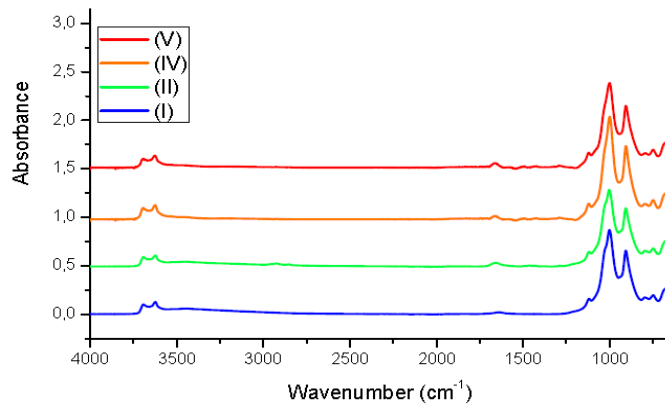


Fig.16. FTIR spectra of (a) pristine HNTs; (b) sonicated HNTs (c) Purified HNTs obtained after sonication at 120 w for 1 h and centrifugation at 8800 g; (d) Purified HNTs obtained after sonication at 120 w for 1 h and centrifugation at 15557 g.

2.3.2 The effect of re-purification on the yield of purified HNTs

As previously mentioned in the experimental section, after all purified samples were washed and dried, the resulting powders from the first step of centrifugation at 1170 g were subjected to the whole purification and separation process again. This re-purification treatment was done twice after the first level. Thus, as it is shown in Fig.17 with the total number of three times purification, the total yield (Y_t) of purified HNTs was successfully increased from 14 % in the primary stage, to 34%, which is higher than previous reports by Rong *et al.* [36]. As it is shown in Fig.17, in the second set of purification process, total yield increased from 14% to 18%, indicating that since HNTs as raw material were formerly subjected to ultrasonication one time, breaking the agglomerations and separating nanotubes were facilitated. However, the increase in the amount of yield compared to the second level of purification is not observed after the third time (16%). This can be explained by the fact that most of the free bundles of HNT were already separated in previous levels.

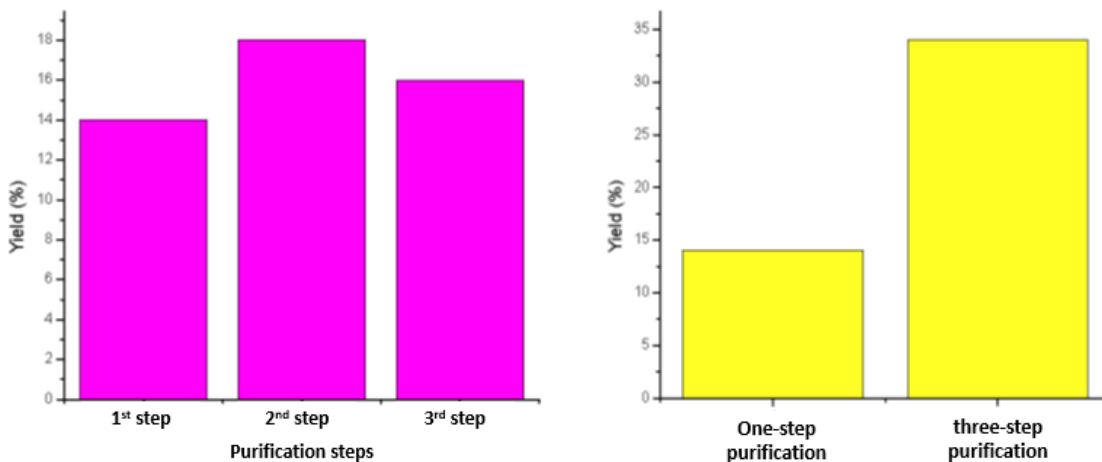
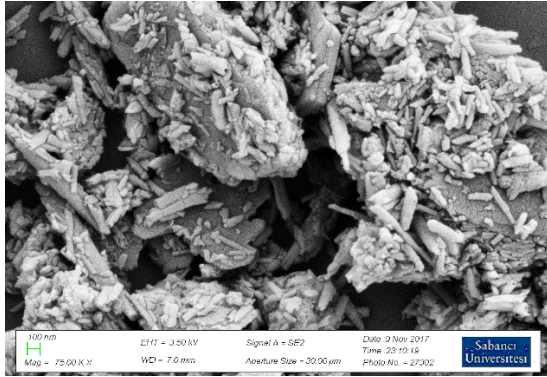


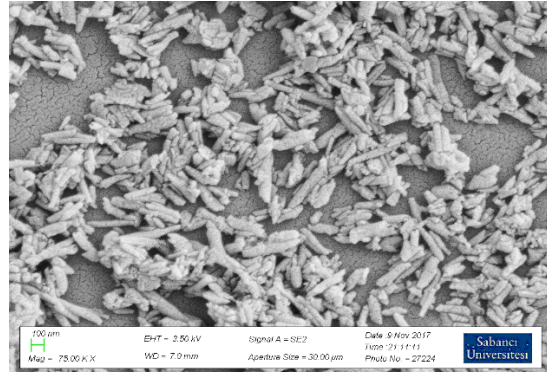
Fig.17. Effect of re-purification on the total yield of purified HNTs.

2.3.3 The effect of Ultrasonic power on the dispersion and size distribution of purified HNTs

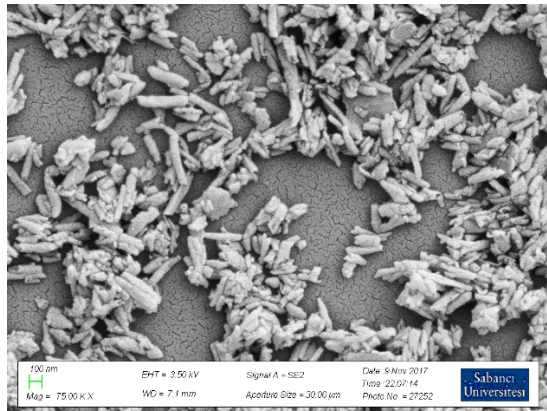
To investigate the effect of ultrasonic power on the dispersion and size distribution of purified HNTs, three different raw HNT samples were subjected to the purification process as described in the experimental section. In the ultrasonication step, samples were treated at 120, 90 and 70 power watts for 1 h, respectively. The FE-SEM images (Fig.18) and the plot showing the average length size of two categories of purified halloysite samples as a function of ultrasonication power (Fig.19) illustrate a dramatic decrease in the average length size of purified HNTs after sonication at 70, 90 and 120 w and centrifuging at 8800 g and 15557 g, separately. While this value for pristine HNT was $\sim 465 \pm 20$ nm, it decreased to $\sim 240 \pm 20$ nm after centrifugation at 8800 g, by increasing the ultrasonication power from 70 to 120 w. Results for samples separated at 15557 g centrifugation show a higher decrease in average length size from $\sim 460 \pm 20$ nm to $\sim 150 \pm 20$ nm, by increasing the ultrasonication power. This falls in line with the prior assumption on the definite effect of the increasing ultrasonic power on narrowing down the size distribution of homogeneous HNT powders.



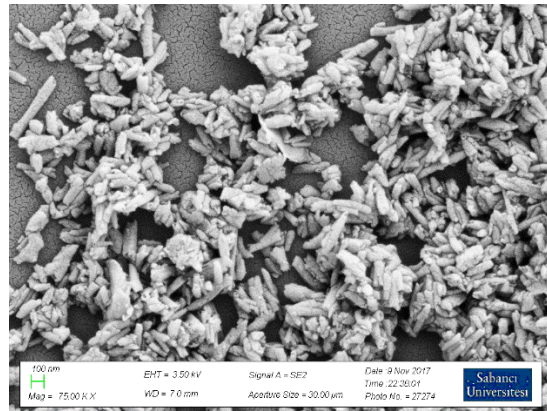
(a)



(b)



(c)



(d)

Fig.18. FE-SEM images of (a) pristine HNTs (b) Purified HNTs obtained after sonication at 70 w for 1 h and centrifugation at 8800 g; (c) Purified HNTs obtained after sonication at 90 w for 1 h and centrifugation at 8800 g; (d) Purified HNTs obtained after sonication at 120 w for 1 h and centrifugation at 8800 g.

All XRD results showing the diffraction patterns for raw HNT and purified HNTs prepared through ultrasonication at 70, 90 and 120 power watts and subsequent three-steps centrifugation (Fig.20), show dominant peaks of halloysite structure (12.1° , 20.1° and 24.6° representing [001], [100] and [002] basal reflection, respectively). The main peaks of halloysite get sharper as the sonication power increases. No impurity peaks

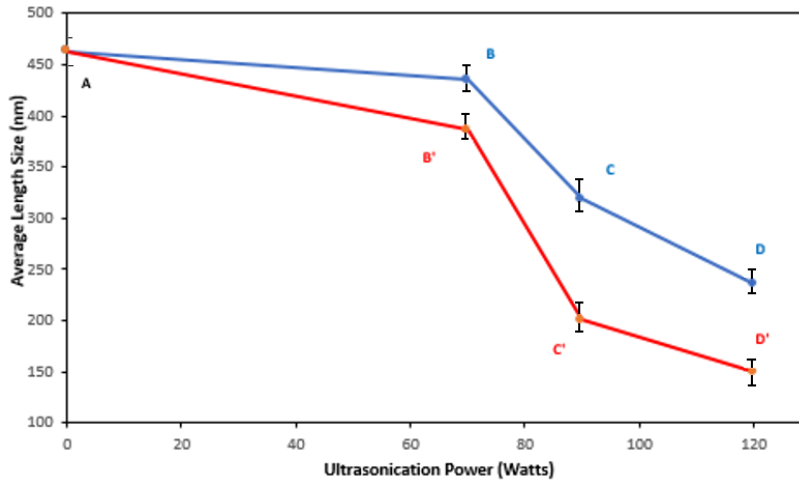


Fig.19. Statistical survey for the effect of ultrasonication power on the dispersion and size distribution of (A) Pristine HNTs (B) Purified HNTs obtained after sonication at 70 w for 1 h and centrifugation at 8800 g; (C) Purified HNTs obtained after sonication at 90 w for 1 h and centrifugation at 8800 g; (D) Purified HNTs obtained after sonication at 120 w for 1 h and centrifugation at 8800 g. (B'), (C') and (D') are the same as (B), (C) and (D) with 15557 g centrifugation force.

were present at 18.1°, 29°, 25.6°, 26.6°, 38.5°, 43°, 47°, 50°, 52.4° and 55.3° (belonging to kaolinite, nacrite and other impurities) in the XRD pattern of purified samples, which suggests that sonication followed by centrifugation at all three different powers were successful in removing components other than halloysite from the purified product. However, by comparing the patterns shown in Fig.20, it is observed that the absence of impurity peaks around 48 -51° in the samples prepared by 120 w ultrasonication power is more evident than those prepared by 90 w and 70 w ultrasonication power. This confirms the direct impact of sonication power on achieving a higher purity level in the final product. Similar results were obtained in the work done by Rong et al. [36]. Furthermore, samples prepared from 90 and 120 w had 34% final yield, which was higher than that obtained from 70 w (30%).

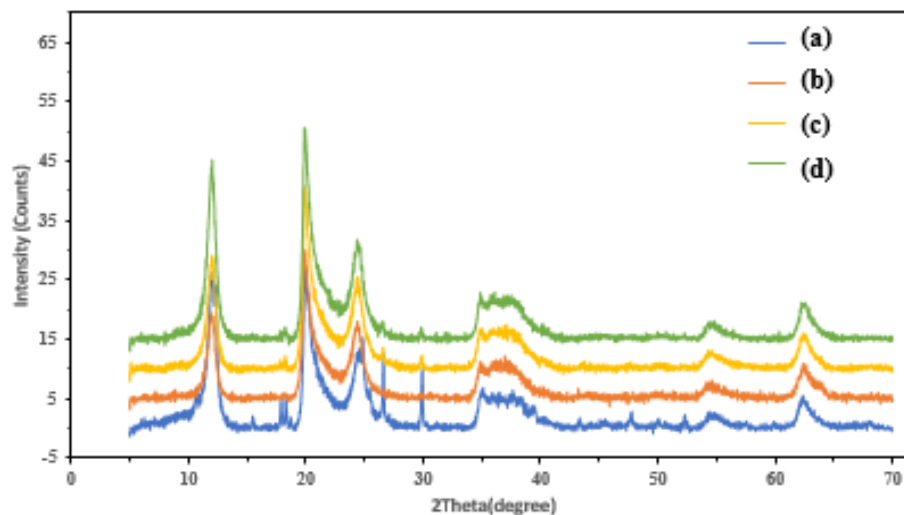


Fig.20. XRD patterns of (a) pristine HNTs (b) Purified HNTs obtained after sonication at 70 w for 1 h and centrifugation at 8800 g; (c) Purified HNTs obtained after sonication at 90 w for 1 h and centrifugation at 8800 g; (d) Purified HNTs obtained after sonication at 120 w for 1 h and centrifugation at 8800 g.

2.3.4 The effect of PVP concentration on the dispersion and size distribution of purified HNTs

In order to study the PVP concentration effect on the dispersion and size distribution of purified HNTs, two different PVP (3% wt. and 6% wt.) and CTAB (0.1 mol/L and 0.2 mol/L) concentrations were chosen. Raw HNTs were added to the solutions and subjected to the purification process as described in the experimental section. Measured DLS results (Fig.21) illustrated a broad size range for raw HNT-from < 100 nm to >1 μ m- and two main very sharp peaks in this interval. As it was shown earlier, Z-average diameter and polydispersity index (PDI) for pristine HNTs were 3478 nm and 0.735, respectively. Sonication in the 6% wt. PVP solution decreased the Z-average and PDI to 368.4 and 0.330, respectively. These values are considerably smaller than those measured in the 3% wt. PVP solution (Z-average size:569.8 nm and PDI: 0.650). This suggests that by increasing the concentration of PVP, HNT particles were better dispersed within the aqueous media, since ultrasonic treatment

was more effective in breaking agglomerations and cutting large nanotubes. After the first level of centrifugation, Z-average diameter of samples in 6% wt. PVP solution further decreased to 276.5 with the PDI value of 0.265, which are smaller than 342.8 nm and 0.249, respectively, obtained in 3% wt. PVP media. In the second centrifugation step, the average hydrodynamic diameter decreased from 302.3 nm to 273.3 nm by changing the solution concentration from 3% wt. to 6% wt. PDI values also dropped from 0.217 to 0.175. According to Fig.21, it can be seen the size distributions in 6% wt. PVP solution have sharper peaks in each step of purification, compared to those in 3% wt. PVP solution. Decreased values in Z-average size and PDI values indicate that using 6% wt. PVP solution was more effective than 3% wt. solution in achieving monodisperse HNT suspensions.

FE-SEM images (Fig.22) also show that dried and sonicated HNTs in 6% wt. PVP media have higher level of dispersion than those sonicated in 3% wt. PVP solution. This can be due to the increased number of particles suspended in the media during ultrasonication and thus breaking and cutting nanotubes in the raw material more efficiently. From the SEM images, it can be realized that PVP and the surfactant facilitate a better dispersion and distribution of raw HNT material.

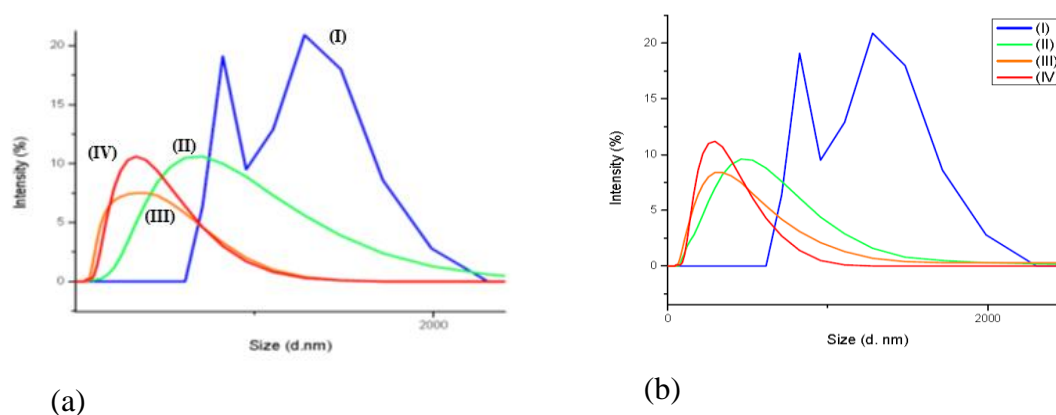
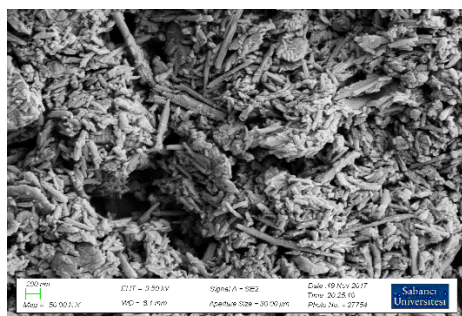
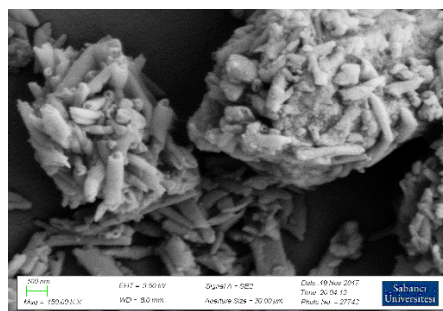


Fig.21. DLS measurement of Size distribution for HNT suspensions in (a) 3% wt. PVP-0.1 mol/L CTAB solution; (b) 6% wt. PVP-0.2 mol/L CTAB solution ((I) pristine HNTs; (II) sonicated HNT at 120 w for 1 h; (III) supernatant of HNTs suspension after sonication and centrifugation at 1170 g; (IV) supernatant of HNTs suspension after sonication and centrifugation at 8800 g).

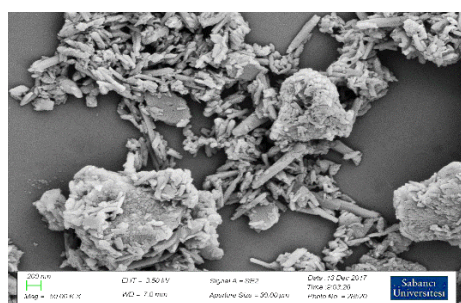
FE-SEM images (Fig.23) show both categories for purified HNTs in 3% wt. and 6% wt. PVP media. It is evident that purified HNTs prepared by 6% wt. PVP have higher level of dispersion than those prepared by 3% wt. PVP solution. This can be an indication of the increased number of particles suspended in the media during ultrasonication and thus breaking and cutting nanotubes in the raw material more efficiently and helping the size separation step. After the sonication, impurities such as kaolinite still remain along with nanotubes, but these nanotubes have shorter length in 6% PVP media than those in 3% PVP media. Also, more individual tubes are observed by increasing the PVP and surfactant concentration. It is clear that PVP and CTAB played an important role in providing a sufficient viscosity gradient media for HNT samples. They allowed particles separated from agglomerates during ultrasonication preserve their separated positions suspended within the solution. After the centrifugation, as it is shown in the FE-SEM images (Fig.23 and Fig.24), the mentioned impurities were removed from the samples and what remains behind is individual halloysite nanotubes with longer length (precipitation from 8800g) or shorter length (precipitation from 15557 g) depending on the centrifugal force. The observation of individual nanoparticles after purification is more apparent in samples obtained from 6% wt. PVP than those obtained from 3% wt. This result again confirms the impact of PVP and surfactant on better HNT dispersion. Hence a better separation of impurities, agglomerates, long and short nanotubes was the result of this parameter in media.



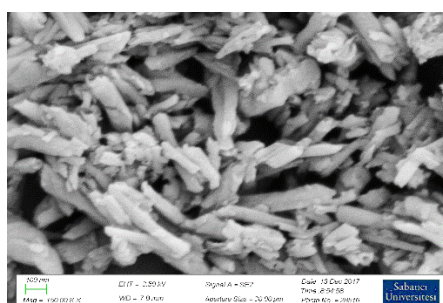
(a)



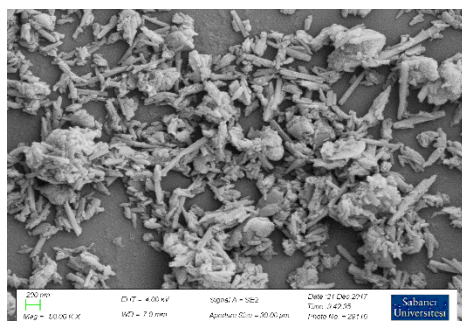
(a)



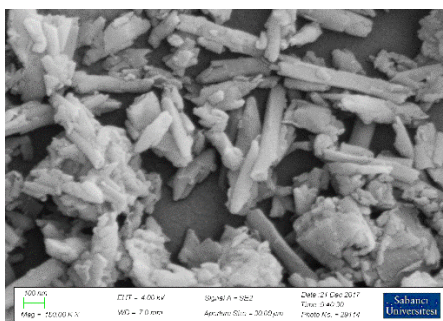
(b)



(b)



(c)

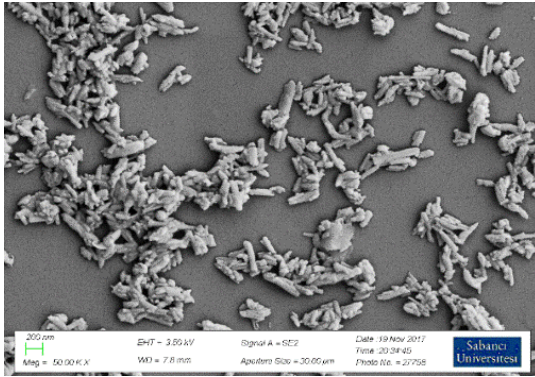


(c)

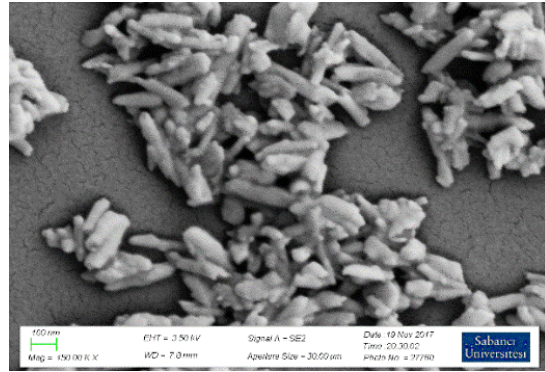
Fig.22. FE-SEM images of (a) pristine HNTs (b) sonicated HNTs in 3% wt. PVP-0.1 mol/L CTAB solution at 120 w for 1 h; (c) sonicated HNTs in 6% wt. PVP-0.1 mol/L CTAB solution at 120 w for 1 h.

As a statistical survey for the effect of PVP concentration on the dispersion and size distribution of purified HNT, we draw the average length size of HNTs as a function of PVP concentration (Fig.25). Pristine HNTs has an average length size of 460 ± 20 nm. This value dramatically drops down to 236.3 ± 20 nm after purification in 3% wt. PVP solution.

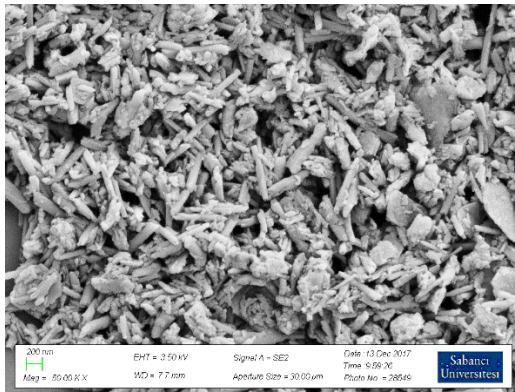
However, purified HNTs in 6% wt. PVP media, showed average length size of 178.2 ± 20 nm, which is smaller than that in 3% wt. PVP. This analysis illustrates that amount of PVP directly affects the purification of pristine HNTs and determines final HNT lengths.



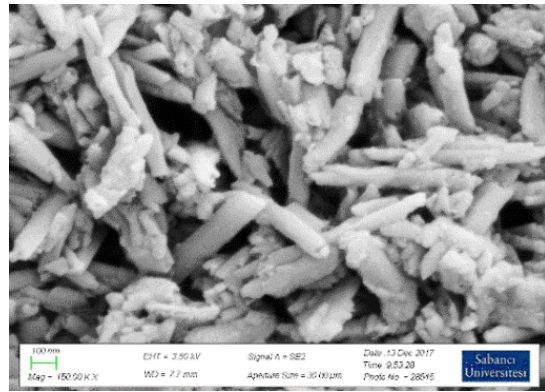
(a)



(a)



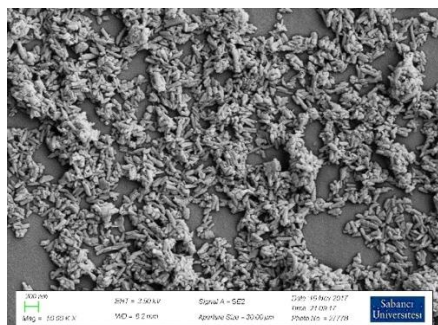
(b)



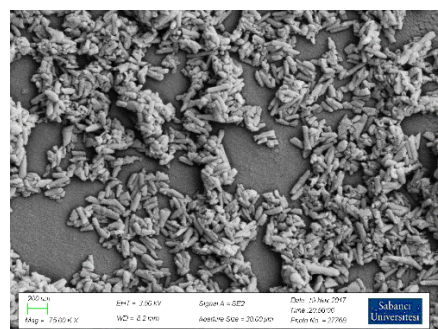
(b)

Fig.23. FE-SEM images of (a) Purified HNTs obtained from 3% wt. PVP solution, after sonication at 120 w for 1 h and centrifugation at 8800 g; (b) Purified HNTs obtained from 6% wt. PVP solution, after sonication at 120 w for 1 h and centrifugation at 8800 g.

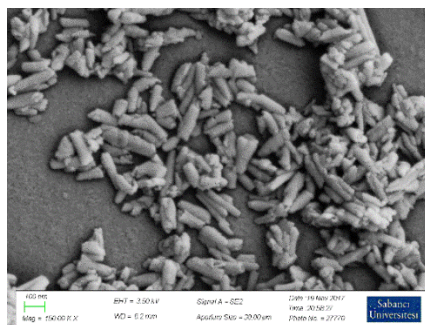
(a)



(b)



(a)



(b)

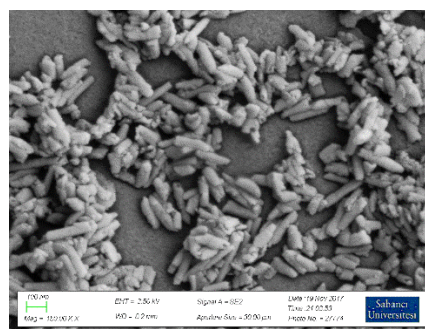


Fig.24. FE-SEM images of (a) Purified HNTs obtained from 3% wt. PVP solution, after sonication at 120 w for 1 h and centrifugation at 15557 g; (b) Purified HNTs obtained from 6% wt. PVP solution, after sonication at 120 w for 1 h and centrifugation at 15557g.

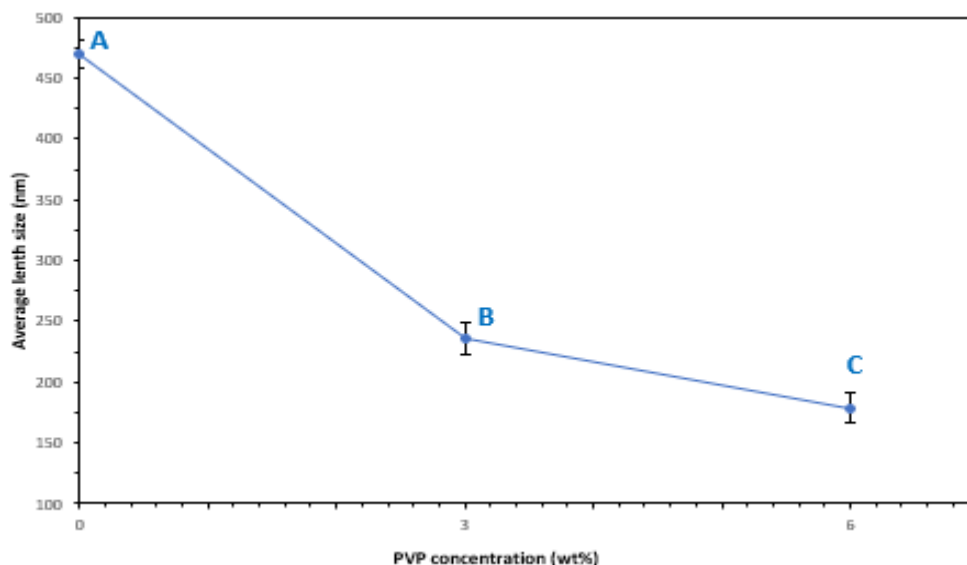


Fig.25. Statistical survey for the effect of PVP concentration on the dispersion and size distribution of (A) Pristine HNTs (B) Purified HNTs obtained from 3% wt. PVP solution, after sonication at 120 w for 1 h and centrifugation at 8800 g; (C) Purified HNT obtained from 6% wt. PVP solution, after sonication at 90 w for 1 hr and centrifugation at 8800 g.

XRD patterns (Fig.26) of both purified HNTs with 3% wt. PVP 6% wt. PVP show the elimination of peaks coming from impurities (18.1°, 29°, 25.6°, 26.6°, 38.5°, 43°, 47°, 50°, 52.4° and 55.3° belonging to kaolinite, nacrite and other impurities) in the raw material, and sharpening of the peaks reflecting the halloysite structure (12.1°, 20.1° and 24.6° attributed to [001], [100] and [002] basal reflection, respectively). Besides, no new peak is emerging after increasing the PVP concentration, confirming the sufficient removal of PVP during the washing of precipitations from each centrifugation step. For a solid investigation of PVP removal from the sample at the end of purification process, FTIR spectra were taken for both purified samples. Since the removal of PVP by general washing procedures can be challenging, FTIR spectroscopy was carried out as an extra characterization method compared to the previous work done by Rong *et al.* [36].

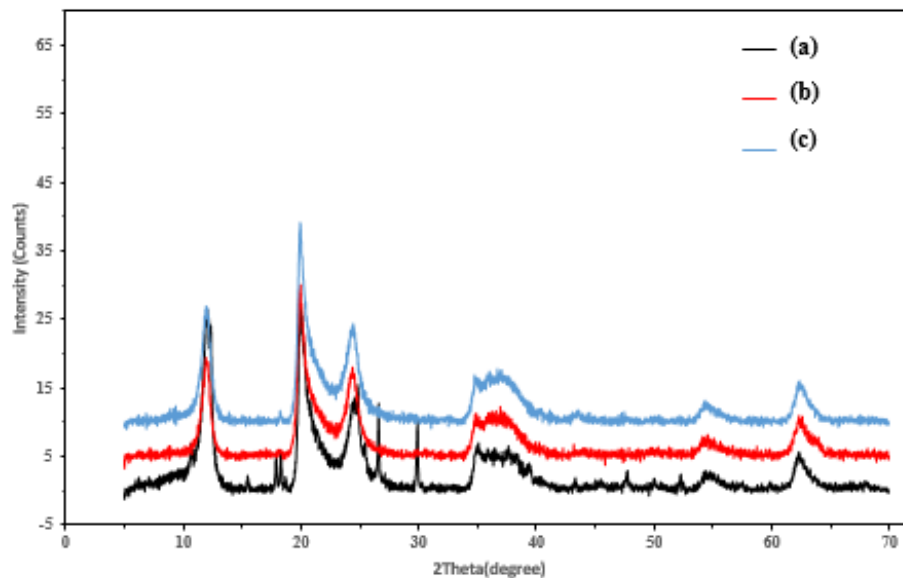


Fig.26. XRD patterns of (a)Pristine HNTs (b) purified HNTs obtained from 3% wt. PVP solution, after sonication at 120 w for 1 h and centrifugation at 8800 g; (c) Purified HNTs obtained from 6% wt. PVP solution, after sonication at 120 w for 1 h and centrifugation at 8800 g.

FTIR spectra (Fig.27) of purified samples prepared from 3% and 6% wt. PVP solution show all main peaks contributed to the standard halloysite structure. Peaks at 3698 cm^{-1} , 3621 cm^{-1} presented in all three diffraction patterns, are contributed to the O–H stretching vibrations of Al–OH bond in internal surface and in interface of Al–O octahedron and Si–O tetrahedron, respectively. The peak at 1635 cm^{-1} coming from water deformation vibration, peaks at 1114 cm^{-1} , 1089 cm^{-1} and 1031 cm^{-1} attributing to stretching vibration of apical Si–O and in-plane Si–O, respectively, are also present in both purified samples as well as the raw material. Besides, other peaks confirming the inner-surface O–H deformation (940 cm^{-1}), Al–OH deformation of internal surface (913 cm^{-1}), Si–O–Si symmetric stretching (796 cm^{-1}), and Si–O–Al perpendicular stretching (754 cm^{-1}), can be observed before and after purification. This means that purification and size separation process did not change the chemical bonding of halloysite nanotubes. However, a new peak around at 1664 cm^{-1} has appeared after purification. This can be attributed to C=O stretching vibrations belonging to the carbonyl group within the PVP structure. The existence of this peak and another small

peak around 2810 cm^{-1} , reflecting aliphatic CH_3 vibrations, means that by increasing the PVP concentration in the solution media, washing them away from the HNT content becomes more difficult. Hence, they still remain on the surface of HNT. This problem can be solved by simply adding more steps to the washing procedure with alternative solvents, to make sure no PVP remains after drying.

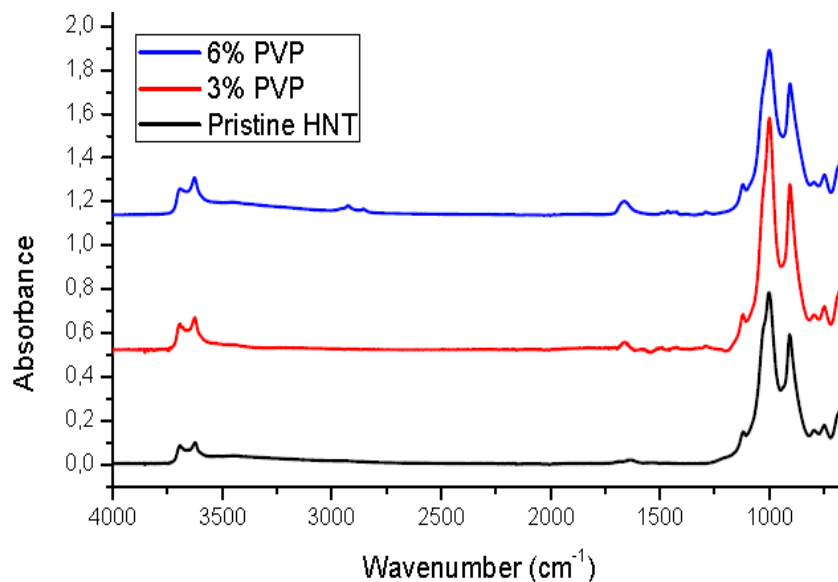


Fig.27. FT-IR spectra of (a)Pristine HNTs (b) purified HNTs obtained from 3% wt. PVP solution, after sonication at 120 w for 1 h and centrifugation at 8800 g; (c) Purified HNTs obtained from 6% wt. PVP solution, after sonication at 120 w for 1 h and centrifugation at 8800 g.

2.3.5 The effect of alkaline treatment on the dispersion and agglomeration of pristine HNTs

The effect of NaOH treatment on the morphology of raw HNT is shown in Fig.28. Raw HNTs are composed of large amounts of agglomerates and other impurities. As it is shown in Fig.29, the average length size and external diameter of raw HNT are $470 \pm 20\text{ nm}$ and $60.2 \pm 8\text{ nm}$, respectively. After treating the nanotubes with alkaline solution, from HNT

treatment with 0.0005 mol/L NaOH to 1.0 mol/L NaOH, degree of agglomeration of the nanotubes decreases systematically, which is an indication of the effectiveness NaOH in dispersing HNT to achieve a more homogeneous suspension.

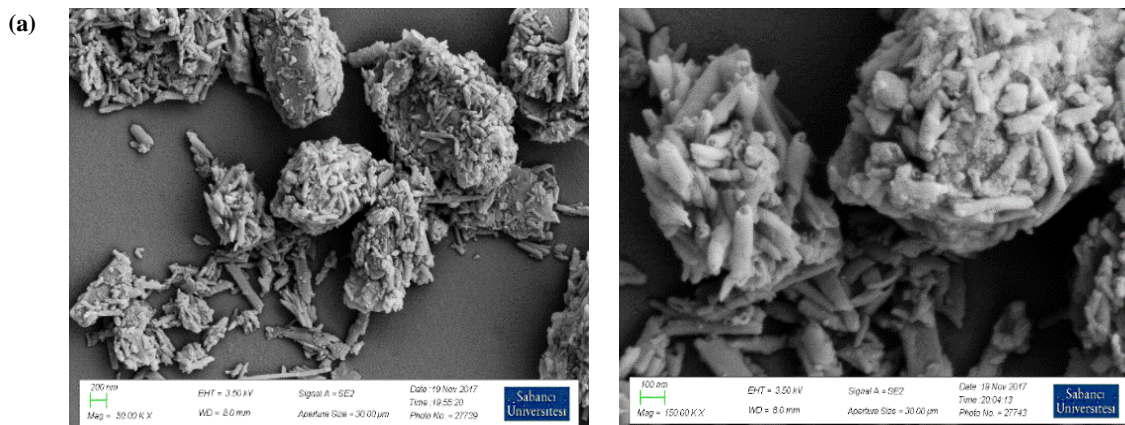
pH values of each of the prepared NaOH solutions was measured and Table 2 shows measured pH values for each suspension sample. pH values differ from 8.48 to 13.96 with increasing NaOH concentration from 0.0005 to 1.0 mol/L. FE-SEM images show that HNTs treated by 0.0005 mol/L NaOH solution still contain some agglomerations, whereas for example, for HNTs treated by 0.02 mol/L NaOH solution, there are no HNT bundles are present, and nanotubes are still packed together to a certain extent. This trend continues by increasing the NaOH concentration in the suspension until after treating HNTs by 1.0 mol/L NaOH solution, we observe no HNT agglomerates, bundles or densely packed nanotubes. According to Joo *et al.* [61], this phenomenon is due to the van der Waals interactions between individual HNTs. At pH = 13.96, the HNT dispersion was at the highest level among the other tested HNTs, and pH = 8.48 had the lowest level of dispersion. In basic environments, HNTs became well dispersed, the end of each HNT got separated from other nanotubes (this is called HNT inner pore opening by Joo *et al.* [63]). This effect of alkaline treatment on the external charge of HNT surface was also investigated by Bretti *et al.* [65], suggesting the dominance of the outer surface charge by increasing the pH.

Table 2. pH values of the prepared alkaline suspensions for pristine HNT treatment.

NaOH concentration in alkaline treated-HNT suspension (mol/l)	pH value
0	7.04
0.0005	8.48
0.001	9.88
0.002	10.17
0.02	11.25
0.2	12.26
1	13.96

On the other hand, FE-SEM images also show that by increasing the NaOH concentration, although the degree of dispersion grows and agglomerates are disappeared more efficiently, some nanosheets and nanoparticles appear outside the nanotubular structures (Fig.28-g). This can be originated from the semi-damaged nanotubes effected by the high pH value. These semi-damaged nanotubes are appearing after NaOH has a concentration of 0.2 mol/L and above, which makes the concentrations below this value suitable for facilitating the agglomerate breaking of halloysite nanotubes without any damage on the tubular structure. Similar morphological results were reported by White *et al.* [60] and Wang *et al.* [64] after pH treatment of HNTs by 1.0 mol/L and 4.0 mol/L NaOH solutions, respectively.

A statistical survey by FE-SEM for the effect of alkaline treatment on the average length size and external diameter of HNTs was conducted. As shown in Fig.29. From Fig.29, it can be observed that by increasing the NaOH concentration from 0.0005 to 0.02 and finally 1.0 mol/L, average length size of HNT narrows down from 470 ± 20 nm (in neutral solution) to 455.9 ± 20 nm and finally 422.6 ± 20 nm, respectively. This fall is in line with our earlier explanation about how alkaline treatment can influence the dispersion of HNT and thus, separating small and large nanotubes from each other. Less number of small nanotubes were obscured by bigger particles. This is the reason that more population of small tubes are observed in FE-SEM images.



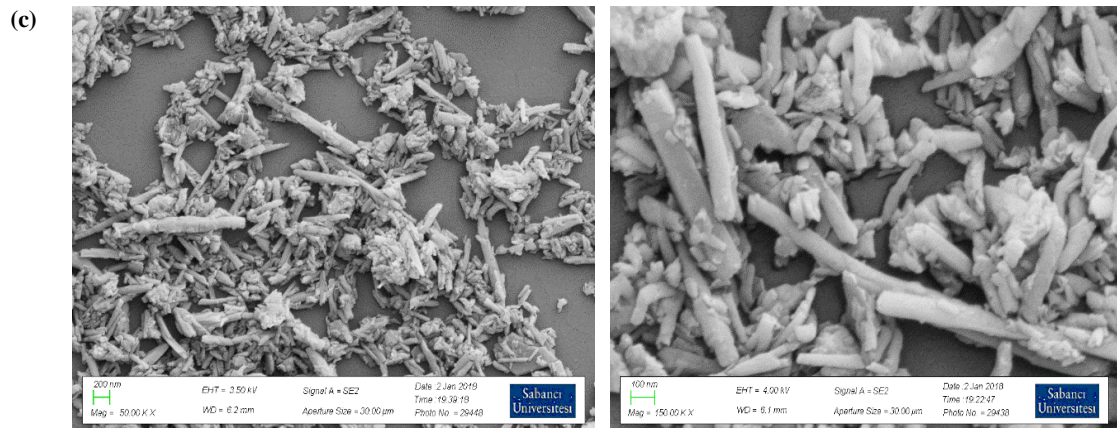
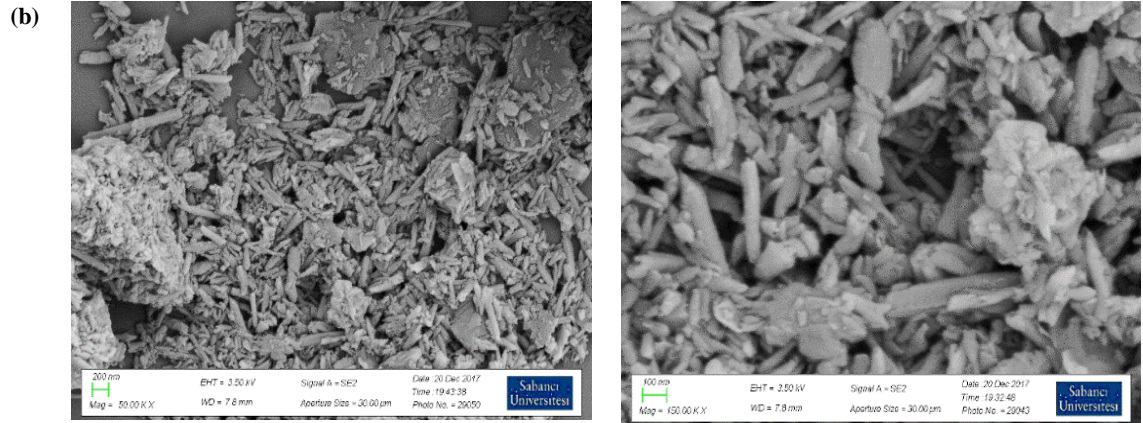


Fig.28. FE-SEM images of (a) pristine HNT (b)alkaline treated HNTs with NaOH (0.0005 mol/L) (c) alkaline treated HNTs with NaOH (0.001 mol/L).



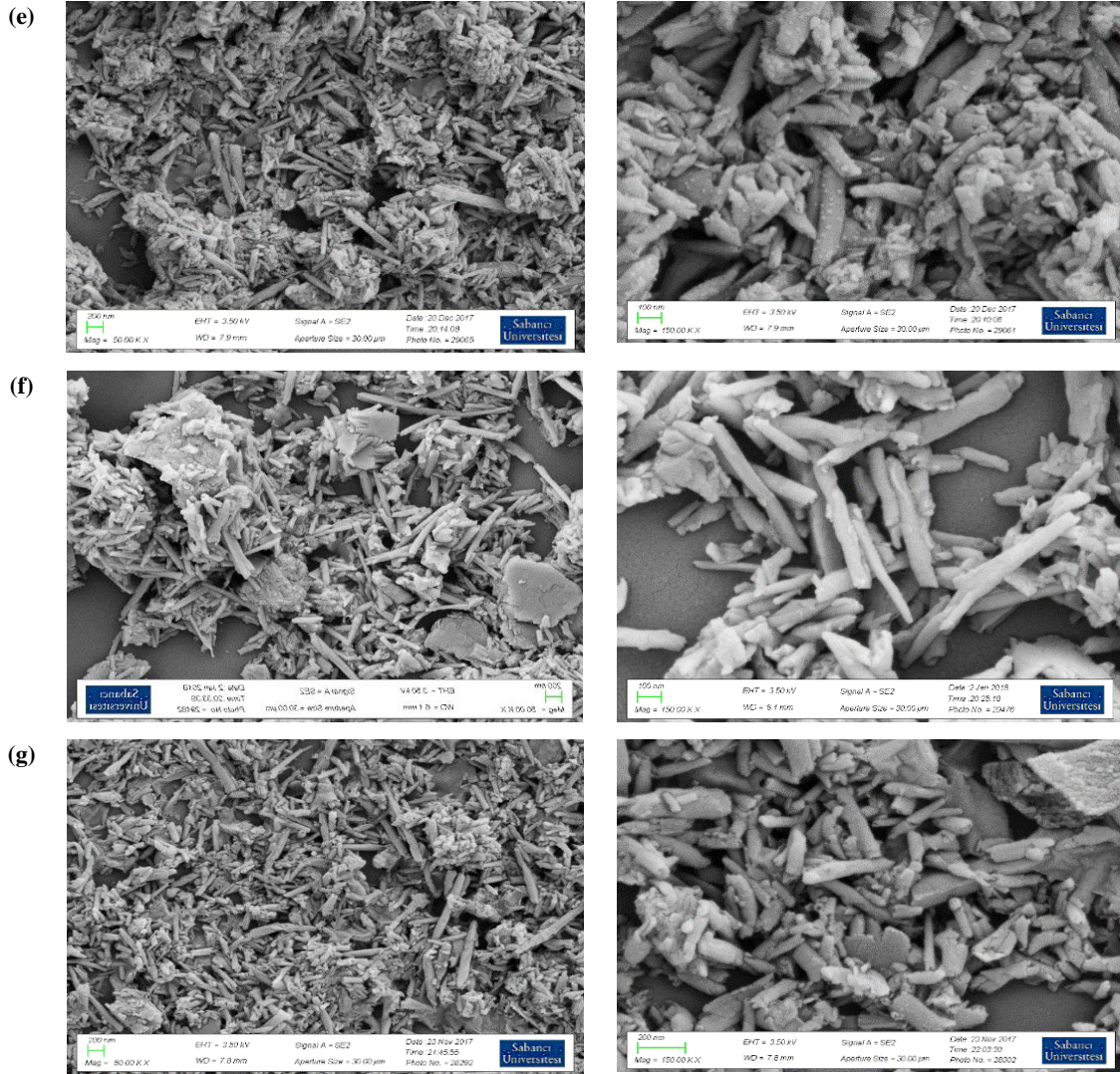


Fig.28. (Continued) FE-SEM images of (d) alkaline treated HNTs with NaOH (0.002 mol/L) (e) alkaline treated HNTs with NaOH (0.02 mol/L) (f) alkaline treated HNTs with NaOH (0.2 mol/L) (g) alkaline treated HNT with NaOH (1.0 mol/L).

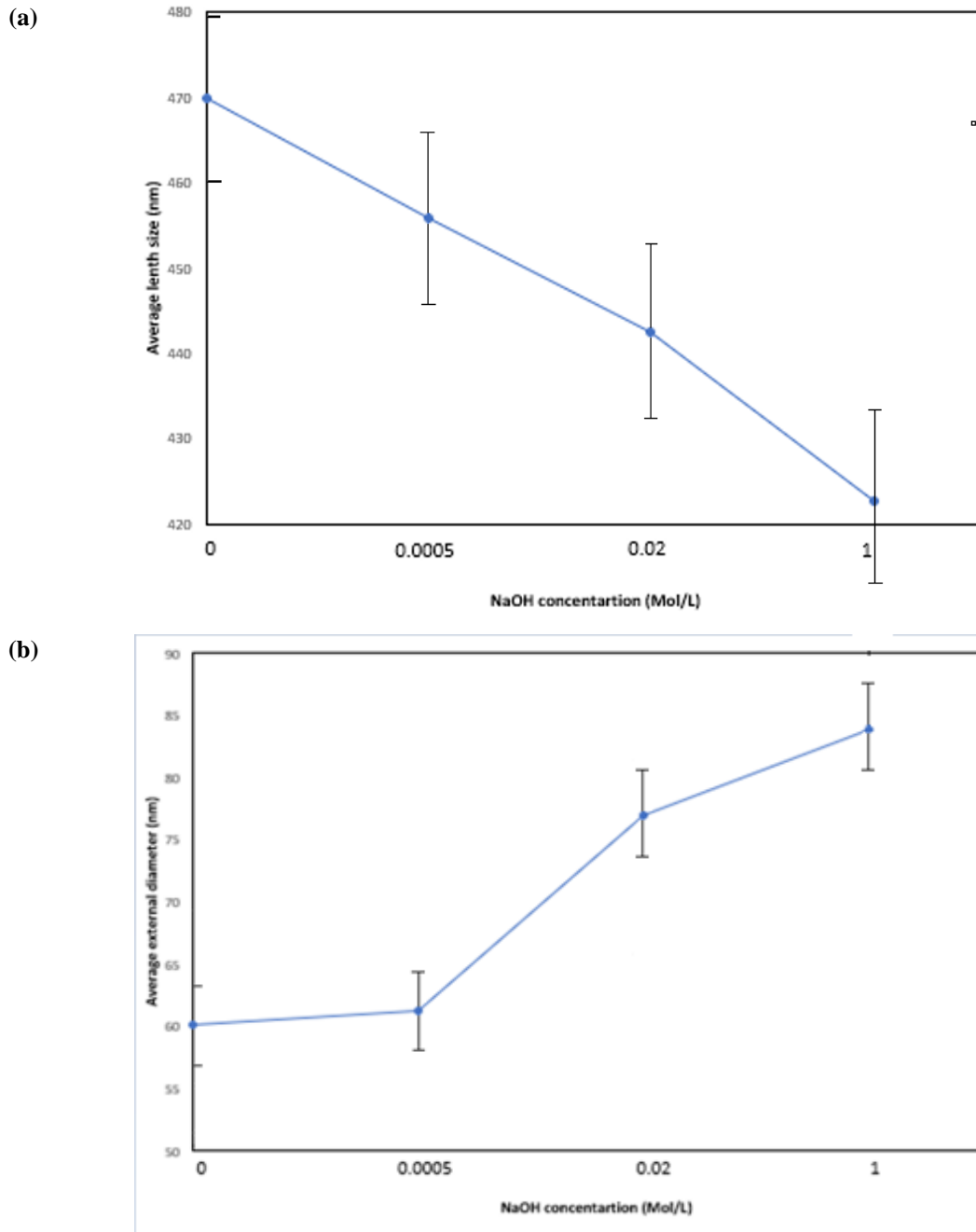


Fig.29. Statistical survey by FE-SEM for the effect of alkaline treatment on the dispersion and agglomeration of pristine HNTs: (a) average length size of HNTs before and after treatment with 0.0005, 0.02 and 1.0 mol/L NaOH solution (b) average external diameter of HNTs before and after treatment with 0.0005, 0.02 and 1.0 mol/L NaOH solution.

In Fig.29-b the effect of NaOH concentration on the average external diameter of HNT is illustrated. By increasing the pH from neutrality to 13.96 (NaOH concentrations rising from 0 to 1 mol/l), the average diameter is increased from 60.2 ± 8 nm to 61.27 ± 8 , 76.99 ± 8 and finally 83.92 ± 8 nm with 0.0005, 0.02 and 1 mol/l NaOH treatment, respectively. This confirms previous studies [61-65, 68] suggesting the influence of basic environment on enlarging the lumen space and expanding the nanotubes diameters.

XRD patterns of raw and alkaline treated HNTs are presented in Fig.30. Raw halloysite indicates a sharp peak attributed to halloysite-(7 °Å) at 12.1° ($d = 7.35$ °Å). Dehydrated state is affirmed by the peaks at 24.6° ($d = 3.58$ °Å) and 20.33° ($d = 4.37$ °Å), which show the [002] and the [020] / [110] basal reflections, respectively. Quartz (SiO₂) and alunite (KAl₃(SO₄)₂(OH)₆) characteristic peaks are also present at $d = 3.34$ °Å and $d = 2.98$ °Å, respectively. Alkaline treatment by NaOH solutions of all concentrations has not altered the HNTs characteristic diffraction peaks. As it was reported by Wang et al. [64], the disposition of HNTs characteristic diffraction peaks happens when NaOH concentration is above 4.0 mol/L. Since, the maximum concentration used for NaOH solution in this work is 1.0 mol/L, no such changes in HNT structure is observed after alkaline treatment with NaOH solution. XRD analysis of treated samples shows no changes in the characteristic peaks of HNT before and after treatment with NaOH solution, even with 1.0 mol/L concentration. This was previously confirmed by White et al. [60]. However, peaks at 47.01° and 53.4° arising from impurities in natural halloysite gradually disappeared by increasing the NaOH concentration of the alkaline solution. The complete disappearance of these two peaks is illustrated in the diffraction pattern of HNT treated by 1.0 mol/L NaOH solution, suggesting the slight removal of some impurities from the system. The results indicate stability in the halloysite crystal structure after alkaline treatment with 0.0005 to 1.0 mol/L NaOH concentration, as well as removal of some minor impurities from the natural HNTs.

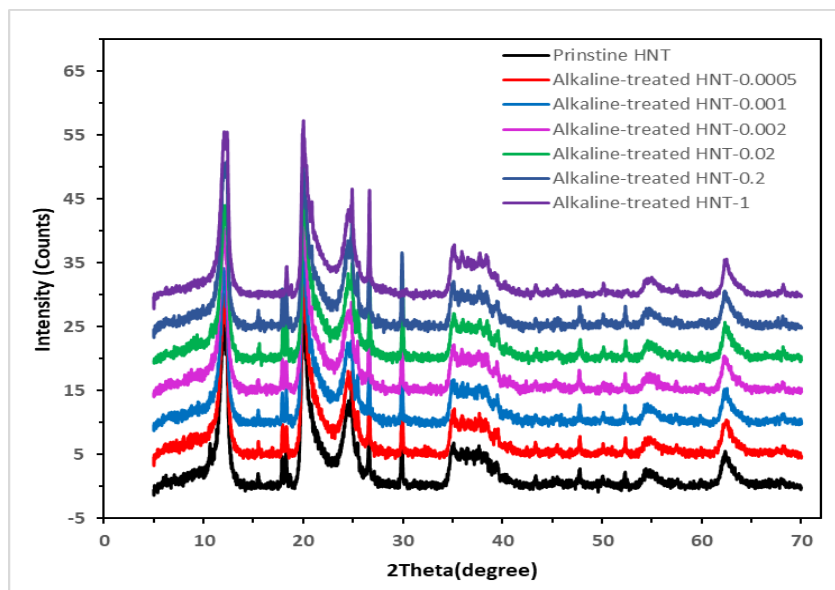


Fig.30. XRD patterns of pristine and alkaline-treated HNTs.

FTIR spectra of raw and alkaline treated HNTs are shown in Fig.31. In the FTIR spectra of raw HNTs, peaks at 3698 cm^{-1} , 3621 cm^{-1} are reflective of the O–H stretching vibrations of Al–OH bond in internal surface and in interface of Al–O octahedron and Si–O tetrahedron, respectively. The peak at 1635 cm^{-1} is attributed to water deformation vibration. Peaks at 1114 cm^{-1} , 1089 cm^{-1} and 1031 cm^{-1} are contributed to stretching vibration of apical Si–O and in-plane Si–O, respectively. Other peaks such as O–H deformation (940 cm^{-1}), Al–OH deformation of internal surface (913 cm^{-1}), Si–O–Si symmetric stretching (796 cm^{-1}), and Si–O–Al perpendicular stretching (754 cm^{-1}), can be observed in the spectra of raw HNT. After alkaline treatment of HNT with NaOH solution, most of main peaks of halloysite structure remained unchanged. The only observed change is in the intensity of the absorption band at 911 cm^{-1} . This peak gradually broadens by increasing the NaOH concentration. This decrease in intensity is indicative of small level for alumina layers removal [60]. Another peak broadening observed in the FTIR results is related to 469 , 536 and 1030 cm^{-1} , suggesting that alkaline-treatment slightly removed the Al–OH and Si–OH groups from natural HNTs. These changes however, are not observed intensely, indicating that our treatment did not disturb the structure of raw HNTs.

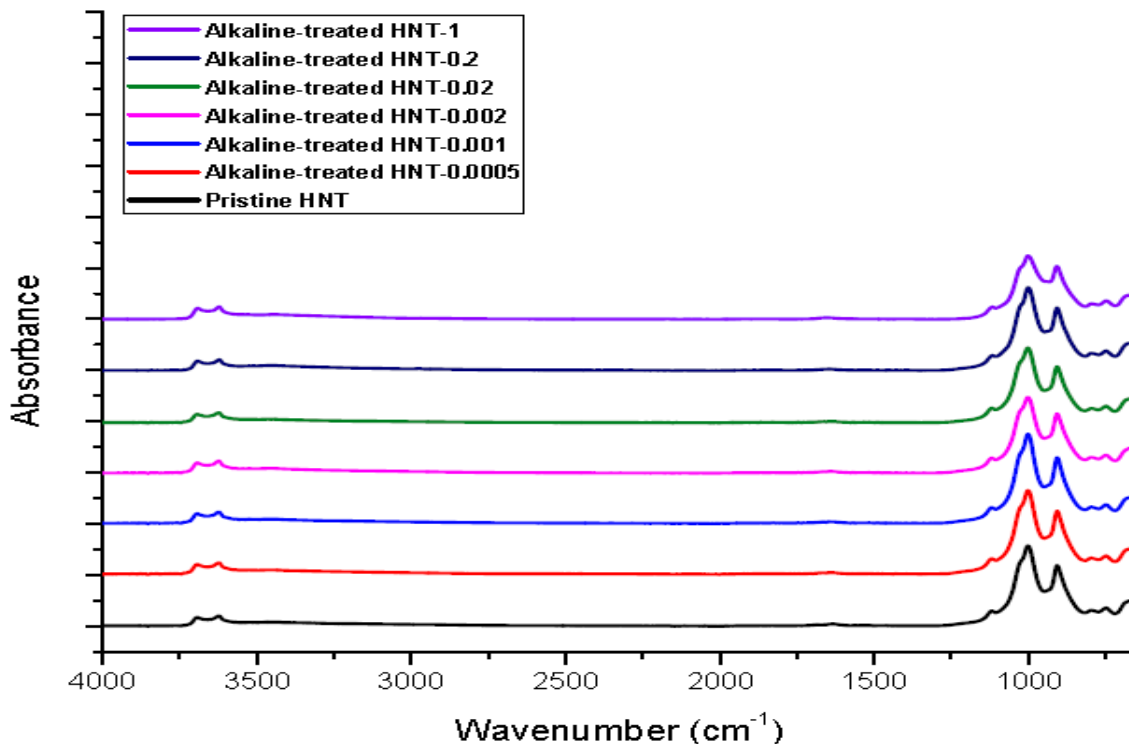


Fig.31. FT-IR spectra of pristine and alkaline-treated HNTs.

TGA analysis of HNT samples before and after alkaline treatment is presented in Fig.32. TGA curve of the natural HNT shows three main sudden mass losses. First one occurs around 90°C, where the physically absorbed water content in HNT is removed. The second sudden mass loss occurs around 247°C as a result of decomposition of structural alunite ($\text{KAl}_3(\text{SO}_4)_2(\text{OH})_6$). This peak is preserved in the curves of all the alkaline treated HNTs, as a proof that alunite was not removed from HNTs, which is consistent with FTIR results [64]. The last sudden and sharp mass loss takes place at 443°C, where the existing structural water content is dehydroxylated at this stage. The amount of mass loss for HNT after alkaline treatment is decreased more as the NaOH concentration is increased. In overall, since no disappearance, sharpening or broadening in the characteristic peaks of TGA curve of natural HNT is observed, we have proved that all alkaline treated sampled preserved the thermal and structural properties of HNTs especially below 1 mol/L NaOH treatment.

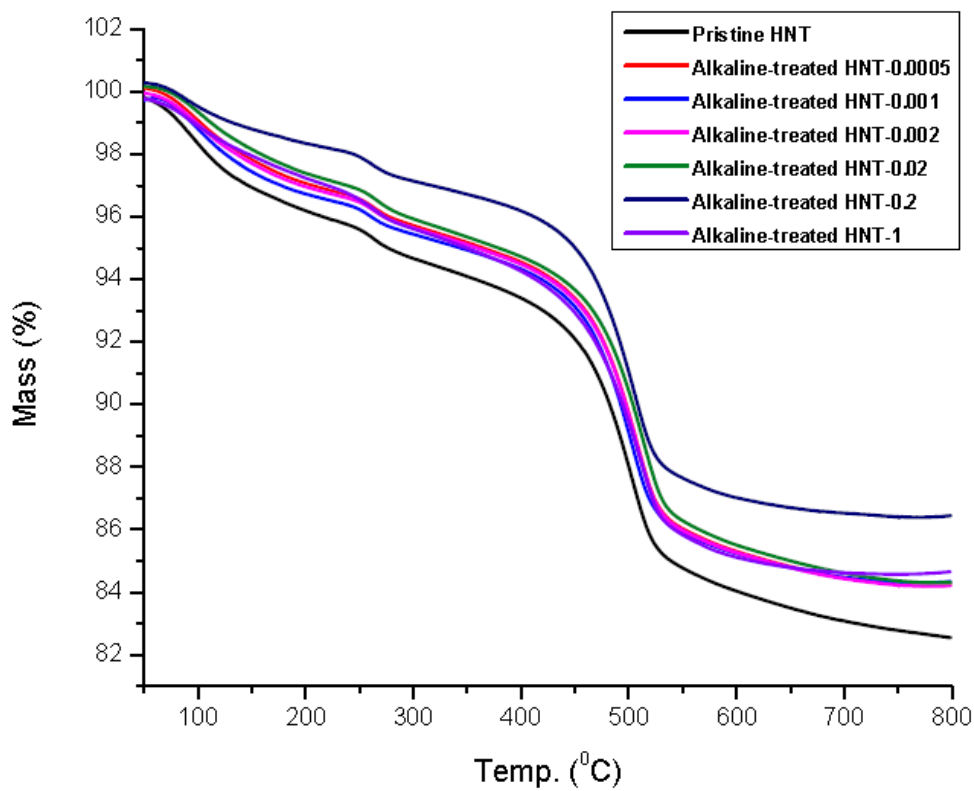


Fig.32. TGA curves of pristine and alkaline-treated HNTs.

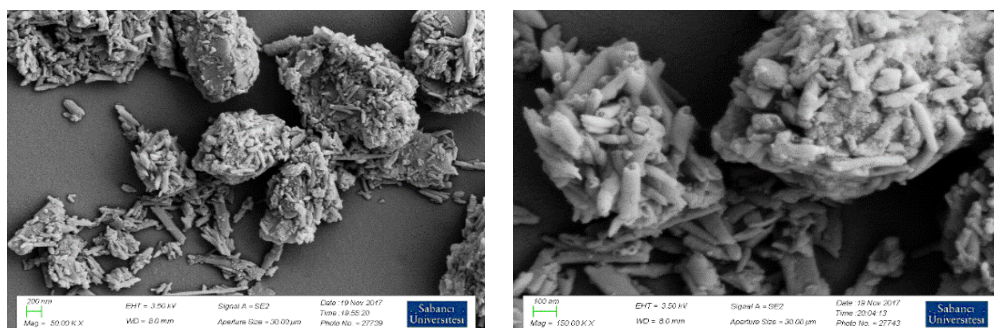
2.3.6 The effect of alkaline treatment of pristine HNTs on the purification and size separation of purified HNTs

In order to investigate the alkaline treatment effect on the purification and size separation of purified HNTs, two concentrations of NaOH, 0.0005 and 0.002 mol/L, were chosen. FE-SEM images (Fig.33 and Fig.34) show both categories for purified HNTs (precipitations of 8800 g and 15557 g) after 0, 0.0005 and 0.002 mol/L NaOH treatments. It is shown that both purified alkaline treated HNTs have equally higher level of dispersion than the purified HNTs without any alkaline treatment. This is an indication of the increased number of particles suspended in the media due to the alkaline treatment and thus breaking and cutting nanotubes more efficiently and facilitating the size separation step. Purified samples from alkaline treated HNTs by 0.002 mol/L NaOH show a more homogeneous distribution than those prepared by 0.0005 mol/L NaOH solution. This is attributed to the effect of higher basic concentrations on the success in breaking agglomerates. No alumina sheets or

amorphous particles are present in either purified samples obtained from alkaline treated HNTs, indicating that pH level is not high enough to disturb the tubular structure of HNTs.

In the statistical survey obtained from FE-SEM images (Fig.35), it is shown that purified HNTs without any pre-alkaline treatment have average length size of 237.52 ± 20 nm (Fig.35-a) and 150.95 ± 20 nm (Fig.35-b) for precipitation from 8800 g and 15557 g centrifugal forces, respectively. These average sizes in length slightly increase for both purified categories of to 244.7 ± 20 nm (Fig.35-a) and 164.87 ± 20 nm (Fig.35-b) by alkaline treatment in 0.0005 mol/L NaOH solution. However, after alkaline treatment by 0.002 mol/L NaOH solution these values drop down to 212.24 ± 20 nm (Fig.35-a) and 140.46 ± 20 nm (Fig.35-b). This falls in line with the FE-SEM results, showing that pH treatment at 0.002 mol/L was more effective in providing a more homogeneous system and separation process for HNTs compared to 0.0005 mol/L NaOH concentration.

(a)



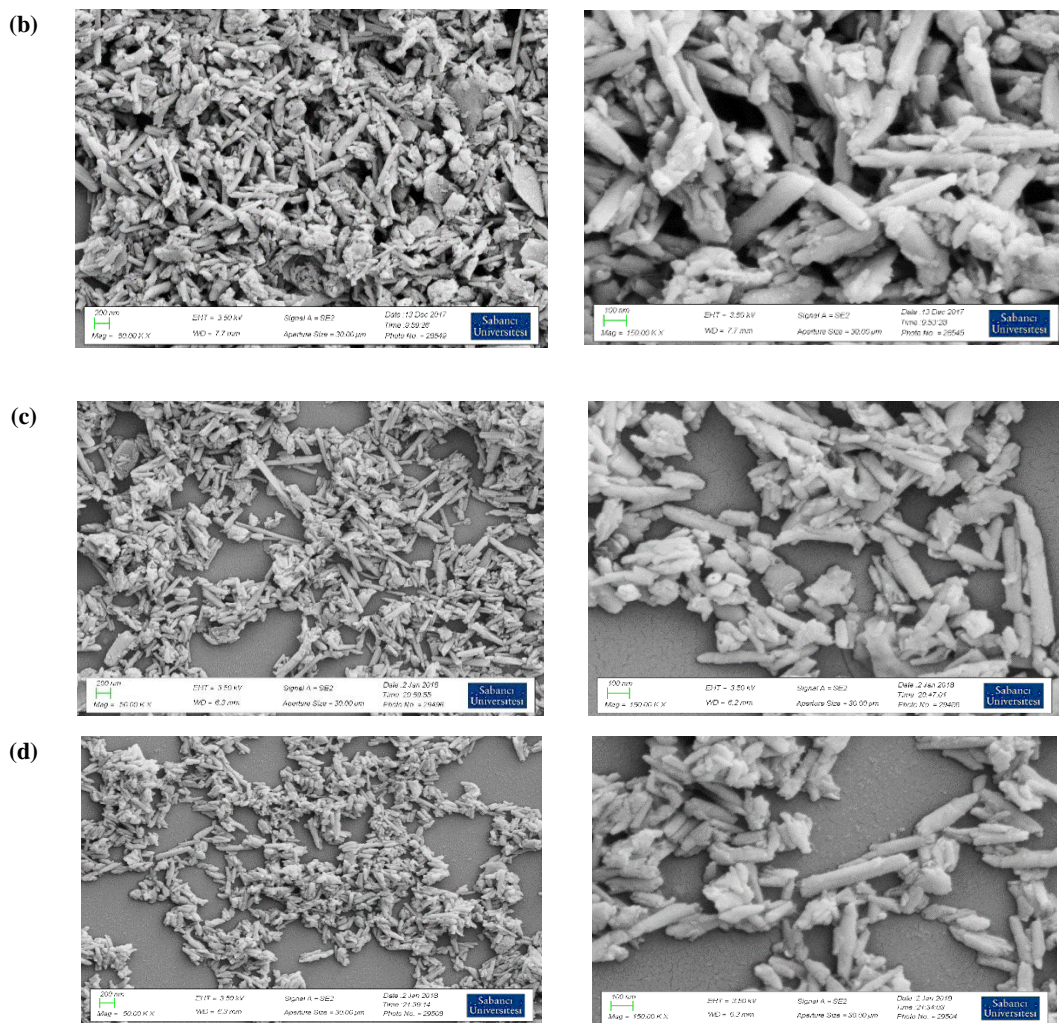
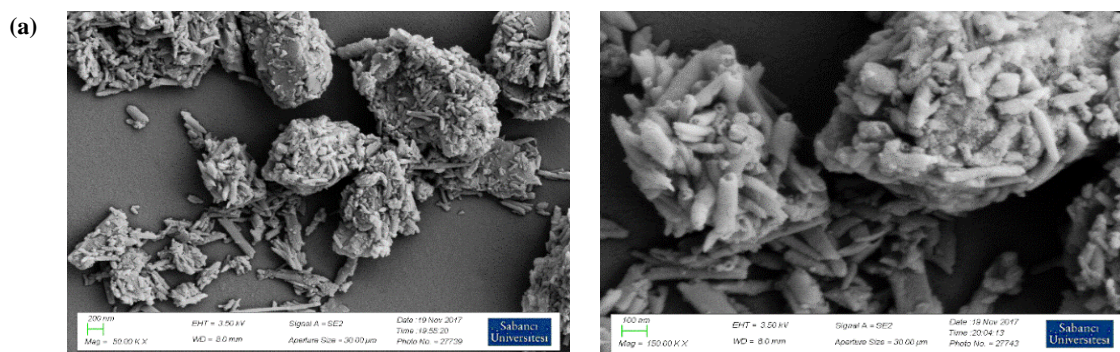


Fig.33. FE-SEM images of (a) Pristine HNTs (b) Purified HNTs precipitated at 8800 g centrifugal force; (c) Purified alkaline-treated HNTs obtained from 0.0005 mol/L NaOH solution and precipitated at 8800 g centrifugal force; (d) Purified alkaline-treated HNTs obtained from 0.002 mol/L NaOH solution and precipitated at 8800 g centrifugal force.



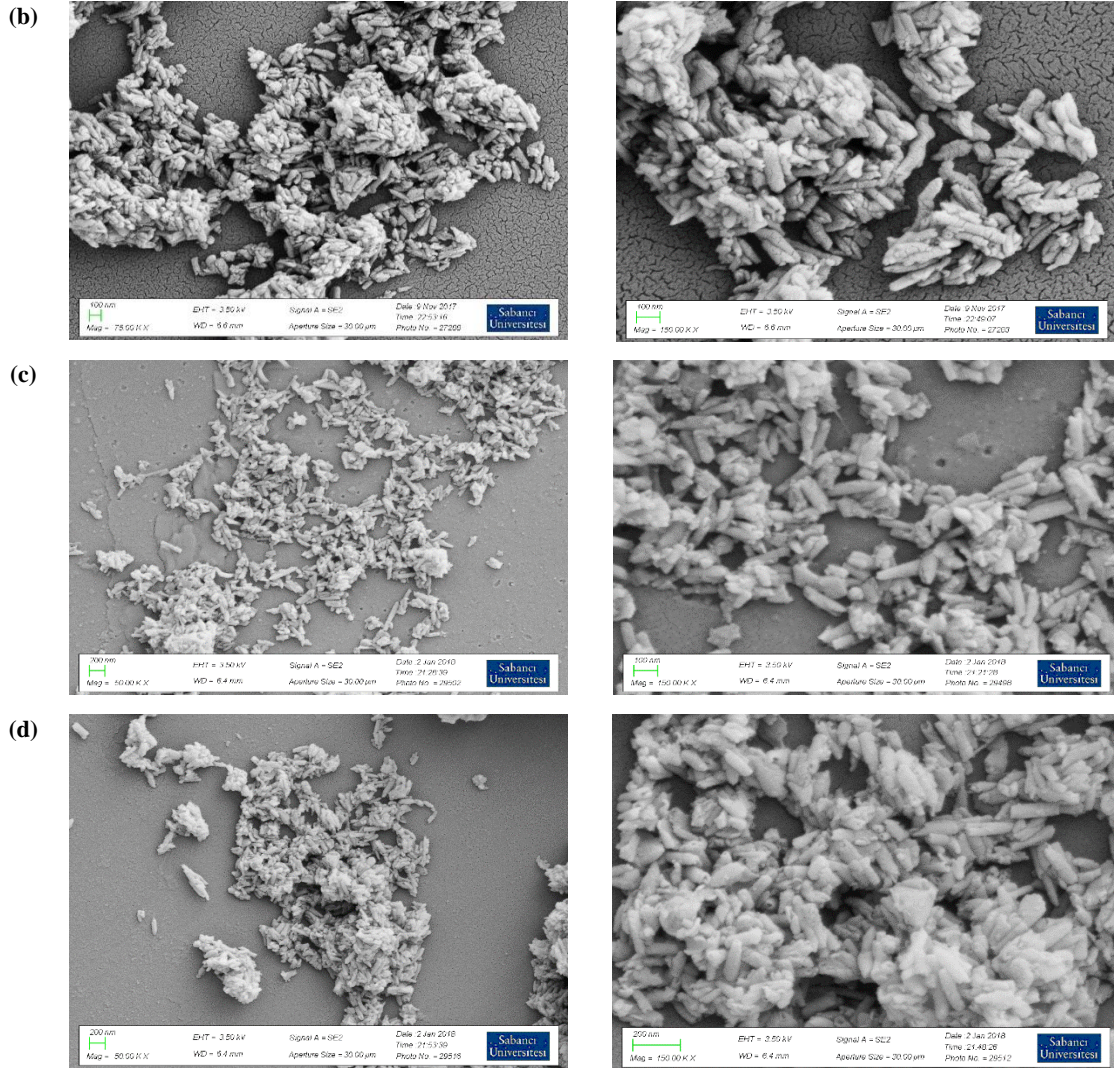


Fig.34. FE-SEM images of (a) Pristine HNTs (b) Purified HNTs precipitated at 15557 g centrifugal force; (c) Purified alkaline-treated HNTs obtained from 0.0005 mol/L NaOH solution and precipitated at 15557 g centrifugal force; (d) Purified alkaline-treated HNTs obtained from 0.002 mol/L NaOH solution and precipitated at 15557 g centrifugal force.

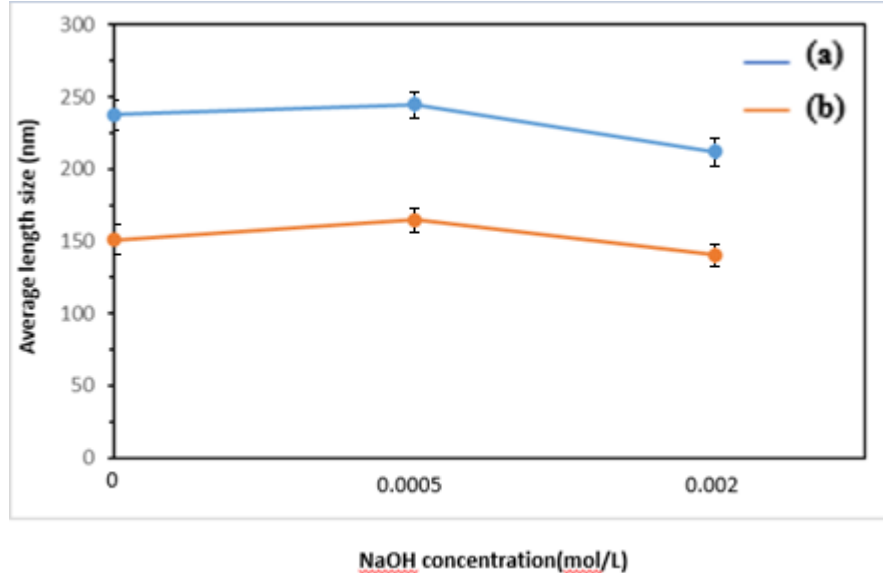


Fig.35. Statistical survey by FE-SEM for the effect of alkaline treatment on the purification and size separation of purified HNTs: (a) average length size of purified alkaline-treated HNTs with 0, 0.0005 and 0.002 mol/L NaOH concentration precipitated at 8800 g centrifugal force (b) average length size of purified alkaline-treated HNTs with 0, 0.0005 and 0.002 mol/L NaOH concentration precipitated at 15557 g centrifugal force.

XRD results in Fig.36 show that although after purification of HNT without any pre-alkaline treatment all the peaks contributed to impurities in the raw material has been disappeared, this is not accurate for the samples which were pretreated by 0.0005 mol/L NaOH solution. We observed that there are still some impurity peaks present at 18.1°, 26.6° and 29° in the XRD pattern of this sample. However, after purification of HNTs, which were primarily subjected to 0.002 mol/L NaOH treatment, no peaks other than main structural HNT are observed. This comparison shows that 0.0005 mol/L NaOH concentration was not enough to eliminate the impurities from the system. Meanwhile, 0.002 mol/L NaOH solution was effective in detaching tubular halloysites from impurities, thus facilitating the separation of nanotubes from these particles during the purification process.

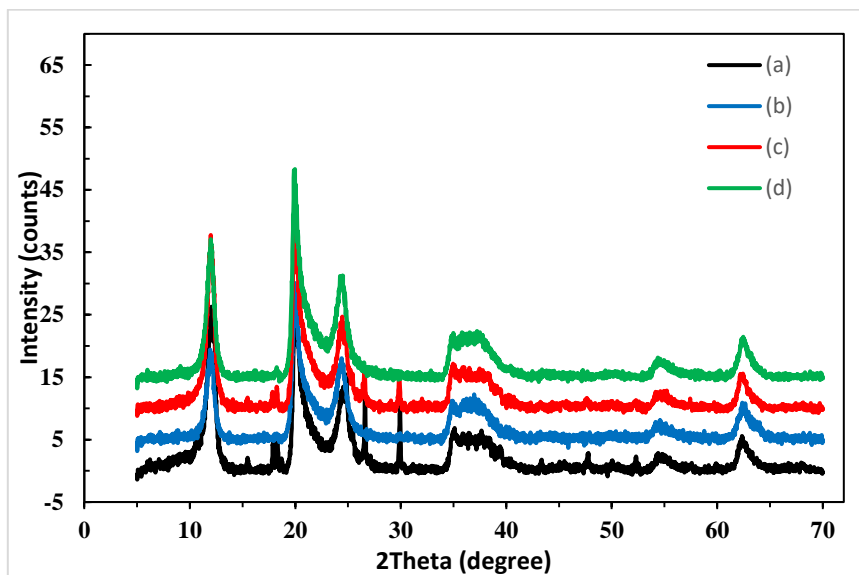


Fig.36. XRD patterns of (a) Pristine HNTs (b) Purified HNTs precipitated at 8800 g centrifugal force; (c) Purified alkaline-treated HNTs obtained from 0.0005 mol/L NaOH solution and precipitated at 8800 g centrifugal force; (d) Purified alkaline-treated HNTs obtained from 0.002 mol/L NaOH solution and precipitated at 8800 g centrifugal force.

FTIR spectra (Fig.37) of raw and all purified HNTs with and without alkaline treatment show the characteristic absorption bands of HNT structure, which were discussed earlier. No new peaks appeared after purification, and no sharpening or broadening of any bands are observed, indicating that HNTs structure is preserved after separation process. These results are consistent with FTIR results of alkaline-treated HNT samples presented in previous section.

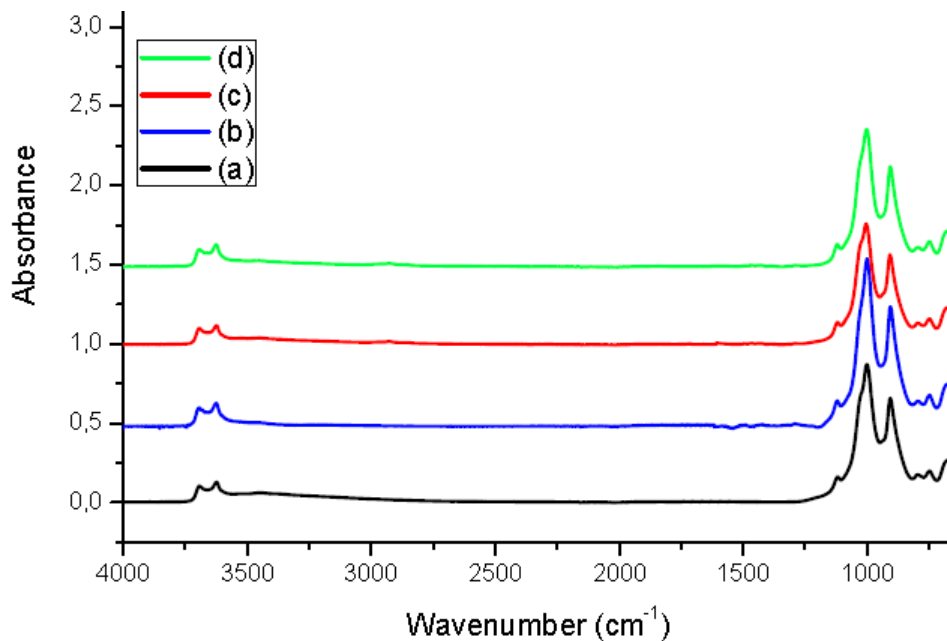


Fig.37. FTIR spectra of (a) Pristine HNT (b) Purified HNT precipitated at 8800 g centrifugal force; (c) Purified alkaline-treated HNT obtained from 0.0005 mol/L NaOH solution and precipitated at 8800 g centrifugal force; (d) Purified alkaline-treated HNT obtained from 0.002 mol/L NaOH solution and precipitated at 8800 g centrifugal force.

TGA curve of all purified samples (Fig.38-b, c and d) show lower mass loss compared to the pristine HNTs curve, illustrating the removal of impurities from the system. Mass loss of purified alkaline treated HNT by 0.002 mol/L NaOH solution is higher compared to the sample treated by 0.0005 mol/L NaOH solution. This is due to the existence of less impurities within the 0.002 mol/L sample. Also, it can be explained as the result of alumina removal and dihydroxylation of water content in Al-OH and Si-OH during the purification process.

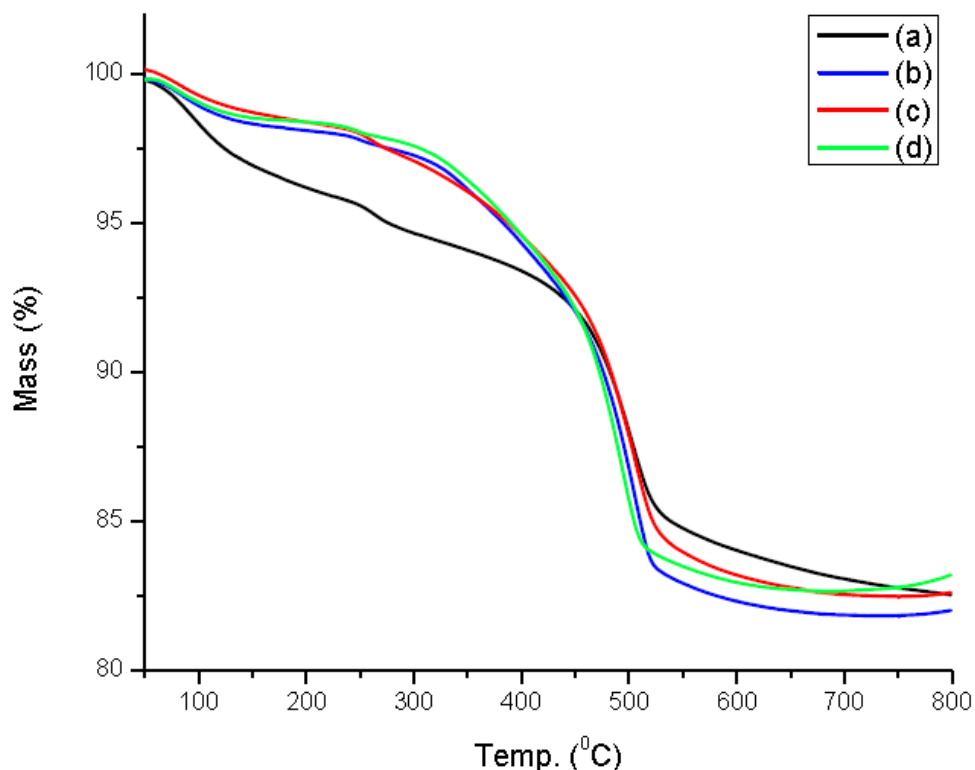


Fig.38. TGA curves of (a) Pristine HNTs (b) Purified HNTs precipitated at 8800 g centrifugal force; (c) Purified alkaline-treated HNTs obtained from 0.0005 mol/L NaOH solution and precipitated at 8800 g centrifugal force; (d) Purified alkaline-treated HNTs obtained from 0.002 mol/L NaOH solution and precipitated at 8800 g centrifugal force.

2.4 Conclusions

A unique method based on the literature was developed to prepare homogeneous HNTs in size by sequencing alkaline treatment, ultrasonication and three-step viscosity gradient centrifugation. The results showed that raw HNTs (150 – 1103 nm in length) that exist in the form of relatively large agglomerations were considerably broken, dispersed and cut in individual nanotubes during the alkaline treatment and ultrasonication. Impurities, in the form of bundles of HNTs or other microparticles, have been successfully removed from pure HNTs (average size of 126 – 179 nm) through a three-step centrifugation. The yield of

purified HNTs were increased by repeating the whole process for three times. Furthermore, PVP concentration and alkaline treatment both had a direct effect on the yield and size distribution of purified HNTs.

3. Part II: Ionic functionalization of HNTs

3.1 Literature survey

3.1.1 Studies on the surface modification of HNTs by organosilane agents

Functionalization of HNTs by organosilane agents is considered to enhance the properties of this naturally available nanotubes for its previously mentioned applications. The use of organosilanes with the chemical formula $R-Si-(OR')_3$ are widely known, due to advantages such as low cost and potential for hydrolysis and thus, condensation reactions with hydroxyl groups existing on the surface of other particles [69].

Numerous research studies have been reported on the investigation of covalently functionalized HNTs with these applications. For example, in an early work, the surface of halloysite was functionalized by using γ -aminopropyltriethoxysilane (APTES) as the modifying organosilane agent. It was found that APTES grafting occurred on the -OH groups of inner walls, nanotube edges and external surface. Also, there was an evidence of oligomerization of free APTES and consequent condensation with the already grafted APTES to compose a cross-linked structure. Water content in the reaction media were controlled by thermal pre-treatment of HNTs. Other factors such as available -OH groups (which could determine the grafted APTES quantity) were extremely dependent on the morphology of HNTs, meaning their internal and external diameters, thickness of walls and length. It was also investigated that kaolinite had much less reactivity with APTES than halloysite. This was because of fairly low amount of -OH groups available on the kaolinite surface. In overall, both properties of HNTs and conditions of pre-treatment were contributing factors in controlling the functionalization process of HNTs by APTES [70].

In another study, modification was performed by the organosilane agent γ -methacryloxypropyl trimethoxysilane (γ -MPS) with the aim of improving HNTs dispersion ability in “ethylene propylene diene monomer (EPDM)” in order to enhance the thermal, structural and tensile characteristics of the mentioned monomer nanocomposites. γ -MPS was grafted on the Al-OH groups inside tubes and at the edges, as well as on the Si-O groups on the external surface of HNTs. It was demonstrated that HNT modification by γ -MPS caused these nanotubes to interact more with EPDM and their dispersion grew within the nanocomposite, which in turn improved the tensile strength. However, modification did not enhance the thermal properties of the nanocomposite. The thermal resistance of the nanocomposites decreased after the modification of the HNTs [19].

Natural HNTs were modified by N- β -aminoethyl- γ -aminopropyl trimethoxysilane (KH-792) to build a novel surfactant for removing Cr(VI) from waste water. Adsorption of Cr(IV) by the modified samples were highly dependent on temperature, contact time, ionic strength and initial pH. Beside these reaction conditions, studies obtained from experiments showed that electrostatic relation between modified HNTs and Cr(IV) was extremely important in achieving a well adsorption. According to these results, it was proved that modified HNTs can be great adsorbents for removing Cr(IV) from waste water, due to their effective performance and low cost [71].

In another study, two aminosilane compounds, diaminosilane (DAS) and triaminosilane (TAS) were grafted on the surface of natural HNTs and the results were compared to the physical adsorption of these silane compound on the HNT surface, which were used as catalyst supports in atom transfer radical polymerization process of methyl methacrylate. It was observed that modified HNTs from grafting by DAS and TAS were not different in their basal spacing from unmodified HNTs, showing there were not any structural changes for HNT after modification by grafting. DAS grafted HNTs and HNTs modified by physical adsorption of DAS both produced a specific polymer with similar polydispersities. However, the HNTs modified through physisorption of DAS showed less conversion and deficient polymerization reaction control. Grafting HNTs with TAS disturbed the activity of catalyst activity and had a harmful impact on polymerization reaction control. This is due to the

existence of hydrogen bonding between hydroxyl groups at HNT surface and amine groups in the silane agent [72].

The promise of using HNTs as a vital cheap carrier for biomolecules in drug delivery was also exploited by numerous researchers. For examples, functionalized HNTs were utilized as carriers for attacking surviving in cancer by the therapeutic gene ASODN. For this purpose, the surface of HNTs were modified with APTES to provide better conditions for the next biofunctionalization, which was building the functionalized HNTs and ASODN complexes. The collected results displayed that the complexes of functionalized HNTs and ASODN had enhanced the intracellular activities regarding the drug delivery and thus, increasing the effect of ASODNs [73].

A study on the description for assisting the functionalization of external surface of HNTs by microwave irradiation was presented. The functionalization of HNTs was through ionic liquids. The modification of HNTs was reported following two steps. First, 3-mercaptopropyl trimethoxysilane was grafted on the HNTs external surface through microwave irradiation, and second, ionic liquids of vinylimidazolium were attached to HNTs surface through thiolene reaction. In the end, it was uncovered that highest level of loading achieved in solvent free conditions, which is considerably environmentally friendly. FTIR and TGA results proved successful functionalization of HNTs, as well as that it only happened on the HNTs external surface. FE-SEM images illustrated the preservation of tubular structure of HNTs after functionalization by the organosilane. Finally, the employed material was used as the Palladium catalyst support in Suzuki reaction, and showed the increased efficiency [74].

In another approach, HNT was employed as filler for poly(hydroxybutyrate-co-hydroxyvalerate) (PHBV) nanocomposites. Modification of HNT was progressed using multiple organosilane agents, such as 3-(glycidyloxy)propyl trimethoxysilane (GOPTMS), 3-(methylamino)propyl trimethoxysilane (MAPTMS), octyltriethoxysilane (OTES) and APTES. Here in this work, like some other previous studies, it was seen that silane grafting resulted in the formation of a crosslinked structure. This occurrence was due to the

hydrolyzation of organosilanes, and their consequent reactions with HNTs surface water and also the already grafted organosilanes on the surface. Dispersion behavior of the prepared nanocomposites built different morphologies depending on the type of silane modifier. It was observed that as the level of some organosilanes oligomerization increased, agglomerations formed, and hence, mechanical and thermal stability decreased. Also, it was reported that reactions of the C=O bond in the polymer with the silanes functional groups could determine the mechanical characteristics of the prepared nanocomposites. For example, reaction between the polymer and amine groups belonging to the silane compounds led to the chemical structure transformation, which resulted in disturbance in the nanocomposites properties. In the case of using OTES and GOPTMS as silane grafting agents, the abovementioned interactions were blocked due to some secondary reactions in PHBV nanocomposites containing modified HNTs. In spite of the defective dispersion behavior of HNTs inside the polymer network, mechanical stability and performance of PHBV was improved [69].

Grafted HNTs using poly (NASS) were produced through a synthesis in three steps to build nanofiltration (NF) membrane with negative charge. According to the results, in the first step, HNTs were modified by APTES successfully. After diffusion of modified HNTs by poly (NASS) into the membrane, the resulting hybrid system showed negative charge, and its hydrophilicity highly increased, compared to commercial membranes. Even though there was an observed decrease in the amount of rejected water-soluble pollutants, diffusion of silane modified HNTs significantly increased. This phenomenon can be applied for desalination purposes, such as waste water treatment and dye removal [75].

It is mentioned that mechanical characteristics, dispersion behavior and interfacial interactions of epoxy nanocomposites could get effected by chemically functionalized HNTs. In this regard, isophorone diisocyanate (IPDI) was chosen as the silane compound., and it was stated that both strong interconnection between epoxy nanocomposite matrix and HNTs and well dispersion behavior improved the mechanical stability of these hybrid nanocomposites [76].

In one investigation, HNTs were functionalized using multiple silane grafting agents, through a post-grafting technique, which was applied in both anhydrous and aprotic environments. Among all modified HNTs, the ones which were functionalized by APTES and MPTMS demonstrated the best silylation performance, respectively. It was concluded that despite of high grafting level for APTES modified HNTs, some primary amine groups were not chemically available to undergo some desired reactions [77].

Modified HNTs were also used as the inorganic part of the hybrid nanocomposites to synthesize waterborne polyurethanes (PU) with enhanced water and mechanical resistance. APTES, polypropylene glycol, 2,2-Dimethylol propionic acid, and Toluene diisocyanate were used to build modified HNTs interconnected with PU in an aqueous media. The results showed that due to the temperature and enthalpy increase in the hard segment, HNTs dealt with this segment of PU. This made the decomposition temperature to decrease. Mechanical stability and toughness increased [78].

3.1.2 Aim of this work

Considering that in the terms of hydrophilicity, diffusion and absorbance, no work has been done on ionic modification of the external surface of HNTs. In this study, the ionic functionalization of HNTs by an ionic solution prepared from the reaction of an organosilane agent 3-(triethoxysilyl)propyl isocyanate (ISO) with n-methyltaurine sodium salt (N-MTSS) was examined. The objective of this work was to illustrate the optimum reaction conditions for grafting the synthesized ionic organosilane on the outer surface of HNT, and to explain the effect of modification on the structure, morphology and dispersion behavior of HNT. In addition, the effect of the surface pre-treatments such as piranha solution treatment and oxygen plasma on the efficiency of grafting of functional groups on the surface of HNTs was studied.

3.2 Materials and experimental procedures

3.2.1 Materials

Pristine HNT powders were provided by Esan, Eczacıbaşı industrial raw materials company (Istanbul, Turkey) and were dried at 110 °C for 12 h to eliminate any residual physically absorbed water content. Triethyl amine was used for HNTs for setting the pH in the basic region in the modification process. 3-(Triethoxysilyl)propyl isocyanate (ISO), N-Methyltaurine sodium salt (N-MTSS), N-dimethylformamide (DMF, Sigma-Aldrich) and Acetone (Sigma-Aldrich) were utilized as silane agent, amine compound and solvents in the functionalization procedure, respectively. DMF and Acetone were dried by molecular sieves prior to be used in reactions. Triethyl Amine (TEA) (>97%) was used to control the pH of the HNTs suspension in some sample, which will be explained further. Sulfuric Acid (>97%, 2.0 mol/L, Sigma-Aldrich) and Hydrogen Peroxide (Sigma-Aldrich) were put to use for making Piranha solution for pretreatment of HNTs.

3.2.2 Experimental procedures

3.2.2.1 Reaction of ISO with N-MTSS

The reaction of ISO with N-MTSS was progress in three different conditions:

- 1) SA-1-17A.: 12.16 ml (40 mmol) liquid N-MTSS (40% wt. aq.) was dissolved in 13.40 ml (30% wt.) dried acetone and stirred until complete dissolvment. Then, 10 ml (40 mmol) ISO was added dropwise to the mixture at room temperature under N₂ atmosphere. The solution was mixed for 4 h.
- 2) SA-1-18A: 1.16 g (8 mmol) dried N-MTSS (white powder) was dissolved in 65 ml dried DMF and stirred until all the N-MTSS content was completely dissolved. Then, 2 ml (8 mmol) ISO was added dropwise to the mixture at room temperature under N₂ atmosphere. The solution was left unmixed for 24 h [79].

- 3) SA-1-22A: 6.92 ml (24 mmol) liquid N-MTSS (40% wt. aq.) was dissolved in 5.62 ml (30% wt.) dried acetone under stirring until it was completely dissolved. Then, 6 ml (24 mmol) ISO was added dropwise to the mixture at 45 °C and under N₂ atmosphere. The solution was mixed for 30 min.

Note that prior to carry out any characterization, all three reaction mixtures described above were stirred at 60 °C until most of the liquid phase is evaporated.

3.2.2.2 Modification of HNTs surface by silane-amine agent solution

Modified HNTs were prepared comparing different methods given below:

- 1) SA-1-17B: 0.6 g pristine HNT was dispersed in the reaction mixture SA-1-17A and ultrasonicated for 30 min. The dispersion was kept under constant stirring at room temperature for 20 hr. Then the temperature was raised to 70 °C until the mixture became muddy.
- 2) SA-1-18B: 0.6 g pristine HNT was added to the mixture SA-1-18A and ultrasonicated for 30 min. Few drops of TEA was added to stabilize the pH to 8. Then the suspension was stirred at room temperature for 24 h.
- 3) SA-1-22B: 0.6 g pristine HNT was subjected to oxygen plasma treatment for 5 min. The treated HNT powder was immediately used for the reaction described in SA-1-22A, and followed by ultrasonication for 30 min, stirring at room temperature for 20 h. The stirring continued at 70 °C until the partial evaporation of liquid phase.
- 4) SA-1-22C: This sample was prepared by the same procedure done for SA-1-22B, with the exception of using HNTs treated by Piranha solution (PT-HNT) as the raw material instead of pristine HNTs.

It should be noted that piranha solution was prepared by slowly adding 10 ml H₂O₂ (34% wt.) to 30 ml H₂SO₄ under strong stirring. PT-HNT was prepared by submerging 1.5 g

pristine HNT in the provided piranha solution at 90°C for 1 h. Treated sample was filtered and washed multiple times with distilled water and vacuum dried at 110° C overnight.

All modified samples were collected and washed five times with distilled water and vacuum dried at 110° C for 12 h.

3.2.3 Characterization Methods

3.2.3.1 Morphological analysis

The morphology of unmodified and modified HNTs were analyzed using Gemini 35 VP FE-SEM.

3.2.3.2 Chemical analysis

FTIR spectroscopy was utilized for the chemical analysis of ionic organosilane agent and all pristine, pre-treated, and modified HNT samples by Bruker Equinox 55 FTIR spectrometer.

3.2.3.3 Thermal analysis

Thermal behavior of all samples was analyzed by TGA using a Netzsch STA 449 C Jupiter instrument which is a simultaneous thermal analyzer and is capable of measuring the data with 0.1°C sensitivity.

3.3 Results and discussion

3.3.1 Characterization of ionic silane agent

The ionic silane compound was prepared through the reaction pathway illustrated in Fig.39. This reaction applies for all three samples SA-1-17A, SA-1-18A and SA-1-22A.

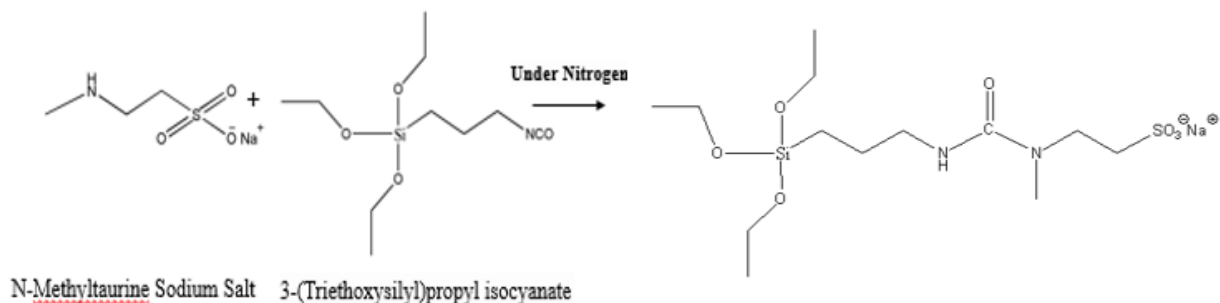


Fig.39. Reaction pathway for ISO and N-MTSS.

FTIR spectra of samples SA-1-17A, SA-1-22A and SA-1-18A are presented below. The absorption band at 3404 cm^{-1} in the SA-1-17A and SA-1-22A (Fig.40-a) is indicative of the O–H stretching vibrations of water content in aqueous N-MTSS. This peak is not however present in SA-1-18A (Fig.40-b), due to using dried N-MTSS as reactant. Peaks at 2977 cm^{-1} , 2930 cm^{-1} and 2883 cm^{-1} are indicative of C–H stretching vibrations in $\text{CH}_2\text{--CH}_3$ bonds of ISO. In Fig.40-a, peaks at 1626 cm^{-1} and 1540 cm^{-1} , which are indicated by arrows in Fig.40 are attributed to amide C=O stretching vibrations and N–H stretching vibration belonging to the urea group in the final product shown in Fig.39. This confirms that the reaction between ISO and N-MTSS was successful in producing the ionic organosilane agent for samples SA-1-17A and SA-1-22A. The peaks attributed to the amide C=O stretching vibrations and N–H stretching vibration belonging to the urea group are sharper in the spectrum of reaction solution SA-1-22A than those in the spectrum of reaction solution SA-1-17A, suggesting that by increasing the reaction temperature from room temperature to 45° C , the reaction time can be decreased from 4 h to 30 min. The possible peak responsible for urea formation is overlapped by the peak attributed to the carbonyl group of DMF in reaction mixture SA-1-18A (Fig.40-b). Other peaks such as 1038 cm^{-1} is contributed to SO_3 symmetric stretch from N-MTSS in the reaction media, and 1366 cm^{-1} , 1392 cm^{-1} , 1439 cm^{-1} are contributed to C–H bending vibrations in ISO. All other peaks belong to either ISO or N-MTSS, and no other new peak other than the ones confirming urea group formation is present in the reaction mixture, suggesting that no undesired byproducts is present within the reaction media [70].

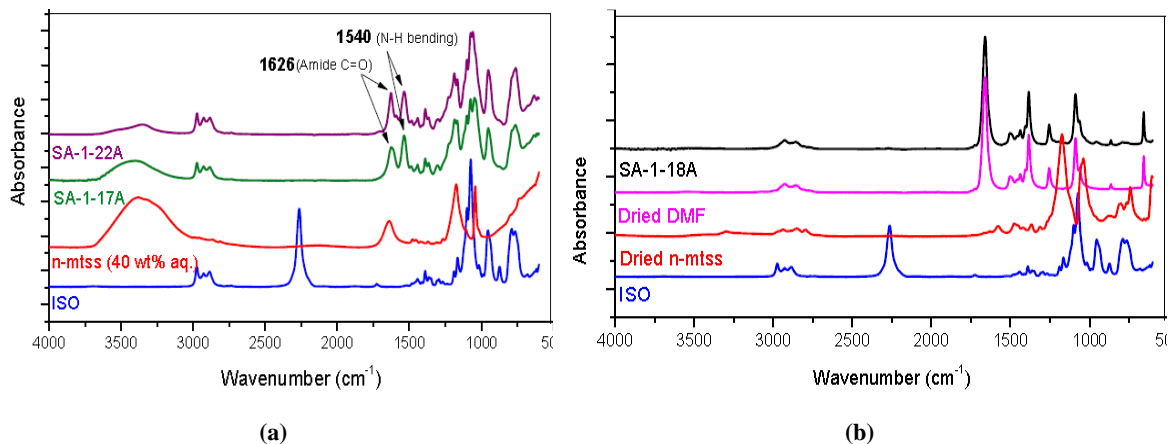


Fig.40. FTIR spectra of ionic silane agent solutions (a) sample SA-1-17A and SA-1-22A (b) SA-1-18A.

3.3.2 Properties of raw and ionically modified HNTs

The ionically modified HNTs were prepared through the reaction pathway illustrated in Fig.41 for samples SA-1-17B and SA-1-18B, and Fig.42 for samples SA-1-22B and SA-1-22C.

FTIR spectra of unmodified and modified HNT are presented in Fig.43. In the FTIR spectra of unmodified HNT, Peaks at 3698 cm^{-1} , 3621 cm^{-1} are representative of the O–H stretching vibrations of Al–OH bond in internal surface and in interface of Al–O octahedron and Si–O tetrahedron, respectively. The peak at 1635 cm^{-1} belongs to water deformation vibration [19]. Peaks at 1114 cm^{-1} , 1089 cm^{-1} and 1031 cm^{-1} are attributed to stretching vibration of apical Si–O and in-plane Si–O, respectively. Other peaks such as O–H deformation (940 cm^{-1}), Al–OH deformation of internal surface (913 cm^{-1}), Si–O–Si symmetric stretching (796 cm^{-1}), and Si–O–Al perpendicular stretching (754 cm^{-1}), can be observed in the spectra of unmodified HNTs. After ionic modification of HNTs, all main peaks of halloysite structure mentioned above remained unchanged. In addition, an absorption band at 1662 cm^{-1} , which is the indicator of C=O stretching vibrations of urea functional group in the ionic silane modifier appears. Some characteristic absorption bands of the organosilane agent, like the

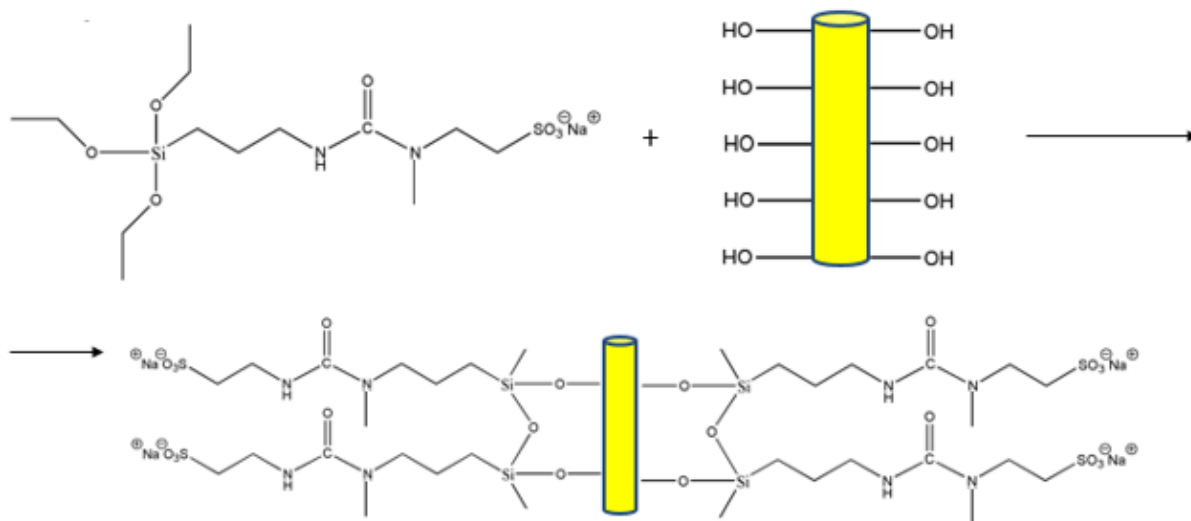


Fig.41. Reaction pathway for modifying the HNT external surface by the ionic silane agent solution for samples SA-1-17B and SA-1-18B.

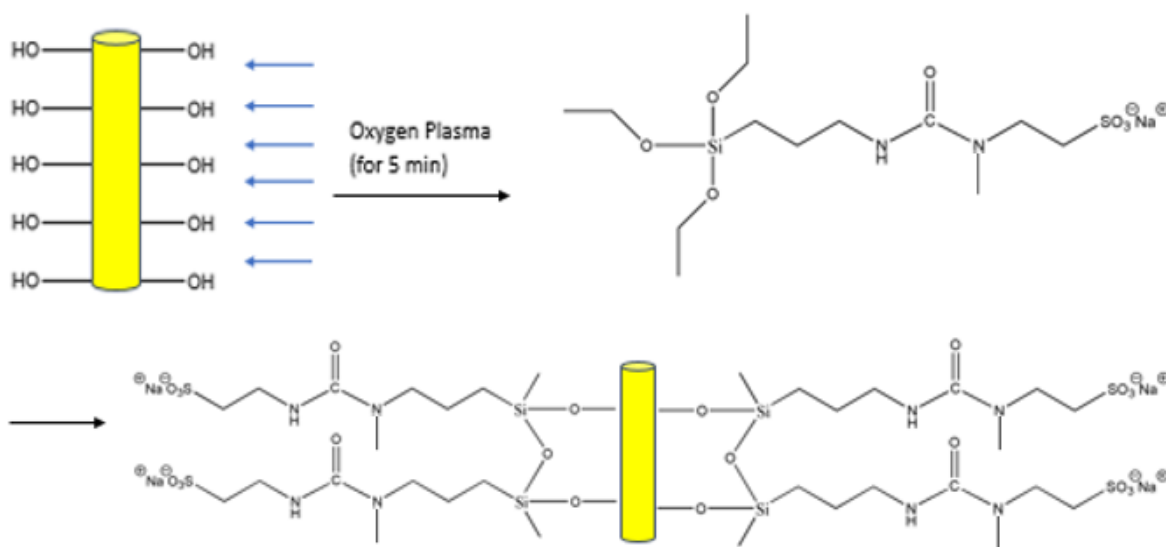


Fig.42. Reaction pathway for grafting the ionic silane agent on the HNT surface for samples SA-1-22B and SA-1-22C.

stretching CH_2 vibrations is evident in the slight uprising of the FTIR spectra in the modified HNTs around 2900 and 2853 cm^{-1} . Also, peak shifts appearing around 1466 cm^{-1} with low

intensities are indicators of the deformation of CH_2 in organosilane compound. This suggests that all ionic functionalized HNTs were prepared successfully. Sample SA-1-22B shows higher intensities for the mentioned new peaks than those appearing in the sample SA-1-17B. This may indicate that silane grafting was more successful for SA-1-22B compared to SA-1-17B, which is consistent with the FTIR results of SA-1-17A and SA-1-22A. Oxygen plasma could activate more silanol groups on the external surface and pore edges of HNTs, leading to more Si–OH reacting with ethyl groups attached to Si in the ionic organosilane agent, and thus higher level of modification. Sample SA-1-18B showed the same trend in the FTIR results, with more intense peaks than SA-1-17B, indicating that using DMF as a polar solvent for the reaction will improve the reaction procedure, since no water is present in the system and therefore the chance of any possible side reactions such as hydrolysis is decreased [53]. In the FTIR spectrum of piranha treated HNT (PT-HNT), an absorption peak at around 1210 cm^{-1} has emerged, contributed to the Si–O–Si asymmetric vibrations belonging to amorphous silica. The intensity ratios of 1089 cm^{-1} to 1031 cm^{-1} and 796 cm^{-1} to 754 cm^{-1} increased. All these changes in absorption bands confirms the appearance of silica and removing a small portion of alumina from the HNT structure after treating by piranha solution (Activation of HNT by piranha). Functionalized samples present new absorption peaks and peaks at 2936 cm^{-1} , and 2870 cm^{-1} , coming from the $-\text{CH}_2$ vibration of asymmetric stretching and CH_3 vibration of symmetric stretching, respectively [80]. The $-\text{CH}_3$ vibrations might also be indication that ethoxy groups belonging to ISO structure in the grafting agent remained unhydrolyzed after modification. These mentioned intensities are higher for sample SA-1-22C, showing the advantages of reaction conditions for grafting agent synthesis such as high temperature, short time and acetone as the solvent, and also using PT-HNT as the raw material as well as oxygen plasma in activation of the external surface.

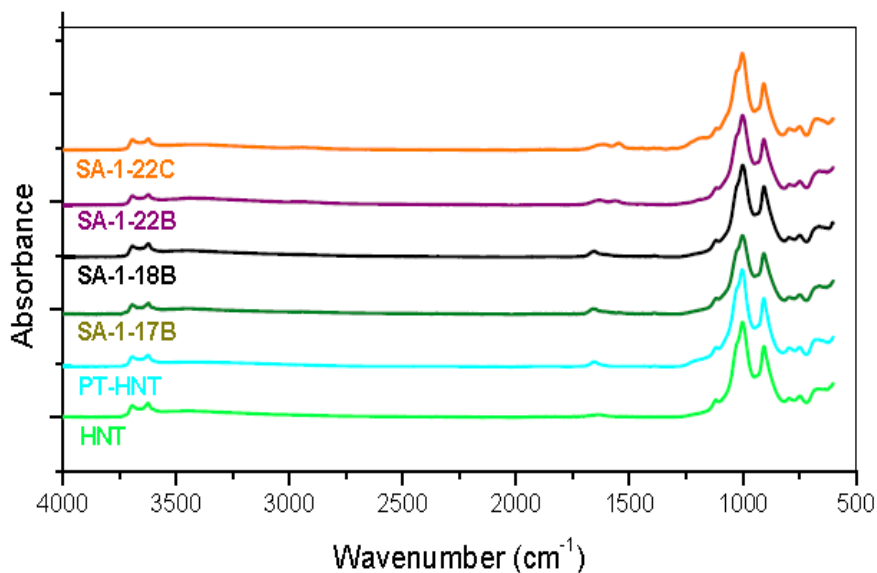


Fig.43. FTIR spectra of ionically modified HNTs.

TGA curves of HNT samples before and after modification is presented below (Fig.44). TGA curve of raw HNTs contain three main sudden mass losses. First one is at 90 °C. At this temperature, the physically absorbed water content in HNTs is dehydrated. The second sudden mass loss happens at 247 °C. This weight loss is a result of decomposition of structural alunite ($\text{KAl}_3(\text{SO}_4)_2(\text{OH})_6$). The last sudden and sharp mass loss takes place at 443 °C due to the removal of existing structural water content of Al–OH and Si–OH at this stage. The modified HNTs present similar thermal behavior as natural HNTs.

In overall, since no disappearance, sharpening or broadening in the characteristic peaks of TGA curve of natural HNTs is observed, we have proved that all functionalized sampled preserved the thermal and structural properties of HNTs. Curve broadenings during all main weight losses correspond to the grafting, proving a higher mass loss compared to pristine HNTs. Furthermore, residual mass of modified HNTs were less than the unmodified HNTs according to Table 3. This change is explained by decomposition of modifying agents at HNT surface [77]. Curves of HNTs and PT-HNTs show residual masses of 84.37% and 83.80%, respectively. The increased weight loss is attributed to the removing of impurities and alumina by the treatment process [80]. Due to reformation of Si–OH and dissolution of alumina, major mass loss of PT-HNTs has shifted to a lower temperature than that of

untreated HNTs. The largest amount of mass loss for modified HNTs belongs to sample SA-1-22C (residual mass of 76.30%), illustrating the process for the sample SA-1-22A was the most suitable, and benefits of both piranha and oxygen plasma treatment of natural HNTs prior to the modification procedure, in efficiency of the ionic functionalization of nanotubes.

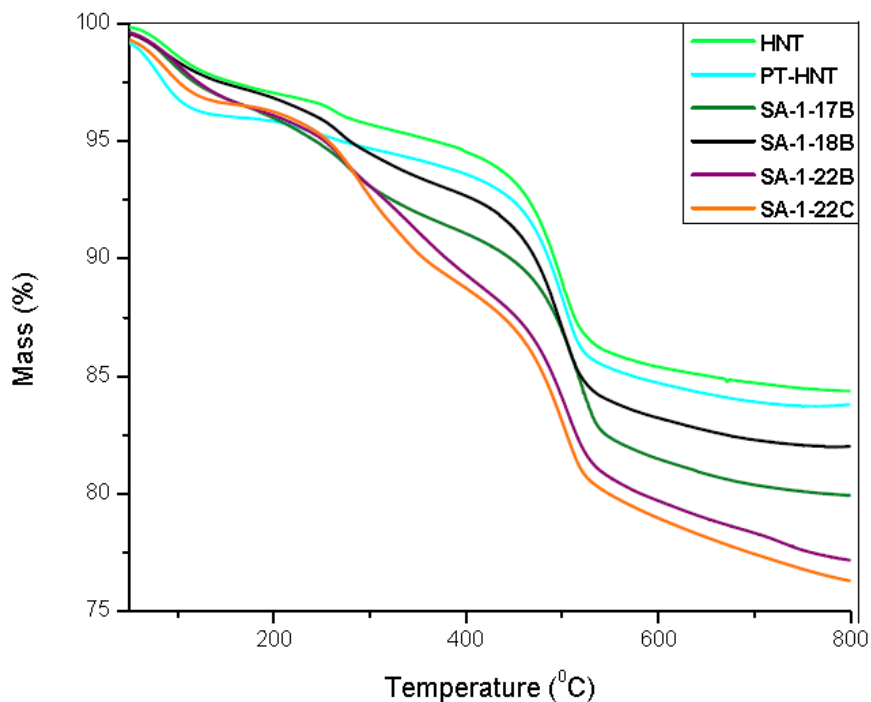


Fig.44. TGA curves of ionically modified HNTs.

The FE-SEM images of natural and modified HNTs (Fig.45) represents that nanotubes of both samples are composed of the similar tubular shapes with wide size ranges [19]. The ionic functionalization showed no effects on the structure and geometry of nanotubes. However, all modified HNTs along with the PT-HNT sample (Fig.46) were well dispersed compared to unmodified HNTs, indicating the ionic modification and piranha treatment helped the dispersion process due to the enhanced surface charge of HNTs.

Table 3. Mass change of ionically modified HNTs during heat treatment, obtained from TGA analysis.

Sample	Mass change (%) at			Residual mass (%)
	50-150°C	150-250°C	250-550°C	
HNT	-2.26	-1.04	-10.55	84.37
PT-HNT	-3.13	-0.79	-9.93	83.80
SA-1-17B	-2.83	-1.99	-12.42	79.93
SA-1-18B	-2.13	-1.52	-11.97	82.01
SA-1-22B	-2.78	-1.72	-14.41	77.18
SA-1-22C	-2.70	-1.38	-15.26	76.30

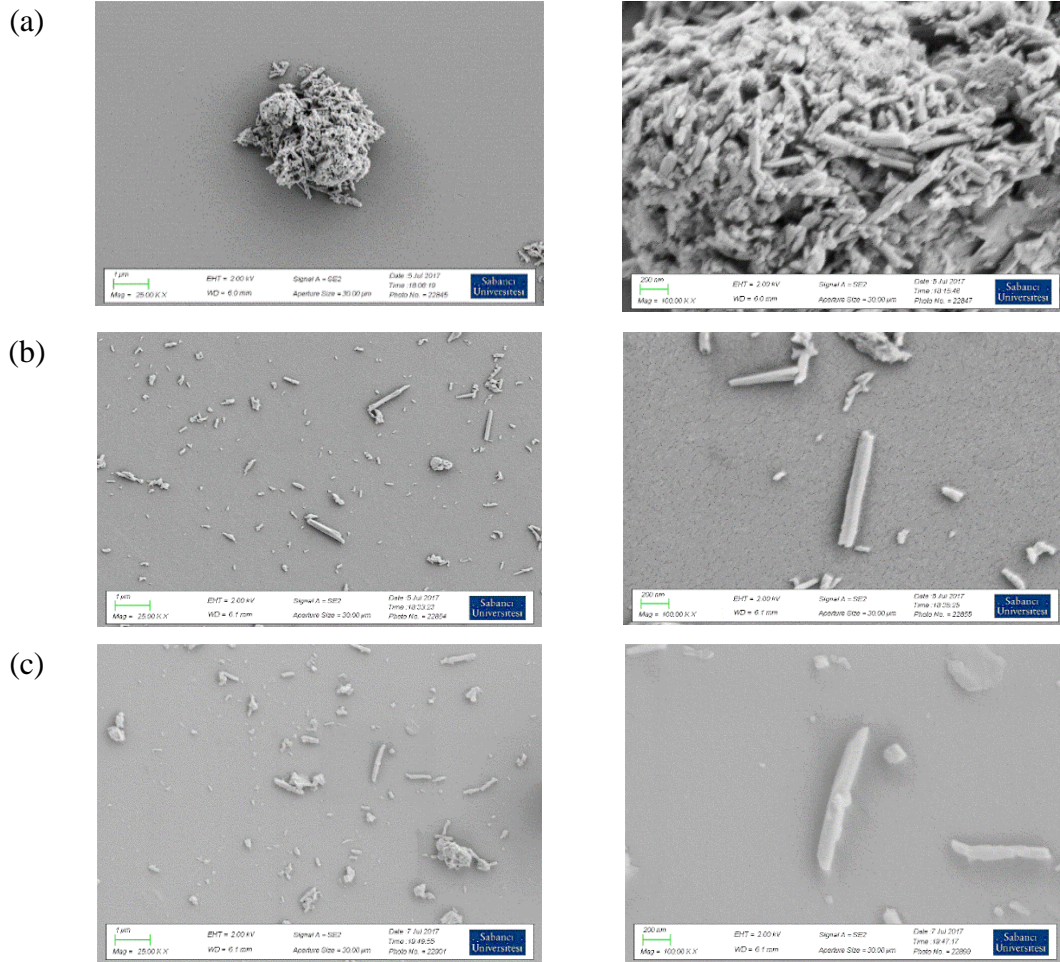


Fig.45. FE-SEM images of (a) pristine HNT (b) sample SA-1-18B (c) sample SA-1-22B.

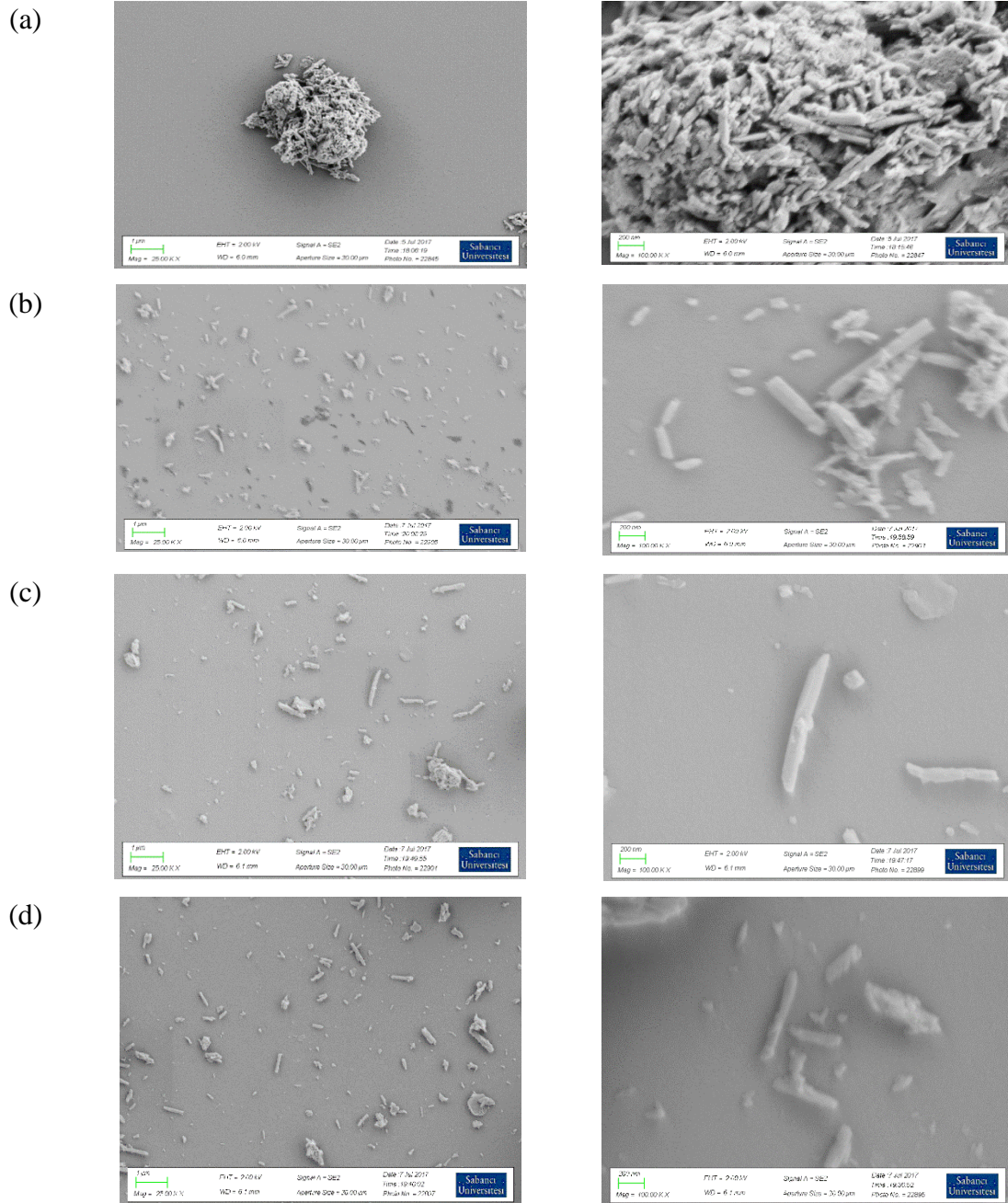


Fig.46. FE-SEM images of (a) pristine HNT (b) PT-HNT (c) sample SA-1-22B (d) sample SA-1-22C.

3.4 Conclusions

ISO and N-MTSS were successfully reacted with each other to obtain the grafting agent with ionic and silane functional groups. Water content, solvent choice, reaction temperature and time were critical to control the reaction. The synthesized ionic organosilane agent was effectively grafted on the HNTs surface. The results showed that ionic functionalization of HNTs showed no effect on the structure and geometry of nanotubes. All modified HNTs were well dispersed compared to unmodified HNTs, indicating that ionic modification improved the dispersion process due to the charged outer surface of HNTs. In addition, pirhana and oxygen plasma pre-treatment of HNTs resulted in the highest level of grafting for HNTs.

4. Conclusions and future work

In conclusion, two investigations regarding the preparation of HNTs with improved, unique characteristics were carried out successfully. One method was focused on the purification and size separation of HNTs, and the other technique was dedicated to ionic functionalization of HNTs.

A unique method based on a previous work was developed to prepare homogeneous HNTs in size by sequencing alkaline treatment, ultrasonication and three-step viscosity gradient centrifugation. The results revealed that raw HNTs (150 – 1103 nm in length) that exist in the form of relatively large agglomerations were considerably broken, dispersed and cut in individual nanotubes during the alkaline treatment and ultrasonication. Impurities, in the form of bundles of HNTs or other microparticles have been successfully removed and pure HNTs (average size of 126 – 179 nm) were obtained through a three-step centrifugation. The yield of purified HNTs were increased by repeating the whole process for three times. Furthermore, PVP concentration and alkaline treatment both had a direct effect on the yield and size distribution of purified HNTs.

With respect to the ionic functionalization process of HNTs, ISO and N-MTSS were successfully reacted with each other to give the ionic organosilane grafting agent with ionic

functional groups. All modified HNTs with the ionic grafting agent were well dispersed compared to unmodified HNTs, indicating that ionic modification improved the dispersion process due to the charged outer surface of HNTs. In addition, pirhana and oxygen plasma pre-treatment of HNTs resulted in the highest level of grafting for HNTs.

These results are critical to enhance properties of HNTs, which enable them to have greater effects in various fields of application, such as waste water treatment.

As an efficient method in modification of HNTs by an ionic functional group, the presented ionic functionalization process can be applied on the separated and purified HNTs as the raw material, to investigate the use of purified and functionalized HNTs as highly promising materials in water purification.

5. References

- [1] Carretero, M.I. and M. Pozo, "Clay and non-clay minerals in the pharmaceutical and cosmetic industries Part II. Active ingredients", *Applied Clay Science*, 2010. 47(3): p. 171-181.
- [2] Patel, H.A., et al., "Nanoclays for polymer nanocomposites, paints, inks, greases and cosmetics formulations, drug delivery vehicle and waste water treatment", *Bulletin of Materials Science*, 2006. 29(2): p. 133-145.
- [3] Garrido-Ramírez, E., B. Theng, and M. Mora, "Clays and oxide minerals as catalysts and nanocatalysts in Fenton-like reactions—a review", *Applied Clay Science*, 2010. 47(3): p. 182-192.
- [4] Nagendrappa, G., "Organic synthesis using clay and clay-supported catalyst", *Applied Clay Science*, 2011. 53(2): p. 106-138.
- [5] Calabi Floody, M., et al., "Natural nanoclays: applications and future trends—a Chilean perspective", *Clay Minerals*, 2009. 44(2): p. 161-176.
- [6] Shahidi, S. and M. Ghoranneviss, "Effect of plasma pretreatment followed by nanoclay loading on flame retardant properties of cotton fabric", *Journal of Fusion Energy*, 2014. 33(1): p. 88-95.
- [7] Ambre, A.H., K.S. Katti, and D.R. Katti, "Nanoclay based composite scaffolds for bone tissue engineering applications", *Journal of Nanotechnology in Engineering and Medicine*, 2010. 1(3): p. 031013.
- [8] Suresh, R., et al., "Nanoclay drug delivery system", *International Journal of Pharmaceutical Sciences and Nanotechnology*, 2010. 3(2): p. 901-905.
- [9] De Azeredo, H.M., "Nanocomposites for food packaging applications", *Food research international*, 2009. 42(9): p. 1240-1253.
- [10] Majeed, K., et al., "Potential materials for food packaging from nanoclay/natural fibres filled hybrid composites", *Materials & Design*, 2013. 46: p. 391-410.

- [11] Lee, S.M. and D. Tiwari, "Organo and inorgano-organo-modified clays in the remediation of aqueous solutions: an overview", *Applied Clay Science*, 2012. 59: p. 84-102.
- [12] Ouellet-Plamondon, C., R.J. Lynch, and A. Al-Tabbaa, "Comparison between granular pillared, organo-and inorgano-organobentonites for hydrocarbon and metal ion adsorption", *Applied Clay Science*, 2012. 67: p. 91-98.
- [13] Yuan, G. and L. Wu, "Allophane nanoclay for the removal of phosphorus in water and wastewater", *Science and Technology of Advanced Materials*, 2007. 8(1): p. 60-62.
- [14] Nazir, M.S., et al., "Characteristic Properties of Nanoclays and Characterization of Nanoparticulates and Nanocomposites, in Nanoclay Reinforced Polymer Composites", *Springer*, 2016, p. 35-55.
- [15] Churchman, G., et al. "Intercalation method using formamide for differentiating halloysite from kaolinite in Clays and Clay Minerals", *Citeseer*, 1984.
- [16] Singer, A., et al., "Halloysite characteristics and formation in the northern Golan Heights. Geoderma", 2004. 123(3): p. 279-295.
- [17] Brown, G. and G.W. Brindley, "Crystal structures of clay minerals and their X-ray identification", *Mineralogical Society London*, Vol. 5. 1980.
- [18] Pasbakhsh, P., G.J. Churchman, and J.L. "Keeling, Characterisation of properties of various halloysites relevant to their use as nanotubes and microfibre fillers", *Applied Clay Science*, 2013. 74: p. 47-57.
- [19] Pasbakhsh, P., et al., "EPDM/modified halloysite nanocomposites", *Applied Clay Science*, 2010. 48(3): p. 405-413.
- [20] Joussein, E., et al., "Halloysite clay minerals—a review", *Clay minerals*, 2005. 40(4): p. 383-426.
- [21] Bailey, S., "Halloysite-a critical assessment. Sciences Geologiques-Memoires", 1990. 86: p. 89-98.

- [22] Tomura, S., et al., "Growth conditions and genesis of spherical and platy kaolinite", *Clays Clay Miner*, 1985. 33(3): p. 200.
- [23] Guo, B., et al., "Structure and performance of polyamide 6/halloysite nanotubes nanocomposites", *Polymer journal*, 2009. 41(10): p. 835-842.
- [24] Dixon, J., "Internal and external morphology of tubular and spheroidal halloysite particles", *Clays and Clay Minerals*, 1974. 22: p. 127-137.
- [25] Singh, B. and R. Gilkes, "An electron optical investigation of the alteration of kaolinite to halloysite", *Clays and Clay Minerals (United Kingdom)*, 1992.
- [26] Robertson, I.D. and R.A. Eggleton, "Weathering of granitic muscovite to kaolinite and halloysite and of plagioclase-derived kaolinite to halloysite", *Clays and Clay Minerals*, 1991. 39(2): p. 113-126.
- [27] Lvov, Y.M., et al., "Halloysite clay nanotubes for controlled release of protective agents", *Acs Nano*, 2008. 2(5): p. 814-820.
- [28] Yuan, P., D. Tan, and F. Annabi-Bergaya, "Properties and applications of halloysite nanotubes: recent research advances and future prospects", *Applied Clay Science*, 2015. 112: p. 75-93.
- [29] R. Price, B.G., Y. Lvov, R., "In-vitro release characteristics of tetracycline HCl, khellin and nicotinamide adenine dinucleotide from halloysite; a cylindrical mineral", *Journal of microencapsulation*, 2001. 18(6): p. 713-722.
- [30] Kamble, R., et al., "Halloysite Nanotubes and Applications: A Review", *Journal of advanced scientific research*, 2012. 3(2).
- [31] Rawtani, D. and Y. Agrawal, "Multifarious applications of halloysite nanotubes: a review", *Rev. Adv. Mater. Sci*, 2012. 30(3): p. 282-295.
- [32] Du, M., B. Guo, and D. Jia, "Newly emerging applications of halloysite nanotubes: a review", *Polymer International*, 2010. 59(5): p. 574-582.

- [33] Wilson, I., "Kaolin and halloysite deposits of China", *Clay Minerals*, 2004. 39(1): p. 1-15.
- [34] Wilson, M., "Clay mineralogical and related characteristics of geophagic materials", *Journal of chemical ecology*, 2003. 29(7): p. 1525-1547.
- [35] Peng, Q., et al., "Adsorption of dyes in aqueous solutions by chitosan-halloysite nanotubes composite hydrogel beads", *Microporous and Mesoporous Materials*, 2015. 201: p. 190-201.
- [36] Rong, R., et al., "Facile preparation of homogeneous and length controllable halloysite nanotubes by ultrasonic scission and uniform viscosity centrifugation", *Chemical Engineering Journal*, 2016. 291: p. 20-29.
- [37] Kearns, G.J., E.W. Foster, and J.E. Hutchison, "Substrates for direct imaging of chemically functionalized SiO₂ surfaces by transmission electron microscopy", *Analytical chemistry*, 2006. 78(1): p. 298-303.
- [38] Foster, E.W., et al., "Patterned Gold-Nanoparticle Monolayers Assembled on the Oxide of Silicon", *Advanced Materials*, 2005. 17(12): p. 1542-1545.
- [39] Sweeney, S.F., G.H. Woehrle, and J.E. Hutchison, "Rapid purification and size separation of gold nanoparticles via diafiltration", *Journal of the American Chemical Society*, 2006. 128(10): p. 3190-3197.
- [40] Robertson, J.D., et al., "Purification of Nanoparticles by Size and Shape", *Sci Rep*, 2016. 6: p. 27494.
- [41] Hanauer, M., et al., "Separation of nanoparticles by gel electrophoresis according to size and shape", *Nano letters*, 2007. 7(9): p. 2881-2885.
- [42] Bikos, D. and T.G. Mason, "Propagation and Separation of Charged Colloids by Cylindrical Passivated Gel Electrophoresis", *J Phys Chem B*, 2016. 120(26): p. 6160-5.

- [43] Wei, G.-T., F.-K. Liu, and C.C. Wang, "Shape separation of nanometer gold particles by size-exclusion chromatography", *Analytical chemistry*, 1999. 71(11): p. 2085-2091.
- [44] Duesberg, G., et al., "Chromatographic size separation of single-wall carbon nanotubes", *Applied Physics A: Materials Science & Processing*, 1998. 67(1): p. 117-119.
- [45] Duesberg, G., et al., "Separation of carbon nanotubes by size exclusion chromatography", *Chemical Communications*, 1998(3): p. 435-436.
- [46] Holzinger, M., et al., "A new purification method for single-wall carbon nanotubes (SWNTs)", *Applied Physics A: Materials Science & Processing*, 2000. 70(5): p. 599-602.
- [47] Moore, K.E., et al., "Separation of Double-Walled Carbon Nanotubes by Size Exclusion Column Chromatography", *ACS nano*, 2014. 8(7): p. 6756-6764.
- [48] Qiu, P. and C. Mao, "Viscosity Gradient as a Novel Mechanism for the Centrifugation-Based Separation of Nanoparticles", *Advanced Materials*, 2011. 23(42): p. 4880-4885.
- [49] Chen, G., et al., "High-purity separation of gold nanoparticle dimers and trimers", *Journal of the American Chemical Society*, 2009. 131(12): p. 4218-4219.
- [50] Bonaccorso, F., et al., "Sorting Nanoparticles by Centrifugal Fields in Clean Media", *The Journal of Physical Chemistry C*, 2013. 117(25): p. 13217-13229.
- [51] Akbulut, O., et al., "Separation of nanoparticles in aqueous multiphase systems through centrifugation", *Nano Lett*, 2012. 12(8): p. 4060-4.
- [52] Fagan, J.A., et al., "Length fractionation of carbon nanotubes using centrifugation", *Advanced Materials*, 2008. 20(9): p. 1609-1613.
- [53] Sharma, V., K. Park, and M. Srinivasarao, "Shape separation of gold nanorods using centrifugation", *Proceedings of the National Academy of Sciences*, 2009. 106(13): p. 4981-4985.

- [54] Sun, X., et al., "Separation of nanoparticles in a density gradient: FeCo@C and gold nanocrystals", *Angew Chem Int Ed Engl*, 2009. 48(5): p. 939-42.
- [55] Bai, L., et al., "Rapid separation and purification of nanoparticles in organic density gradients", *Journal of the American Chemical Society*, 2010. 132(7): p. 2333-2337.
- [56] Qiu, P. and C. Mao, "Viscosity gradient as a novel mechanism for the centrifugation-based separation of nanoparticles", *Adv Mater*, 2011. 23(42): p. 4880-5.
- [57] Miller, J.B., J.M. Harris, and E.K. Hobbie, "Purifying colloidal nanoparticles through ultracentrifugation with implications for interfaces and materials", *Langmuir*, 2014. 30(27): p. 7936-46.
- [58] Miller, J.B., J.M. Harris, and E.K. Hobbie, "Purifying colloidal nanoparticles through ultracentrifugation with implications for interfaces and materials", *Langmuir*, 2014. 30(27): p. 7936-7946.
- [59] Fagan, J.A., et al., "Centrifugal length separation of carbon nanotubes", *Langmuir*, 2008. 24(24): p. 13880-13889.
- [60] White, R.D., D.V. Bavykin, and F.C. Walsh, "The stability of halloysite nanotubes in acidic and alkaline aqueous suspensions", *Nanotechnology*, 2012. 23(6): p. 065705.
- [61] Joo, Y., et al., "Opening and blocking the inner-pores of halloysite", *Chemical Communications*, 2013. 49(40): p. 4519-4521.
- [62] Joo, Y., et al., "Aggregation and stabilization of carboxylic acid functionalized halloysite nanotubes (HNT-COOH)", *The Journal of Physical Chemistry C*, 2012. 116(34): p. 18230-18235.
- [63] Joo, Y., et al., "Opening and blocking the inner-pores of halloysite", *Chem Commun (Camb)*, 2013. 49(40): p. 4519-21.
- [64] Wang, Q., J. Zhang, and A. Wang, "Alkali activation of halloysite for adsorption and release of ofloxacin", *Applied surface science*, 2013. 287: p. 54-61.

- [65] Bretti, C., et al., "Thermodynamics of Proton Binding of Halloysite Nanotubes", *The Journal of Physical Chemistry C*, 2016. 120(14): p. 7849-7859.
- [66] Ouyang, J., et al., "High morphological stability and structural transition of halloysite (Hunan, China) in heat treatment", *Applied Clay Science*, 2014. 101: p. 16-22.
- [67] Tazaki, K., "Microbial formation of a halloysite-like mineral", *Clays and Clay Minerals*, 2005. 53(3): p. 224-233.
- [68] Yu, L., et al., "Recent advances in halloysite nanotube derived composites for water treatment", *Environmental Science: Nano*, 2016. 3(1): p. 28-44.
- [69] Carli, L.N., et al., "The effects of silane coupling agents on the properties of PHBV/halloysite nanocomposites", *Applied Clay Science*, 2014. 87: p. 311-319.
- [70] Yuan, P., et al., "Functionalization of halloysite clay nanotubes by grafting with γ -aminopropyltriethoxysilane", *The Journal of Physical Chemistry C*, 2008. 112(40): p. 15742-15751.
- [71] Luo, P., et al., "Preparation and characterization of silane coupling agent modified halloysite for Cr (VI) removal", *Industrial & Engineering Chemistry Research*, 2011. 50(17): p. 10246-10252.
- [72] Barrientos-Ramírez, S., et al., "Surface modification of natural halloysite clay nanotubes with aminosilanes. Application as catalyst supports in the atom transfer radical polymerization of methyl methacrylate", *Applied Catalysis A: General*, 2011. 406(1): p. 22-33.
- [73] Shi, Y.-F., et al., "Functionalized halloysite nanotube-based carrier for intracellular delivery of antisense oligonucleotides", *Nanoscale research letters*, 2011. 6(1): p. 608.
- [74] Massaro, M., et al., "Eco-friendly functionalization of natural halloysite clay nanotube with ionic liquids by microwave irradiation for Suzuki coupling reaction", *Journal of Organometallic Chemistry*, 2014. 749: p. 410-415.

- [75] Zhu, J., et al., "Preparation and characterization of negatively charged PES nanofiltration membrane by blending with halloysite nanotubes grafted with poly (sodium 4-styrenesulfonate) via surface-initiated ATRP", *Journal of Membrane Science*, 2014. 465: p. 91-99.
- [76] Zhang, J., et al., "Chemical functionalization for improving dispersion and interfacial bonding of halloysite nanotubes in epoxy nanocomposites", *High Performance Polymers*, 2014. 26(7): p. 734-743.
- [77] Peixoto, A.F., et al., "Physicochemical characterization of organosilylated halloysite clay nanotubes", *Microporous and Mesoporous Materials*, 2016. 219: p. 145-154.
- [78] Wu, Y., et al., "Preparation of waterborne polyurethane nanocomposite reinforced with halloysite nanotubes for coating applications", *Journal of Applied Polymer Science*, 2016. 133(37).
- [79] Vogel, B.M., et al., "Interfacial modification of silica surfaces through γ -isocyanatopropyl triethoxy silane-amine coupling reactions", *Applied Surface Science*, 2008. 254(6): p. 1789-1796.
- [80] Sun, P., et al., "Effective activation of halloysite nanotubes by piranha solution for amine modification via silane coupling chemistry", *RSC Advances*, 2015. 5(65): p. 52916-52925.